EPFL

Thèse n° 9866

Construction of MOF/Polymer Composites for Metal Ion Capture

Présentée le 15 janvier 2020

à la Faculté des sciences de base
Laboratoire des matériaux inorganiques fonctionnels
Programme doctoral en chimie et génie chimique

pour l'obtention du grade de Docteur ès Sciences

par

Daniel Teav SUN

Acceptée sur proposition du jury

Prof. M. K. Nazeeruddin, président du jury
Prof. W. L. Queen, directrice de thèse
Prof. C. Brown, rapporteur
Dr Y. Liu, rapporteur
Prof. A. Boghossian, rapporteuse

École polytechnique fédérale de Lausanne

2020

“This world would be in darkness without a sense of duty”

ABSTRACT

Metal ion capture is of environmental and economic significance. The industrial revolutions have discharged increasing amounts of heavy and precious metals into complex water sources. The key is that these types of metal ions tend to be at trace amounts in water mixtures containing high concentrations of inorganic and organic interferents. It is extremely difficult to extract and concentrate such species from these complex water mixtures. In this thesis, we show that novel inner pore structural modifications inside of metal-organic frameworks or MOFs, achieved via *in-situ* polymerization can enhance specific metal ion capture performance from aqueous media.

One unique property of MOFs is the presence of open metal sites along the pore surface, which can give rise to interesting redox activity. By taking advantage of this phenomenon, in Chapter 2 we show that a MOF named Fe-BTC polymerizes dopamine to polydopamine (PDA) inside its porous network via its Fe^{3+} open metal sites. The heavy metal scavenging PDA, now pinned on the internal MOF surface results in a material that has high capacities for Pb^{2+} and Hg^{2+} and removes over 99.8 % of these contaminants from a 1 ppm solution rapidly, yielding drinkable levels in seconds and maintains its properties in river water, waste water (obtained from Swiss industry) and sea water spiked with only trace amounts of lead and mercury. The material is further shown to be resistant to fouling due to its unique pore architecture and is fully regenerable over many cycles. Further, a number of characterization techniques are defined and employed to help fully understand the interface of these materials.

By changing the polymer building blocks, in Chapter 3 we demonstrate that a new material, Fe-BTC/PpPDA, is able to selectively and rapidly extract ultra-trace amounts of gold from several complex water mixtures that include waste water, fresh water, ocean water, and solutions used to leach gold from electronic waste and incinerated sewage sludge. The material has an exceptional removal capacity and completely extracts gold from these complex mixtures in under 2 minutes. Further, due to the high cyclability, we demonstrate that the composite can effectively concentrate gold and yield purities up to 23.9 K.

For large-scale implementation, these materials must be scaled up and considered in a dynamic continuous flow through operation. As such, the objectives are to 1) construct a continuous flow through apparatus, 2) scale up the synthesis of the MOF/Polymer composites, 3) optimally structure the fine powder material and 4) optimize and model continuous fix-bed column

experiments. In Chapter 4, the progress for these endeavors from the Clean Water Initiative is shown.

RÉSUMÉ

La capture des ions métalliques a une importance environnementale et économique. Les révolutions industrielles ont déversé des quantités croissantes de métaux lourds et précieux dans des sources d'eau complexes. Ces types d'ions métalliques ont tendance à être à l'état de traces dans des mélanges d'eau contenant de fortes concentrations d'interférents inorganiques et organiques. Il est extrêmement difficile d'extraire et de concentrer ces espèces de ces mélanges complexes d'eau. Dans cette thèse, nous montrons que de nouvelles modifications structurelles des pores internes de metal-organic frameworks (MOFs), obtenues via une polymérisation in situ, peuvent améliorer les performances de capture spécifiques d'ions métalliques en milieux aqueux.

Une propriété unique des MOF est la présence de sites métalliques ouverts le long de la surface des pores, ce qui peut donner lieu à une activité redox intéressante. En tirant parti de ce phénomène, nous montrons au chapitre 2 qu'un MOF nommé Fe-BTC polymérise la dopamine en polydopamine (PDA) dans son réseau poreux via ses sites métalliques ouverts Fe^{3+}. Le PDA piégeant les métaux lourds, à présent épinglé sur la surface interne du MOF, donne un matériau qui possède des capacités de capture élevées pour Pb^{2+} et Hg^{2+} et élimine plus de 99,8% de ces contaminants d'une solution à 1 ppm rapidement, produisant des eaux avec des niveaux buvables en quelques secondes et conservant ses propriétés dans l'eau de rivière, les eaux usées (fournies par l'industrie suisse) et l'eau de mer ne contenant que des traces de plomb et de mercure. En outre, le matériau résiste à l'encrassement grâce à son architecture unique de pores et peut être entièrement régénéré sur plusieurs cycles. En outre, un certain nombre de techniques de caractérisation sont choisies et utilisées pour aider à comprendre pleinement l'interface de ces matériaux.

Au chapitre 3, en modifiant les éléments constitutifs des polymères, nous démontrons qu'un nouveau matériau, le Fe-BTC / PpPDA, est capable d'extraire sélectivement et rapidement des quantités ultra-traces d'or de plusieurs mélanges d'eau complexes comprenant des eaux usées, de l'eau douce, des océans, et les solutions utilisées pour extraire l'or des déchets électroniques et des boues d'épuration incinérées. Le matériau possède une capacité d'extraction exceptionnelle et extrait complètement l'or de ces mélanges complexes en moins de 2 minutes. De plus, en raison de la cyclabilité élevée, nous démontrons que le composite peut efficacement concentrer l'or et donner des puretés allant jusqu'à 23,9 K.

Pour une mise en œuvre à grande échelle, ces matériaux doivent être mis à l'échelle en considérant un flux continu et dynamique. Les objectifs sont les suivants: 1) construire un appareil à écoulement continu, 2) augmenter la synthèse des composites MOF / polymère, 3) structurer de manière optimale le matériau en poudre fine et 4) optimiser et modéliser les expériences de colonne en lit fixe en continu. Le chapitre 4 présente les progrès réalisés dans le cadre de ces initiatives pour une eau saine.

SYMBOLS AND ABBREVIATIONS

MOF	Metal-organic Framework
PSM	Post Synthetic Modification
NBS	N-bromosuccinimide
Py	Pyridine
BTC	1,3,5-Benzene Tricarboxylate
PDA	Polydopamine
PpPDA	Poly-p-phenylenediamine
PHQ	Polyhydroquinone
PTA	Polytyramine
PmAP	Poly-m-aminophenol
SCXRD	Single Crystal X-ray Diffraction
PXRD	Powder X-ray Diffraction
XPS	X-ray Photoelectron Spectroscopy
ATR	Attenuated Total Reflectance
DRIFTS	Diffuse reflectance infrared fourier transform spectroscopy
TGA	Thermo gravimetric Analysis
SEM	Scanning Electron Microscopy
TEM	Transmission Electron Spectroscopy
STEM	Scanning Transmission Electron Miscroscopy
EDX	Energy Disperson X-ray spectroscopy
EELS	Electron Energy Loss Spectroscopy
NMR	Nuclear Magnetic Resonance
BET	Brunaeur-Emmett-Teller
DFT	Density Functional Theory
ICP-OES	Inductively Coupled Plasma – Optical Emission Spectroscopy
ICP-MS	Inductively Coupled Plasma – Mass Spectrometry
MALD-TOF-MS	Matrix-assisted laser desorption/ionization time of flight mass spectrometry
WHO	World Health Organization
EPA	U.S. Environmental Protection Agency
UN	United Nations
CPU	Computer Processing Unit
TV	Televisions
PC	Personal Computers
WEEE	Waste Electrical and Electronic Equipment
E-Waste	Electronic Waste

ABSTRACT **3**

RESUME **5**

SYMBOLS AND ABBREVIATIONS **7**

TABLE OF CONTENTS **8**

CHAPTER 1 – INTRODUCTION **12**

1.1 Metal Ions 12

1.2 Water Contamination by Heavy Metals 13

1.3 Highly Valuable Commodities in Complex Liquid Mixtures 15

1.4 Matrices 17

1.5 Trace Extraction of Metal Ions 21

1.6 Metal-Organic Frameworks (MOFs) 22

1.7 MOF/Polymer Composites for Metal Ion Capture 26

1.8 MOTIVATION AND OUTLINE OF THE THESIS 28

CHAPTER 2 - RAPID, SELECTIVE HEAVY METAL REMOVAL FROM WATER BY A MOF/POLYDOPAMINE COMPOSITE **31**

2.1 Introduction 32

2.2 Results and Discussion 33

2.2.1 Design, Synthesis and Characterization 33

2.2.2 Heavy Metal Extraction from Water 35

2.3 Conclusion 41

2.4 Synthetic Methods and Procedures 42

CHAPTER 3 - RAPID, SELECTIVE EXTRACTION OF TRACE AMOUNTS OF GOLD FROM COMPLEX WATER MIXTURES WITH A MOF/POLYMER COMPOSITE **45**

3.1 Introduction 46

3.2 Results and Discussion 47

3.2.1 Design, Synthesis and Characterization 47

3.2.2 Gold Extraction from Complex Water Mixtures 50

3.3 Conclusion 53

3.4 Synthetic Methods and Procedures 55

CHAPTER 4 – CLEAN WATER INITIATIVE – NEX GEN FILTER DEVICES 59

4.1 Introduction 60

4.2 Results and Discussion 61

4.2.1 Scale up of MOF/ MOF/Polymer Composites and Structuring 61

4.2.2 Design of 1st Generation Continuous Flow Through Apparatus 62

4.2.3 Continuous Fix-Bed Column Experiments and Preliminary Results 63

4.3 Conclusion 67

SUMMARY 69

EXPERIMENTAL PART 72

General Methods for Synthesis 72

Material Characterization 73

Powder X-ray Diffraction 73

Nitrogen Adsorption Measurements 73

X-ray Photoelectron Spectroscopy 73

In-situ FT-IR with Carbon Monoxide 73

Scanning and Transmission Electron Microscopy with Microtomy 74

Attenuated Total Reflection Infrared Spectroscopy 74

Thermogravimetric Analysis 74

Matrix-assisted Laser Deposition/Ionization Time of Flight Spectroscopy 74

General Metal Ion Capture Experiments 75

Inductively Coupled Plasma – Optical Emission and Mass Spectrometry 75

APPENDIX 80

Appendix to Chapter 2 80

Appendix to Chapter 3 114

Appendix to Chapter 4 137

ACKNOWLEDGEMENTS **140**

REFERENCES **141**

CURRICULUM VITAE **153**

“Knowing is half the battle”

Chapter 1 Introduction

1.1 Metal Ions

Metals are used in all parts of industrial activity and our daily lives. Interestingly, the properties of metals such as hardness, reactivity and/or electronic profiles are dictated by the variation of the number of electrons, neutrons and protons in a given atom.[26-27] This gives rise to individual identities along the periodic table. Some of these metals are susceptible to oxidation and dissolve into liquids such as water or organic solvents. They transform into metal ions that have hydration or solvent shells and float in solution (Figure 1.1).[29] These ions play major roles in industrial applications such as metal production,[31] purification,[33] catalysis,[34] chemical separations[35] and even in our living biochemical systems.[36] For instance, natural occurring metal ions such as Na^+, Ca^{2+}, K^+ or Mg^{2+} in water are important electrolytes for the human body as they regulate hydration and body pH.[37] Whereas heavy metal ions, such Pb^{2+} or Hg^{2+}, play no role in human homeostasis and if trace amounts are consumed or exposed to, induce multiple organ damage and cause adverse birth defects.[38] Other metals ions such as the platinum group and noble metals are extremely valuable in their pure neutral oxidation state form (Figure 1.3).[39-41] Thus, with the ever-increasing production of modern electronics, catalysts and infrastructure, the purification of these precious metals from sources other than virgin mines are being intensively explored.[1-3] For decades, scientists have been developing new porous materials to examine their effectiveness in capturing metal ions from liquid sources. These sources include natural bodies of water, industrial wastewater mixtures and liquid solutions used to leach metal ions out of solid waste. It is indisputable that the capture of metal ions from liquid sources is both of significant environmental and economic relevance.

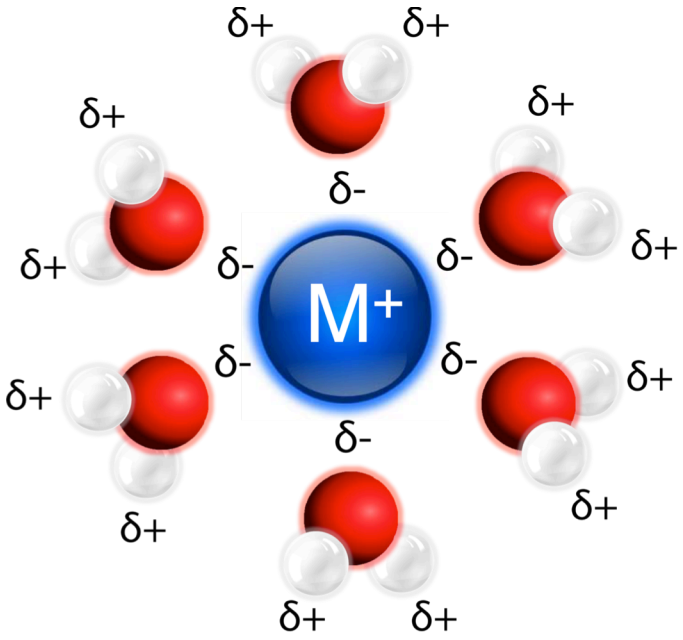

Figure 1.1. Solvation shell around a Metal Ion.

1.2 Water Contamination by Heavy Metals

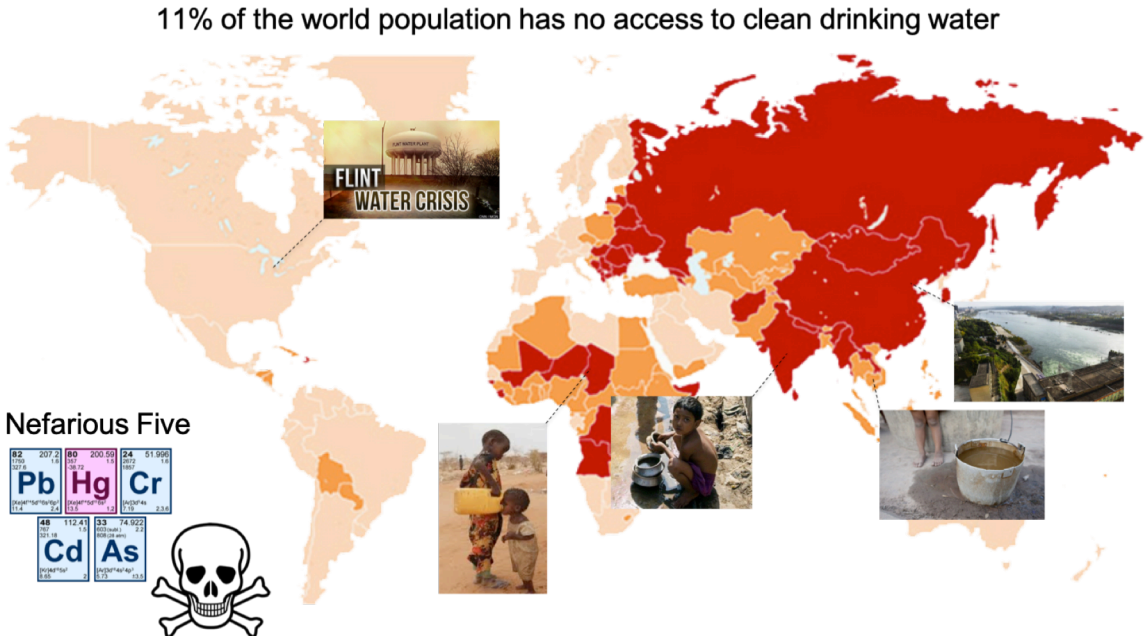

Figure 1.2. World map and some of the many locations where heavy metal contamination in water is prominent.

It is without a doubt that the world's clean water supply is steadily decreasing as industrial activities continue to flourish along with continued climate change (Figure 1.2). Further a rapidly increasing population will create new water intensive areas globally especially in developing countries. This shortage of water will not only impact human health in underdeveloped areas, but can also impact the more developed countries' energy sector. As seen in the U.S. 2012 drought, the absence of an abundant clean water supply had strained the energy systems nationally. The water energy nexus illustrates that it cost energy to produce and send municipal clean water to the populace. Vice versa it also takes water to produce energy for the public. Solutions for the energy efficient production of clean potable water are becoming imperative for not only environmental and human well-being, but as well as the preservation of long-term energy security.

As for environmental and social concern, water contamination with heavy metals exists worldwide.[38] With an estimated 1 billion people without access to clean drinking water and 2 million casualties per year, water contamination is one of the world's leading causes of death.[42] This problem is only expected to worsen as the World Health Organization (WHO) estimates that climate change will limit access to clean water for as much as half of the world's population in the next decades.[43] Heavy metal ions, particularly Pb^{2+}, Hg^{2+}, Cd^{2+}, Cr^{6+} and $As^{3+,\ 5+}$ are extremely

toxic at trace amounts as they induce acute organ damage and are classified carcinogens (Figure 1.2). There are many locations globally where these contaminants are at concentrations deemed too high for consumption and are still employed for municipal uses (Figure 1.2).[44-45] This stems from the 19th and 20th century industrial revolutions, where the increasing uses of these toxic metals are being employed or are a by-product in the building of infrastructure, material applications and/or mining operations. Consequently, foreign toxic heavy metals still are currently discharged and mixed into waste streams and natural bodies of water that already contain complex mixtures of natural occurring light metals and large organics. As such, environmental damage is prominent globally.

For instance, recently Virginia Tech researchers uncovered extensive lead contamination in Flint, Michigan[46] and in December of 2016 a study by Reuters reported over 3000 areas in the US with poisoning rates twice that of Flint.[47] These media reports have shed light on a major environmental crisis and our inability to decontaminate large quantities of water even in developed first world countries. Exposure is even worse in underdeveloped countries where lack of resources and awareness limit the use of expensive industrial wastewater treatment processes. Some examples include the ground water in India that is littered with toxic hexavalent chromium[48] and the Mekong River that runs through Cambodia contains internationally illegal concentrations of lead and arsenic.[44] With this in mind, obviously drinking water contamination with the aforementioned heavy metal ions is of great environmental concern and many scientists are developing porous materials for the capture of such toxic species to produce clean potable water.

Although there are many effective ways to clean water from bacteria, pathogens and organics; heavy metals tend to be a difficult separation problem as they are generally in complex water mixtures where inorganic interferents can be up to hundreds of times the concentration of the contaminants. First, large organic molecules like humic acid tend to foul state of the art adsorbents such as activated carbons or mesoporous silica. Next, the common inorganic interferents tend to be at relatively high concentrations of Na^+, K^+, Ca^{2+} and Mg^{2+} noticeably found in all water sources. It is difficult to extract toxic heavy metals at trace amounts to below concentrations lower than what organizations like the United States Environmental Protection Agency (U.S. EPA) or World Health Organization (WHO) deems drinkable. Next to climate change, water purification is a major humanitarian effort that needs attention for the survival of next generation.

1.3 Highly Valued Commodities in Complex Water Mixtures

Other metals that are rare with radiant and lustrous appearances have been the basis for jewelry production and currency for centuries. Further these types of metals tend to have unique electronic properties and redox activity that are sought out for the manufacturing of modern-day electronics,[49] catalysts[50] and in some case energy applications.[51-53] It is irrefutable that the separation and purification of such metals is of significant economic relevance. As such, scientists have been designing new porous materials and methodologies to capture such metal ions deemed valuable from liquid sources. These sources include natural bodies of water, industrial wastewater or solutions used to leach out metal ions from ore, incinerated sewage ash or electronic waste. As such, it is to no surprise that recent studies have shown that now it is more cost-effective to urban mine precious metals from electronic waste rather than the virgin mining of ore as scientists look towards new routes of sustainability.[23]

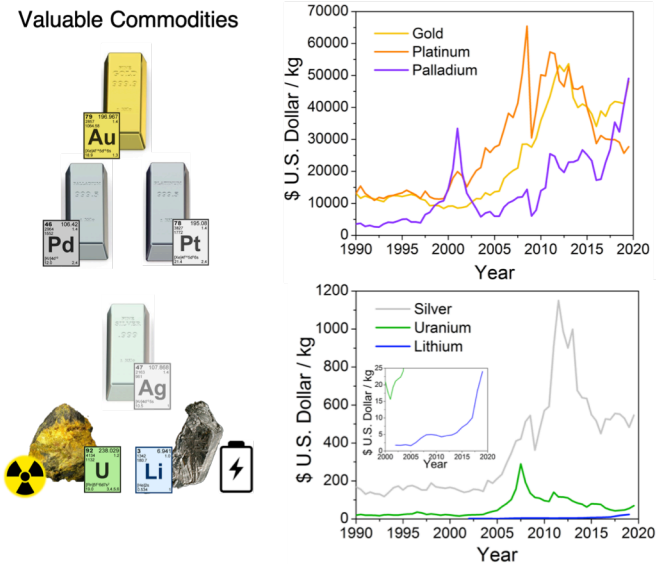

Figure 1.3. The price per kg history of gold, silver, platinum, palladium, uranium and lithium.[1-4]

In 2016 alone, 60 billion U.S. dollars of precious metals were estimated in electronic waste produced in Europe alone.[54-55] Commonly the separation of such commodities involves the desired metal in the solid waste to be oxidized into metal ions by chemical means subsequently leaching them into liquid solutions.[56] Further industrial activities that employ such high value metals in their production or operations tend to lose a significant amount in their liquid downstream processes and thus there is increasing opportunities to recover value that is ultimately lost. The precious metals, Ag^{+}, $Pt^{2+,\ 4+}$, Pd^{2+}, Au^{3+}, which are obvious valuable commodities in their neutral oxidation state, have been historically major players in material applications, modern electronics and catalysts (Figure 1.3). For example, the most prominent use of platinum other than electronics, is as a catalyst in a number of industrial sectors that include the automotive, petroleum, pharmaceutical and fine chemicals industries. Some of these platinum

catalysts are homogenous in nature and after they are catalytically spent, tend to be ultimately lost in the downstream operations. This is but one example of an avenue where scientists could develop sustainable protocols or materials to recover such metal ions from solution to be recycled and used once again. Currently there are traditional methods to separate these precious metals, but they tend to utilize harsh chemical conditions. If the waste produced from such processes is not treated properly, they can damage the environment extensively. Since these precious metals are extremely valuable and needed in our modern society, it is imperative that we developed new green and environmentally friendly methodologies for their selective extraction and separation from complex liquid sources. This includes creating green protocols for 1) the oxidation of the metal into solution, 2) its separation from the complex liquid mixture and 3) its reduction to its neutral oxidation state depending on the application.

The separations of precious metals are obvious metal ions that are well targeted by scientists as seen in the literature. But another arena, in which the separation of specific metal ions will play major roles, is the energy sector. Climate change is real and undeniable. Currently we are already seeing many of its side effects such as the melting of artic glaciers, record breaking temperatures and a diminishing drinkable water supply worldwide. It is expected that humanity will be met with dire consequences in less than 20 years if we do not transform our energy system from using fossil fuels to sustainable carbon free emitting energy sources. Thus, scientists are intensively studying other means of renewable energy production. It will take a diverse portfolio of renewable energy operations to overcome the beast that is the fossil fuel industry. For instance, nuclear power is one such important avenue to explore. However, for nuclear energy production to become feasible on large scales, a sustainable supply of uranium is essential. Current land reserves, estimated to be ~4.85 million tons, will likely be exhausted in the coming decades. This has prompt scientist to look for other sources of uranium. For instance, wastewater produced in nuclear plants contain not only uranium ion but other radioactive isotopes that can be reused for nuclear energy production. Further, because of the increasing use of new battery technologies, the separation of lithium from spent batteries or brine reservoirs is also gaining attention. This is to combat the energy storage problem, as a sustainable supply is needed with the increase production of lithium ion based batteries. New technologies that can selectively extract such species, like precious metals or uranium and lithium, from these complex water mixtures will not only help solve our energy problems, but will revolutionize what future mining activities may look

like. The recycling and recovery of such valuable metal commodities is an essential aspect of sustainability for our modern industries and energy sectors.

1.4 Matrices

1.4.1 Surface Water

It is imperative to go over the possible water matrices that these metal ions tend to be in. The matrix can influence the desired metal ion's speciation and the possible inorganic or organic interferents present can compromise material performance. Generally, fresh water sources can be classified into two groups: surface water and groundwater.[57] Surface water is the water found on the surface of the earth, which includes water in lakes, rivers, streams, wetlands and artificial reservoirs. This water is usually not very high in mineral content, and is often classified as "soft water" compared to other sources of water such as the sea or waste streams. Because of this and its availability, it is used for municipal and domestic operations and consumption. In general, the pH of surface water is commonly between 6.5 and 8.5 depending on the metal composition and the geography and season will influence that composition. Typical major metal ions found in surface water tend to be Ca^{2+}, Mg^{2+}, Na^{+}, K^{+}. For instance, the Rhone river in the Swiss alps will have a lower mineral content in the summer due to the melting snow increasing various run off streams from the mountain. Although one of the major sources for humanity,[58] surface water is often the most exposed to contaminants that include animal wastes, pesticides, insecticides, industrial waste, algae and many other organic and inorganic materials.

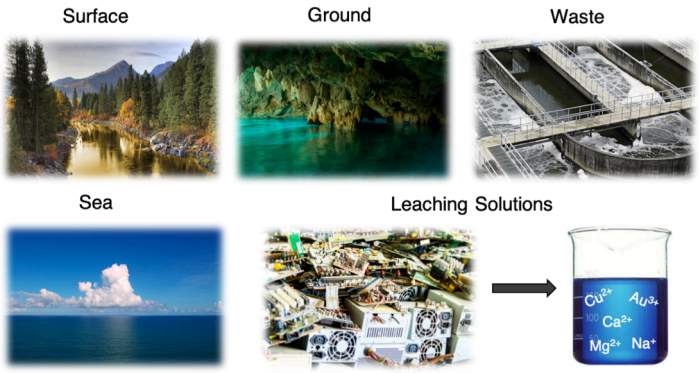

Figure 1.4. Different types of water matrices.

1.4.2 Ground Water

Groundwater is the water located under the earth's surface, contained in or by a subsurface layer of soil or rock.[57] Rain that soaks into the ground, rivers that disappear beneath the earth, melting snow are but a few of the sources that recharge the supply of underground water. Because of these many sources, ground water may contain any or all of the contaminants found in surface

water as well as the dissolved minerals it picks up during its journey to the deep. However, groundwater usually contains less contamination than surface water because the sediment and the soil tend to act as a filter to remove the toxic species.[59] Unlike surface water, ground water is free from pathogenic organisms such as salmonella and malaria. Rather it tends to store pesticide chemicals and nitrate while surface water usually contains living bacteria and other microorganisms. Further, ground water maintains a constant temperature whereas the temperature of surface water alters according to the surroundings affecting the aforementioned composition. Typical pH of ground water ranges from 6 to 8.5. Clearly, there are major differences in the composition between surface and ground water. Moreover, as the depth increases, the salt content also increases.[60] Nowadays, due to rapid population growth globally and intensive domestic activities, as well as expanding industrial and agricultural production, the surface and ground water are susceptible to hazardous chemicals especially heavy metals by the discharge of untreated domestic and industrial waste. The heavy metals (Pb^{2+}, Hg^{2+}, Cd^{2+}, Cr^{6+}, $As^{3+, 5+}$) can be found in these freshwater sources. Ag^{+}, Au^{3+}, Pd^{2+}, $Pt^{2+, 4+}$, Li^{+} and UO_2^{2+} can also be found but usually at trace amounts if not next to mining or industrial operations.

1.4.3 Sea Water

Rivers carry dissolved ions, which are collected from ground and surface water runoff, into the sea.[61] Covering more than 70 percent of earth's surface, it contains common alkali and alkaline earth metal ions at concentrations up to 20,000 ppm and a plethora of organics.[62] On average the salinity of seawater is roughly 3.5 %, which is approximately 35 grams of dissolved salts per liter. Typical pH of seawater ranges from 7.5 to 8.4, but this value may vary depending on geographic factors. There is virtually every commercially important metal ion in the sea, but at trace amounts. Although at low concentrations, due to the vast amount of seawater in the world, there are millions of tons of commodities for the taking if separated effectively and economically. For instance, there is 20 million tons of gold present in the world's oceans.[63] Unfortunately, the typical concentration of gold tends to be in the low ppt regime and is miniscule when compared to other competing metal ions. Another example is a potential carbon free energy source we mentioned earlier. Currently, there is an estimated 4.5 billion tons of uranium in the oceans, an amount able to help supply the world with energy. To put this in perspective, over 300 000 L of seawater would need to be filtered to extract a single gram of uranium.[64] Further there are brine reservoirs in South America that contain tons of lithium, a main component in modern commercial batteries.[65] New innovative technologies able to selectively concentrate and recover commodities from these

sources can disrupt future mining activities. This is an extremely difficult challenge as seawater is the most complex matrix in the world.

1.4.4 Industrial Wastewater

Wastewater originated from industries, street runoffs and landfills normally contain many metals ions and have a high total organic content.[66-67] This can cause the formation of organic metal ion complexes that can disrupt an adsorbent's performance. The most common industries that produce wastewater are metal finishing and plating, printed circuit board manufacturing, wood processing, inorganic pigment manufacturing, petroleum refining, and semiconductor manufacturing. These industrial operations tend to discharge heavy or precious metals in their downstream processes that eventually make it to the environment. Because of the various types of industrial activity, the pH can range along the whole spectrum. As such, some adsorbents have to be stable against extremely acidic or basic conditions. Various methods are applied to remove these heavy and valuable metal ions, such as expensive chemical precipitation,[68] coagulation-flocculation,[69] complexation,[70] activated carbon adsorption,[71] ion exchange,[72] solvent extraction,[67] foam flotation,[73] electrolytic reduction,[74] cementation,[75] and membrane technologies.[76] Unfortunately, in underdeveloped countries, surface water contamination with heavy metals is more prominent due to lack of awareness and these expensive treatment processes for industrial wastewater. Both heavy and valuable metals are most definitely found in wastewater. Looking at the glass half full; this provides researchers opportunities to develop new solutions for industry with the intent of protecting the environment and humanity.

1.4.5 Leaching Solutions

Leaching solution from electronic waste and mining operations are employed to generate generally toxic liquid mixtures containing heavy and precious metal ions for separation purposes.[77-78] Electronic waste includes all discarded obsolete electronic products, among which televisions (TVs), personal computers (PCs), and computer monitors comprise the most significant components.[79] It is estimated that electronic waste contributes as much as 70% of the total heavy metals and 40% of total lead (Pb) in the waste stream being sent to landfills and waste treatment plants.[80] Common toxic heavy metals from electronic waste leaching solutions tend to be Cu, Fe, Al, Zn, Ni, Al, As, Cd, Cr, Pb. Obviously valuable commodities can also be found in electronic waste as they are major important components in electronic devices. This includes Au, Pt, Pd, Ru and Ag and thus many industrial operations are employed to purify them. In 2016

alone, 45 million tons of e-waste were generated and less than 20% went into a recycling scheme.[54] The projected worth of precious metals that year was estimated to be 67 billion U.S. dollars. Once again, It is no surprise that recent studies suggest that urban mining of metals from electronic waste is becoming more cost-effective than the virgin mining of ores (Figure 1.5).[74] Mining and mineral processing operations utilize these similar leaching techniques and as such discharge huge amounts of heavy and precious metals making their way into natural bodies of water located near the operations. Although valuable commodities are present in these sources it is difficult and energy intensive to separation for instance gold from light metals. New innovated technologies that can reduce energy costs for such separation processes will have a major impact on these industrial activities possibly influencing how metals are mined in the future.

1.4.6 Traditional Metal Recovery/Separation Methodologies

Currently to recover the precious metals from the waste or ore, many technologies employ conventional pyrometallurgical,[81] hydrometallurgical,[82] and biometallurgical[83] processing techniques. Emerging separation methods consists of electrochemical,[84] supercritical fluid,[85] mechanochemical,[86] and ionic liquids[87] processing technologies. Pyrometallurgical technology refers to treating various wastes under high-temperature conditions and recycling them via high-temperature chemical reactions. Currently, pyrometallurgy processing for precious metals recovery includes mainly high-temperature incineration, vacuum carbon thermal reduction and chlorination volatilization methods. Hydrometallurgical technology for valuable metal recovery consists of two main processes, namely dissolution and leaching of metals, and separation and purification of the metals. Aqua regia can effectively dissolve the metals in waste materials, but it produces toxic nitrogen oxide fumes. Cyanide leaching[88] has been used for over a century, due to the selectivity and stability of the precious metal complex. However, the high toxicity of cyanide may cause serious environmental and human safety problems. In recent years, some green leaching systems, with

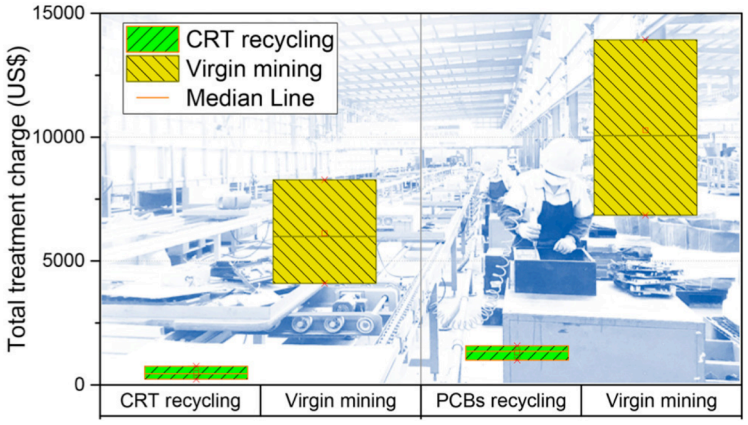

Figure 1.5. Chart indication that now it is more cost effective to urban mine than the virgin mining of ore.[23]

high leaching speed and high efficiency, have been proposed and have gained considerable progress, such as halide, thiourea, and thiosulfate leaching.

Methods include solvent extraction, adsorption on activated carbon, ion exchange, precipitation, cementation, and electrolysis have been developed. While pyrometallurgical and hydrometallurgical methods are efficient, they cause secondary pollution such as dioxin and furan emissions, and toxic wastewater generation. Thus biometallurgical technology has been developed as an alternative technique which includes two main approaches: bioleaching and biosorption. The biometallurgical process has the advantages of simplicity, strong maneuverability, low cost and little environmental pollution. However, most of the applications of biometallurgy for recovering valuable metals are still at the laboratory scale because of low leaching rates and long operating times. They also tend to deal with selectivity problems resulting in the fouling of the adsorbent compromising performance.

1.5 Trace Extraction of Metal Ions

The most significant challenge for these types of separations is the ability to extract and concentrate trace amounts of the desired metal ion from complex liquid solutions. Although matrix compositions vary, as aforementioned they usually contain high concentrations of inorganic species compared to the desired metal ion.[89-90] Such species are of the alkali and alkaline earth metals commonly Ca^{2+}, Na^{+}, Mg^{2+} and K^{+}. In addition to these inorganic species liquid sources, matrices also regularly contain a variety of organic species such large humin molecules.[91] These interferents alone already make the effective separation of these contaminants and commodities extremely difficult and they are virtually found in all matrices and are known to foul adsorbents compromising capture efficiency. Although employed industrially, this is the current limitation for state-of-the-art mesoporous materials such as the derivatives of activated carbon and silica.[92] As such, the major objective in the field is to design and develop porous materials that are tailor-made to selectively capture the desired metal ion, while inhibiting the capture of the aforementioned interferents simultaneously.[64] Further, for successful implementation in drinking water or wastewater treatment technologies, a material must not only be selective but must competitively have a high removal capacity, rapid rate of removal, long-term stability and is recyclable.[89] To design such material will require the knowledge and understanding of the speciation and properties of the desired metal ion, the understanding of the matrix composition and properties of a given matrix and most importantly creativity in adsorbent design.

1.6 Metal-organic Frameworks

1.6.1 Adsorption

Adsorption is the process in which an analyte is physically or chemically adhered to a given surface.[93] This type of separation is desirable in industry as the energy cost is significantly lower than other separation processes (Figure 1.6). An analyte whether in liquid, vapor or gas phase simply needs to be put into contact with the adsorbent and then will interact and adhere to the surface of the adsorbent usually without any input of extra external energy. This is the reason why it is the preferred method for metal ion capture as other methods such chemical precipitation, ion exchange, membranes, distillation and reverse osmosis have high economic and energy cost, low removal efficiency and produces high quantities of chemical sludge.[94] Thus, high porosity is one of the most sought properties in the discovery of new materials for adsorption separation processes. It offers quick diffusion and high adsorption capacities for targeted chemical species and in turn significantly reduces energy and operating costs. In the last century, a portfolio of diverse porous materials has been discovered and developed. Recently, in the last 20 years, a new class of hybrid inorganic-organic materials have been the forefront of material science making major contributions in gas/liquid separations, storage, catalysis and more niche applications such as drug delivery, sensors and devices. This class of materials is known as Metal-organic frameworks or MOFs.

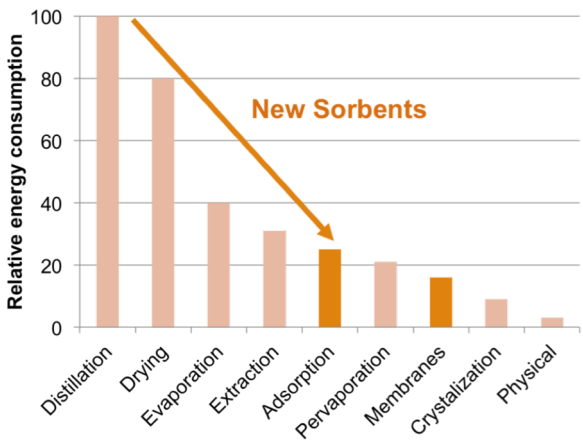

Figure 1.6. Comparing the energy consumption of different separation techniques used in industry.

1.6.2 History of MOFs

Metal–organic frameworks (MOFs) are a family of crystalline porous materials, which are assembled from metal ion/cluster connecting points and organic bridging ligands.[95-96] While today thousands of MOF structures have been developed,[97] the history of MOFs can trace back to the 1960s[98-99]. In 1990, Hoskins and Robson reported the design and construction of a new class of scaffolding-like materials comprising infinite polymeric frameworks of 3D-linked molecular rods.[100] They predicted that these materials with large empty cavities and low densities should be

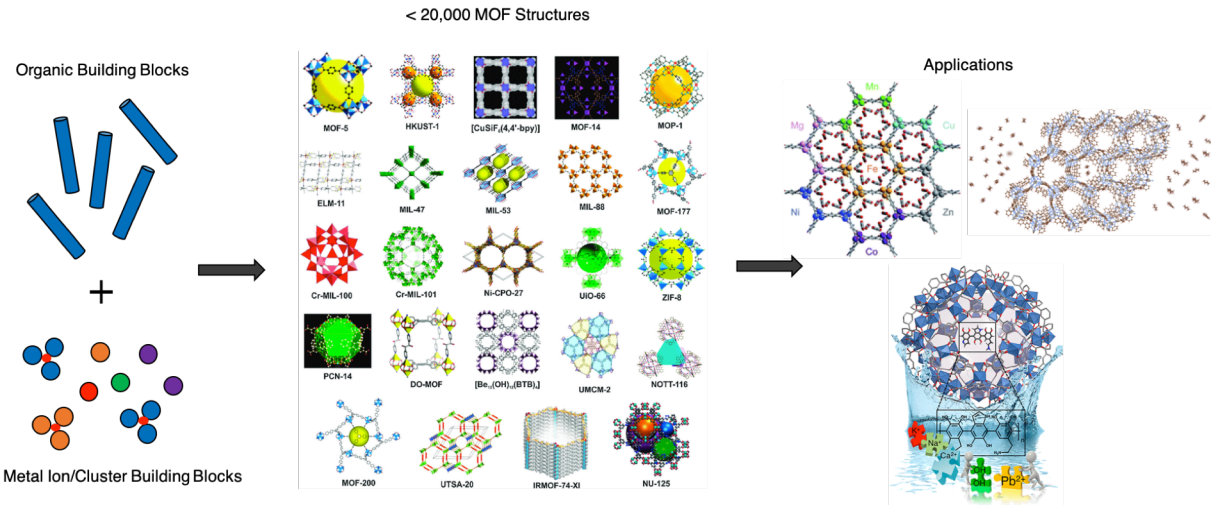

Figure 1.7. Representation of the building blocks used to make MOFs, the different common frameworks of MOFs and potential applications MOFs have been employed for.

accessible while maintaining high thermal, chemical, and mechanical stability. Five years later, Yaghi et al. synthesized a 3D crystalline and open material by hydrothermal route and for the first time the term metal–organic framework (MOF) was introduced.[101] Later in 1997, Kitagawa et al explored the application of MOFs for methane storage at high pressures.[102] Then, in 1998, Yaghi et al. for the first time demonstrated MOF-5 showed permanent porosity after guest solvent removal.[103] Since then the field of MOFs has grown rapidly and attracted immense attention due to the nearly endless structural possibilities for constructing different MOF materials. MOFs illustrate numerous unique characteristics such as highly accessible surface area, structural flexibility, tunable chemical structures, controllable synthesis, tunable pore size and surface functionality.[104] These advantages of MOFs promoted the study of these materials for various applications, including gas capture and separation, catalysis, sensing, imaging, drug delivery, light harvesting, ionic exchange, conductivity, water adsorption for heat transformation, sorption of toxic substances from air and water, etc.[105-110]

1.6.3 Synthesis of MOFs

To synthesize MOFs, principally the conditions of the method should facilitate the formation of the metal-ligand bonds at the same time allow these bonds to be broken and reformed for the structure propagation and high-order.[104] The conventional synthesis of MOF can be divided into two types: solvothermal and nonsolvothermal according to the reaction temperature. The solvothermal synthesis is the most common and straightforward method. Normally for this type of synthesis, the reaction is performed by mixing a metal salt with an organic linker in a high boiling point solvent usually taking place in closed vessels under autogenous pressure at relative high

temperature. While quite a lot of MOFs were synthesized using solvothermal methods, still some MOFs such as MOF-5, MOF-74, MOF-177, HKUST-1 or ZIF-8 could be obtained through the nonsolvothermal synthesis for which the reactions take place at the room temperature, relative low temperatures or even by mechanical stress.[111] Certainly the reaction temperature will have a strong influence on the morphology of the crystals, MOF formation time, thermal and chemical stabilities and so on. Apart from the reaction temperature, MOF synthesis is also very sensitive to other parameters such as reaction time, reaction pressure, solvent, and concentration of reactants, pH and property of the precursors. The variations of these parameters can affect both the topology, the crystal size and phase purity. To investigate the influence of these parameters on the formation of MOFs with a relative high efficiency, the high-throughput method is applied to accomplish this tedious work and to optimize syntheses procedures thus accelerate the discovery of new MOFs. However, this method does not shed any light on the reaction mechanism or the formation of intermediate phases. Thus, in situ and ex situ investigations under solvothermal conditions have been carried out.[112] These investigations allow the detection of crystalline intermediates, the assessment of individual reaction parameters, and formulating an idea about the crystallization mechanism thus optimize the synthesis conditions for new MOFs. It should be noted that not all MOF systems form in a similar manner. In other words, every system is different and insight on one system most likely will not give any insight in another system. Generalizing the crystallization of MOFs is extremely difficult and is still a major challenge in the field.

1.6.4 Post Synthetic Modifications of MOFs

Through direct synthesis mentioned as above, a large number of organic linkers and inorganic nodes that can be combined, could generate a portfolio of novel materials. However, post-synthetic modification (PSM) of MOFs allows for the systematically modifying the structure and offering functional highly porous materials that are not accessible from direct synthesis.[113] In a PSM, the reactant diffuses into the interior of the MOFs to react with either the ligand or the metal nodes while the connection and topology of the parent MOF is not altered after the reaction. This PSM approach can be used to modify the pores, surface, stability, hydrophobicity, sorption, catalysis properties, luminescence, and magnetism etc.[104] Firstly, through PSM it is possible to incorporate a more complex functional group that could restrict the formation of the MOF. Second, since the modification is performed directly on crystalline solids, the purification and isolation of the modified products are easy. Third, a given MOF structure can be modified with different reagents and thus generate a large number of topologically identical but functionally diverse

MOFs. Fourth, control over both the type of substituent and the degree of modification allows introduction of multiple functional units into a single framework. This allows scientists to tune and optimize the MOF properties. Until now many PSM approaches have been developed, which typically can be divided into non-covalent PSM, covalent PSM, tandem PSM, protonation, post-synthetic doping with metals or metal exchange, post-synthetic ligand exchange. There are also some new PSM reactions including post-synthetic installation, post-synthetic *in-situ* polymerization and post-synthetic oxidation, which broaden the concept of PSM.

1.6.5 Characterization of MOFs

To characterize the prepared MOFs, different techniques are involved, for instance, in the diverse fields of diffraction, adsorption, combustion, microscopy and spectroscopy. Single crystal X-ray diffraction (SXRD) is the best way to determine the structures of MOFs and powder X-ray or neutron diffraction (PXRD) is often used to determine bulk crystallinity of MOF samples. These characterization techniques establish crystallinity and phase purity of the porous material.[89] Gas adsorption/desorption isotherms are measured to confirm porosity and calculate surface area as well as MOF pore volumes and pore size distributions. Powder x-ray diffraction and porosity measurements are the two most important pieces of characterization data used to study and employ MOFs. You will find these techniques used in all MOF papers published in the literature. Other types of characterization techniques tend to be supplementary and can contribute to the understanding of the MOF system. For instance, thermogravimetric analysis (TGA) is the technique for determining the thermal stability of a MOF and in some cases to estimate the solvent-accessible pore volume. It can also give other indications such as if more organics are added to the system after modifying the framework post-synthetically. Scanning electron microscopy (SEM) and transmission electron microscopy (TEM) coupled with energy dispersive X-ray spectroscopy (EDS) are used to characterize the crystal size and morphology as well as the elemental composition and distribution. Inductively coupled plasma optical emission spectroscopy (ICP-OES) or mass spectrometry (ICP-MS) can be used to confirm purity or elemental ratios in a MOF sample after digestion in acid. Although more difficult, solid state nuclear magnetic resonance (NMR) spectroscopy can be used to determine MOF purity, quantifying linker ratios in mixed linker MOFs, and leftover modulator, as well as the absence of solvent after activation.[114] Diffuse reflectance infrared fourier transform spectroscopy (DRIFTS) is used to probe the presence or absence of IR active functional groups in a MOF in addition to more information about the behavior of MOFs interacting with specific gases (CO, CO_2, H_2 etc.) at different

temperatures.[115] For example, CO prefers to interact with unsaturated lewis acids that can be found along the pore surface of MOFs. Performing *in-situ* IR experiments with CO can tell if there are open metal sites present in the system as solvent removal and even give some information on the metal site's electronic environment.

Due to their huge porosity and pore geometry, MOFs have definitely been investigated for the capture of metal ions from water although less prominent than gas storage/separation or catalysis applications.[89-90, 116-117] The advantages of using MOFs as adsorbents for removal of metal ion from water are listed as follow: 1. MOF's are rigid structures with permanent porosity, which promote high performance. 2. The high surface area and porosity of MOFs provides a surface where there is a high density of active sites and thus benefit for improving metal uptake capacity. 3. The MOFs surface can be a platform to graft specific functional groups with free N, O, and S containing species such as thiol, amine, sulfur, nitro, carbonyl, and so on that can interact and grab the desired metal ion. These functional groups could be tuned to capture metal ions with high efficiency and selectivity. Though the advantages of MOFs as adsorbents for metal ions are appreciated, there are still some issues that need attention. First, the water stability is a basic and very important factor for MOFs, if to be applied for water purification. While some stable MOFs have been synthesized, most of MOFs are sensitive and unstable in water especially in a relatively large range of pH. Thus, it is imperative that MOFs with high water stability be chosen or where improvement of the water stability of some promising MOF candidates before use can be conducted. Second, devices for practical use that can keep or enhance performances are desirable. Though batch, filter column and membranes are three possible solutions, there still exist limitations on mass production and more should be investigated to make full use of MOFs scale up while retaining high quality. Third, MOFs if not incorporated into a membrane must be structured to reduce pressure drops along the column when performing continuous dynamic operations typically used in industry. The infinite SBUs and ligands that are used to construct highly porous rigid MOFs provides interesting chemistry that can be utilized to improve specific metal ion capture performance.

1.7 MOF/Polymer Composites

Polymers are materials consisting of one or multiple monomeric units that are chemically linked together. There is over a century of polymer chemistry research in the scientific literature[118]. This subdiscipline of chemistry has been the foundation of many major scientific breakthroughs leading to countless products we use in our everyday lives. The appeal to utilize such chemistry is the

tunability and design of monomeric units that when chemically linked together and repeated, lead to extraordinary properties such as high mechanical strength, elasticity or desired functionality. As such, there have been many efforts by organic chemists to construct interesting monomeric units for various applications. It is to no surprise that in the last decade, scientists have combined different polymers and the recently discovered highly porous MOFs together with the intent to intertwine their properties into one system. In fact, there are numerous combinations that can be explored if we consider the various MOFs and polymers present in the literature as building blocks. Combining the well-defined field of polymer chemistry with a new field focused on the most porous materials in the world will most certainly result in the discovery of interesting new properties for the many chemical separations performed today.

MOF/Polymer composites can be made in a variety ways. The easiest method is simply blending the fully synthesized polymer dissolved in a solvent with the MOF powder. By this method, typically the crystallites of the MOFs are embedded into the bulk polymer depending on the reaction conditions leaving the MOF's pores open and intact. There also have been reports that suggest some polymers are actually interpenetrating into the MOF pores[119]. But, the extent of how much of the polymer is interpenetrating into the MOFs is not quantified. Further the pore size and shape must be large enough for the polymer to diffuse through. Despite this, there have been reports clearly demonstrating an enhancement in performance for a variety of separations when MOF and polymers are incorporated together into a system. For example, mixing together the zirconium based MOF UiO-66 with an amine on its ligand (UiO-66-NH_2) with the polymer polysulfone into thin membranes promotes high CO_2 permeability[120]. When the MOF wt. % reaches above 30%, porous highways are formed through the membrane and it is thought that the amine functional groups speed up CO_2 through the membrane compared to other gases. Another example is a study incorporating an amine rich PEI polymer into MIL-101 Cr, a famous, stable and extremely porous telephthalate based MOF (> 4000 m^2/g) discovered by the late Gerald Ferey in 2005[97, 121]. In collaboration, Krista Walton, David Scholl and Christopher Jones illustrated that they could increase the specific binding energy of CO_2 at low pressures likely due to the increase in adsorption sites from the PEI. This is reflected in the higher uptake of CO_2 for the MIL-101-Cr/PEI composite compared to the bare framework at low pressures. These methodologies allows for the potential to employ tailor-made adsorbents in applications related to the capture of CO_2 from air to combat climate change.

Another methodology to construct MOF polymer composites can be done by diffusing monomers into the porous networks and using the surface chemistry to facilitate polymerization reactions. One of the first demonstrations of this methodology was by Kitagawa, where he and his team oxidatively polymerized pyrrole molecules between a 2-D layer open framework containing Fe^{3+} sites. The Fe^{3+} sites actually facilitate the *in-situ* polymerization reaction by taking electrons from the pyrrole molecules reducing it to the Fe^{2+} sites. The resulting polypyrrole can then be isolated from the 2-D framework now existing as stack sheets. This work demonstrated that redox reactions could occur on surfaces that contain metal sites. In the diverse field of MOFs, there are many structures that actually exhibit open metal sites, which can act as lewis acids. For instance, it is known that the MOF-74 family contain open metal sites when desolvated or activated in MOF terms[122]. It was then found that these open metal sites along the 1-D channel are the major adsorption sites for carbon dioxide[105] as Queen and Brown described. Further these metal sites in some cases are also known to participate in electron transfer events[122-123]. The interface between redox active monomers that can undergo oxidative/reductive polymerization and MOFs with these redox active sites along its pore surface and their superior porosity provide the perfect platform in the discovery of new porous composite materials for many chemical separations in air or water.

1.8 MOTIVATION AND OUTLINE OF THESIS

Research pertaining to metal ion separation in water is moving towards the forefront of material science and is becoming indisputably relevant for environmental and economic security. The motivation of this thesis is to design and construct novel porous composites made up of MOFs, which are some of the most porous and chemically interesting materials today and polymers, which are historically the most employed materials in the world, and unite both their exceptional properties into one system. The objective is then to employ and evaluate these new materials for the effective capture of different metal ions with a water and commodity purification relevance in mind. Further, the intention is to attempt to commercialize these materials. As such, although we demonstrate that different MOF frameworks can be employed in this platform, Fe-BTC, a MTN topology type framework was chosen as the main MOF building block in this thesis as it is quite porous (> 2000 m^2/g), has redox active metal sites to facilitate *in-situ* oxidative polymerization reactions and is made in water with cheap starting reagents (1.25 CHF per kg on the ton scale). Further, all polymerization reactions are done under mild conditions such as room temperature and in alcohols as the solvent media.

Each chapter provides the blueprints for the construction and characterization of different MOF/Polymer composites with a specific type of metal ion separation evaluated. Chapter 2 focuses on designing a material to decontaminate heavy metals from water. For the first time, dopamine is diffused into the Fe-BTC framework and undergoes spontaneously oxidative *in-situ* polymerization to polydopamine. This study not only illustrates the material's extraordinarily performance for rapid and selective Pb^{2+} and Hg^{2+} removal from water, but also provides a set of characterization techniques that together help fully understand these class of MOF/Polymer composites. Chapter 3 is built off the previous study, recognizing that Hg^{2+} undergoes a reduction event to Hg^{1+} when treated with Fe-BTC/PDA. Since Au^{3+} also has a higher reduction potential than Hg^{2+}, we surmised that we could develop materials to extract Au^{3+} ions from water. We report the synthesis and characterization of a number of new MOF/Polymer composites demonstrating monomer versatility and notably one of those materials, Fe-BTC/PpPDA is shown to have the ability to selectively, rapidly extract and concentrate trace amount of gold from any complex water mixture even the sea.

Last, chapter 4 introduces the design and construction of our Clean Water Initiative's first generation continuous flow through apparatus. For commercial feasibility, we must consider these materials in a continuous flow through operation primarily used in industry. This apparatus allows us to implement and evaluate some of the aforementioned materials into filter devices. Although preliminary results are shown, experiments are still underway to realize the most cost effective filter.

“Failure is instructive”

CHAPTER 2 - RAPID, SELECTIVE HEAVY METAL REMOVAL FROM WATER BY A MOF/POLYDOPAMINE COMPOSITE

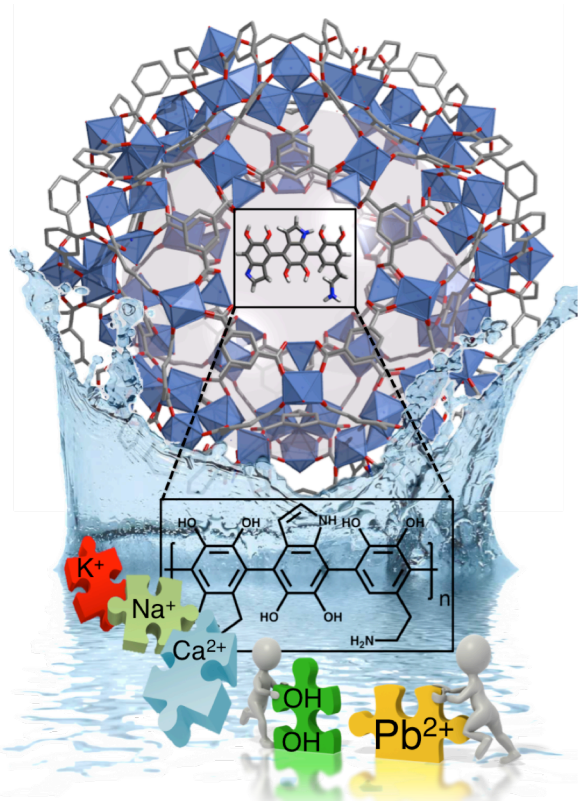

Drinking water contamination with heavy metals, particularly lead, is a persistent problem worldwide with grave public health consequences. Existing purification methods cannot often address this problem quickly and economically. Here we report a cheap, water stable metal-organic framework/polymer composite, Fe-BTC/PDA, that exhibits rapid, selective removal of high quantities of heavy metals, such as Pb^{2+} and Hg^{2+}, from real world water samples. In this work, Fe-BTC, is treated with dopamine, which undergoes spontaneous polymerization to polydopamine (PDA) within its pores via the Fe^{3+} open metal sites. The PDA, pinned on the internal MOF surface, gains extrinsic porosity resulting in a composite that binds up to 1634 mg Hg^{2+} and 394 mg Pb^{2+} per gram of composite and removes over 99.8 % of these ions from a 1 ppm solution, yielding drinkable levels in seconds. Further, the composite properties are well-maintained in river and sea water samples spiked with only trace amounts of lead, illustrating unprecedented selectivity. Remarkably, no significant uptake of competing metal ions is observed even when interferents, such as Na^{+}, are up to 14,000 times the concentration of Pb^{2+}. The material is further shown to be resistant to fouling when tested in high concentrations of common organic interferents, like humic acid, and is fully regenerable over many cycles.

This chapter is based on published work: *Sun et al. ACS Cent. Sci.* 2018, 4, 3, 349-356

2.1 Introduction

With an estimated 1 billion people without access to clean drinking water and 2 million casualties per year, water contamination is currently one of the world's leading causes of death[42]. This problem is only expected to worsen as the World Health Organization (WHO) estimates that climate change will limit access to clean water for as much as half of the world's population[124], and a recent United Nations report projects that the world could face a 40% water shortage in as few as 15 years[125]. A surge in energy production and an exponential increase in heavy metal use in industrial processes have caused a rise in human exposure to toxic heavy metals in recent decades[126]. The high toxicity and prevalence of cadmium, chromium, lead, arsenic, and mercury put them among the greatest concern. These metals, which play no role in human homeostasis, induce multiple organ damage, cause birth defects, and are classified carcinogens[126]. To maintain environmental and human well-being, it is imperative that we find new solutions for the cheap, energy efficient remediation of trace contaminants from water[127-128].

The high abundance of lead has steered its incorporation into a number of products such as pigments, paints, ceramic glazes, jewelry, toys, etc. Further, municipal drinking water in many countries is still delivered through lead pipes or pipes joined with lead solder. Consequently, aging infrastructure makes lead one of the most prominent metals seen in human exposure cases. Recently, the media has shown extensive lead exposure in several developed countries shedding light on our inability to rapidly clean contaminated water on large scales. Virginia Tech researchers uncovered extensive lead contamination in Flint, Michigan[46] and in December of 2016 a study by Reuters reported over 3000 areas in the US with poisoning rates twice that of Flint[129]. Unfortunately, exposure is even worse in underdeveloped countries where lack of resources and awareness limit the use of expensive industrial wastewater treatment processes[44-45]. Given these problems, the WHO has recently declared lead as 1 of 10 chemicals of major public health concern necessitating action by Member States to protect the population[130].

Commercial heavy metal remediation methods such as chemical precipitation, sorbents, and membranes have many disadvantages that include high economic and energy cost, low removal efficiency, difficult regeneration and/or fouling, and the production of high quantities of chemical sludge[127]. As a result, even well documented cases of contamination in developed countries are left without remediation. These inadequacies have sparked our interest in the exploration of inexpensive metal-organic frameworks (MOFs) for water purification. This class of porous materials has quickly moved to the forefront of materials research due to their unprecedented

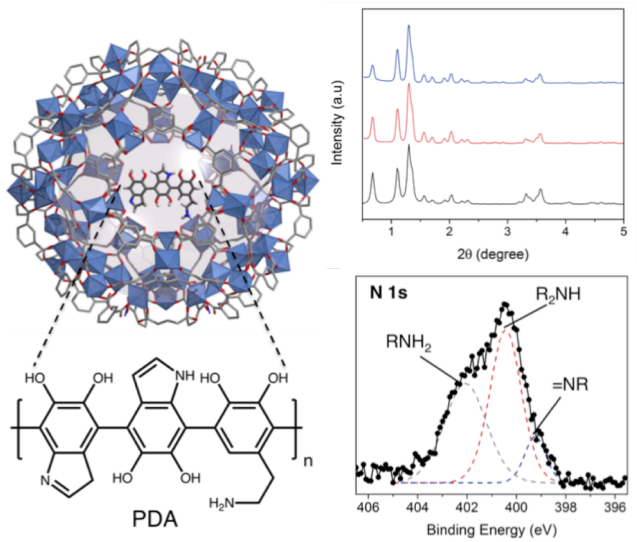

Figure 2.1 Characterization of Fe-BTC/PDA. (Left) Polyhedral view of a large cage in the Fe-BTC with PDA embedded inside the channels. The purple sphere represents void space inside of the cage prior to dopamine addition. (Top) The simulated XRD pattern of Fe-BTC (black) compared to synchrotron XRD data (λ = 0.50084 Å) of Fe-BTC (red) and Fe-BTC/PDA-19 (blue). (Bottom) X-ray photoelectron spectroscopy data obtained from the N1s spectrum of Fe-BTC/PDA-19.

internal surface areas, facile chemical tunability, and extraordinary capability to selectively adsorb large quantities of guest species[131-133]. The potential to deploy MOFs in water purification is related to the ease with which their internal surfaces can be post-synthetically decorated with high densities of strong adsorption sites[134-136]. Further, recent reports show that amorphous polymers with intrinsic porosity can compete in both rate and capacity with benchmark adsorbents for water treatment[137-139]. Therefore, we hypothesize that MOFs could be used to introduce extrinsic porosity to polymers comprised of high-densities of metal-scavenging functionality (Figure 2.1). In this work, a biologically[140] and environmentally friendly MOF, Fe-BTC (alternatively known as MIL-100; BTC=1,3,5-benzenetricaboxylate)[141-142], which features triangular Fe_3O clusters interlinked by BTC^{3-} ligands, is used as a porous template for the anaerobic polymerization of dopamine. Polydopamine (PDA) contains amine and catechol functionalities that are not only capable of scavenging metals, but also provide a pathway to adhere the polymer onto the internal MOF surface[143]. The latter inhibits the dispersion of the hydrophilic PDA into water and hence facile separation post-water treatment. The resulting composite combines high capacity, selectivity, and record-breaking removal rate of Pb^{2+} and Hg^{2+} ions, making it a highly promising material for decontamination of drinking water.

2.2 Results and Discussion

2.2.1 Design, Synthesis and Characterization

Fe-BTC, synthesized using known procedures[144], possesses empty mesoporous cages of 25 and 29 Å diameter that can be accessed *via* microporous windows of *ca.* 5.5 and 8.6 Å diameter, respectively. The resulting material has a BET surface area of 2324 m^2/g and open metal coordination sites (Appendix Figure 2.2), which can be used to append PDA on the internal MOF

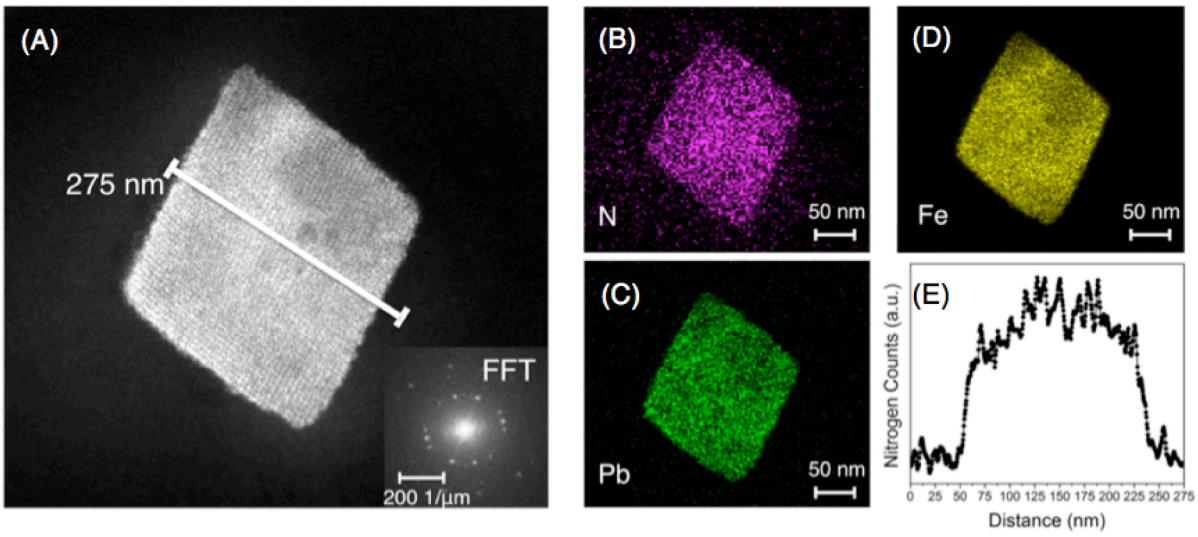

Figure 2.2. HAADF-STEM images. (A) HAADF-STEM image of a sliced single crystalline of Fe-BTC/PDA-19 and (B-D) corresponding EDX elemental mapping. (E) STEM-EDX line profile of nitrogen across the region indicated in (A). The line profile is 275 nm long and is integrated over 100 nm. Elemental mapping was done after the composite was soaked in a high concentrated aqueous solution of Pb^{2+}.

surface. Density functional theory (DFT) calculations were utilized to assess the feasibility of PDA binding to Fe^{3+} sites (Appendix Figure 2.10 and Table 2.2). The calculated relative binding energies indicate that the O and N containing functionalities on the polymer are expected to bind readily to the metal ion, implying that the polymer has a high affinity for the internal MOF surface.

The Fe-BTC/PDA composite is formed by mixing the desolvated MOF with dopamine (see methods). The redox active Fe^{3+} sites[145] are found to promote the anaerobic oxidation of dopamine to form PDA, which causes a color change in the MOF from light orange to dark purple. While the anaerobic oxidation of dopamine *via* Fe^{3+} has been previously reported, to the best of our knowledge it has not been carried out in a porous adsorbent[146]. The resulting composite is found to contain a modest loading of PDA, 19 mass % (denoted as Fe-BTC/PDA-19) via combustion analysis (Table 2.1) and exhibits a BET surface area of 1134 m^2/g, with no apparent loss in crystallinity (Figure 2.1). Fe-BTC/PDA stability was tested by soaking the material for up to two months in Rhone river water containing 0, 1, and 1000 ppm Pb^{2+}. No leaching of iron was observed per ICP-OES, which shows a concentration less than the detectable limit (<10 ppb). Also, after long term soaking there is no apparent trace of PDA found in the water samples via MALDI-TOF-MS experiments (Appendix Figure 2.3). Last, powder X-ray diffraction shows that the structural integrity of the MOF is maintained after the soaking process (Appendix Figure 2.3). Dopamine polymerization was evident by X-ray photoelectron spectroscopy (XPS). The N 1s

region of the spectrum was used to look for primary, secondary, and tertiary amines that are indicative of dopamine, polydopamine and its intermediates, and tautomers of the intermediates[147]. The presence of secondary and tertiary amines, which are not present in dopamine, are evidence for the indole formation, a signature of the polymerization process[147-148] (Figure 2.1). To give further evidence of the polymerization, the composite was soaked in a 4M HCl solution as an attempt to partially destroy the porous template, and MALDI-TOF-MS spectra show proof of PDA in solution consisting up to 7-monomeric units (Appendix Figure 2.6). Scanning electron microscopy (SEM) reveals no polymer formation on the crystal facets (Appendix Figure 2.7). In order to test conclusively whether the polymer is distributed throughout the MOF, Fe-BTC/PDA-19 was embedded in an epoxy resin and serially sectioned in 100 nm thick slices using an ultramicrotome. Energy dispersive X-ray spectroscopy (EDX) analysis in a scanning transmission electron microscope (STEM) provided evidence that nitrogen, a signature of the polymer, is indeed located throughout the MOF crystal (Figure 2.2 and Appendix Figure 2.8). The result was further confirmed by STEM electron energy loss spectroscopy (EELS) (Appendix Figure 2.9). Attenuated total reflectance infrared (ATR-IR) and Raman spectroscopies were used to provide evidence that the polymer is interacting with open Fe^{3+} sites of the MOF (Appendix Figure 2.11). IR data obtained from PDA nanospheres reveals a peak at ~1506 cm^{-1}, which has previously been assigned to an indoline stretching vibration[149-150]. For Fe-BTC/PDA, this peak is instead split into two bands occurring at ~1482 cm^{-1} and ~1556 cm^{-1}, a signature of the formation of an Fe^{3+}-PDA complex[149-150]. Further, when compared to Fe-BTC, the Raman spectrum obtained from Fe-BTC/PDA, shows a new peak at ~642 cm^{-1}, which previous reports attribute to stretching modes of Fe^{3+}-catecholate complexes[151]. These results, which also coincide with the aforementioned DFT calculations, indicate that PDA is indeed pinned to the MOF's pore surface through the Fe^{3+} open metal sites.

2.2.2 Heavy Metal Extraction from Water

The accessibility of metal-scavenging catechols within the pores of Fe-BTC/PDA-19, as indicated by a positive Prussian blue test (Appendix Figure 2.12) spurred the exploration of the composite for water treatment. Fe-BTC and Fe-BTC/PDA-19 were soaked in distilled water containing 1 ppm of As^{3+}, Cd^{2+}, Cr^{6+}, Hg^{2+} or Pb^{2+} (Figure 2.3 and Appendix Figure 2.13). When compared to Fe-BTC, the composite material significantly enhances the removal of all metals excluding Cr^{6+}. The removal capacities of As^{3+}, Cd^{2+}, Pb^{2+}, and Hg^{2+} were improved by factors of 6.1, 6.1, 92, and 60, respectively. Additionally, the composite reduced the concentrations of both Pb^{2+} and Hg^{2+} below

what is deemed drinkable by the U.S. Environmental Protection Agency (EPA, < 15 ppb for Pb^{2+} and < 2ppb for Hg^{2+})[33]. As such, Pb^{2+} and Hg^{2+} extraction were explored for the remainder of the study.

The high performance observed for Fe-BTC/PDA-19 prompted us to determine the effect of polymer loading on the composite's removal capacity. Fe-BTC was loaded with 28, 38, and 42 mass % PDA resulting in BET surface areas of 757, 488 and 165 m^2/g, respectively (Figure 2.4 and Appendix Table 2.1). The composites were then used to treat Rhone river water spiked with 1000 ppm Hg^{2+} (Figure 2.4). Removal capacities up to 1634 mg Hg^{2+} per gram of composite were observed for Fe-BTC/PDA-42, almost 10 times that observed for the unmodified Fe-BTC. For Pb^{2+}, the trend is similar (Figure 2.4) with removal capacities up to 394 mg per gram of composite, 2.6 times the capacity of unmodified Fe-BTC. Given the enhanced performance of the composite compared to the MOF, we establish that the high density of heavy metal scavenging groups on the polymer backbone is the fundamental contributor to the high removal capacities. Several other parameters such as selectivity, removal rate, and resistance to organic interferents were also tested for Fe-BTC/PDA-42. Other than higher capacities, this material shows similar performance to Fe-BTC/PDA-19. As such, the composite with the 19 mass % loading is the material discussed throughout this work, because it was the most extensively studied.

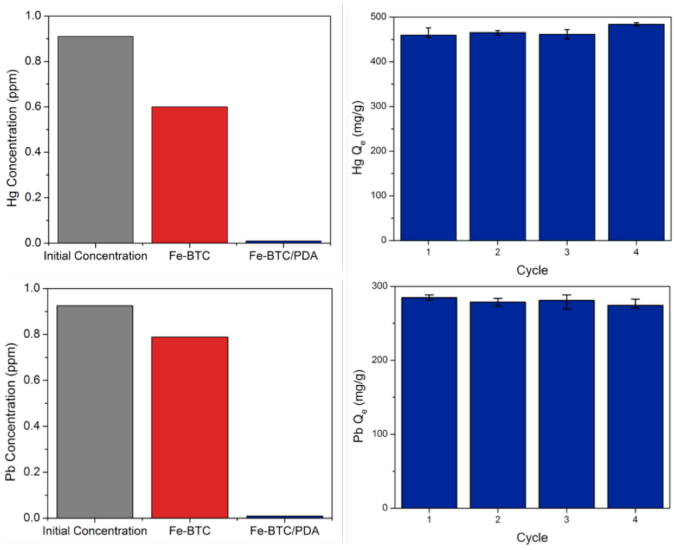

Figure 2.3. Evaluation of Heavy Metal Remediation. Concentration of (Top, left) Hg^{2+} and (Bottom, left) Pb^{2+} in distilled water before treatment and after treatment with Fe-BTC or Fe-BTC/PDA-19, respectively. Uptake capacity of Fe-BTC/PDA-19 after saturation and regeneration cycles using (Top, right) Hg^{2+} (with regeneration via ascorbic acid) and (Bottom, right) Pb^{2+} (with regeneration via ethylenediaminetetraacetic acid (EDTA)).

Efforts were also made to demonstrate the structural tunability of these novel MOF/polymer composites. For this, many dfferent redox active polymers, containing –OH, –SH, and $–NH_2$ metal scavenging functionality, were loaded into two MOF templates, including Fe-BTC and Cu-TDPAT[34] (TDPAT = 2,4,6-tris(3,5-dicarboxylphenylamino)-1,3,5-triazine). It can be seen in Appendix Figure 2.24 and Table 2.6 that these materials, not only readily form, but also offer fast

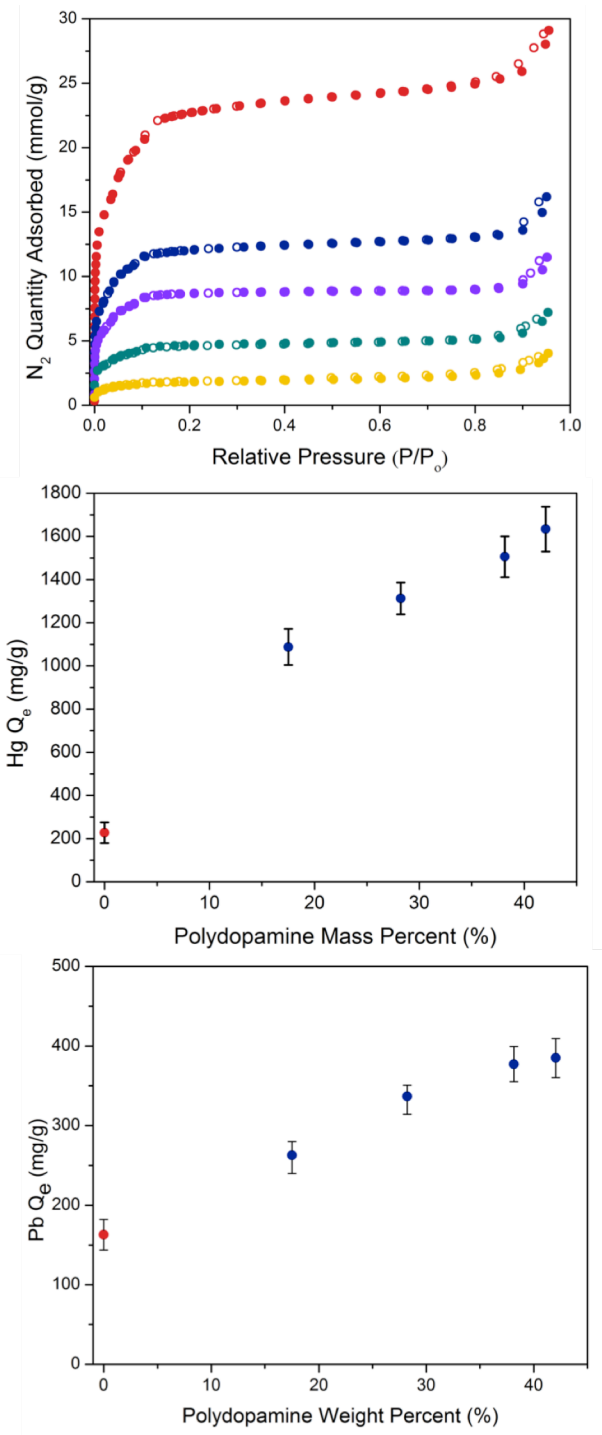

Figure 2.4. Tuning Composite Removal Capacity. (Top) N_2 adsorption and desorption isotherms for Fe-BTC (red) and several Fe-BTC/PDA composites with 19 (blue), 28 (purple), 38 (cyan) and 42 (yellow) mass % loading of PDA. The polydopamine loading level provides tunability of the (Middle) Hg^{2+} and (Bottom) Pb^{2+} removal capacity.

Pb^{2+} removal rates, and into the drinkable regime as observed for Fe-BTC/PDA. Studies intended to demonstrate the use of these materials for the extraction of many other analytes from water and air are currently underway.

To date, there is an increasing number of studies assessing heavy metal uptake in porous adsorbents[19, 35-38]. Throughout the literature these materials are typically assessd based on a metric known as the calculated distribution coefficient, k_d (Appendix Figure 2.16), which reflects a material's affinity to heavy metals. The consensus is that k_d values higher than 1.0×10^4 mL/g are considered to be excellent. The k_d values of Fe-BTC/PDA, 5.5×10^6 mL/g and 1.7×10^6 mL/g for Hg^{2+} and Pb^{2+}, respectively, are among the highest reported, particularly for lead (Appendix Figure 2.14). To date, only two studies report materials with lead k_d values that are higher than Fe-BTC/PDA, which are a MOF containing Zn paddlewheels (known as Zn_3L_3(BPE)1.5, $k_d = 2.3 \times 10^6$)[39] and a Ni/Cr layered double hydroxide (known as DPA-LDH, $k_d = 1.99 \times 10^8$)[40]. While the k_d is a sufficient measure for a quick initial comparison of materials, it is seen that these materials suffer from long equilibration times (30 to 60 minutes)[41,42] and loss in capacity with regeneration[152]. As such, we have provided an extensive comparison of Fe-BTC/PDA to the best performing materials reported to date in Appendix Table 2.4 and 2.5. It should be noted that successful implementation of a material in

drinking water or wastewater treatment technologies require full evaluation of long-term stability, cost-effectiveness, ability to resist clogging from large organic interferents, recyclability, rate of removal and selectivity over common inorganic interferents. Fe-BTC/PDA is found to perform well in all aforementioned arenas.

Most current adsorbent technologies for water purification, such as activated carbon and functionalized silica, are mesoporous, (2 nm - 50 nm in size) allowing large organic molecules to diffuse inside. This process often fouls adsorbents, compromising removal capacity[39,40]. Given this, the composite's susceptibility to a common large organic interferent, humic acid, was tested. Fe-BTC/PDA-19 was used to treat solutions with and without humic acid (100 ppm of humic acid and Hg^{2+} and Pb^{2+} concentrations ranging from 200 to 900 ppm) (Appendix Figure 2.17). The composite indeed maintains capacities in the presence of humic acid, likely due to Fe-BTC's unique architecture. The small pore apertures, 5.5 and 8.6 Å, act as gateways into the mesoporous cages, preventing large organic molecules from diffusing into the MOF, while still allowing metal ions to diffuse through.

Since the composite's heavy metal uptake shows a clear pH dependence (Appendix Figure 2.18), the material's reversibility was probed using ascorbic acid and ethylenediaminetetraacetic acid (EDTA). The composite material was first saturated with Pb^{2+} or Hg^{2+} and then treated in the aforementioned additives for 4 hours, followed by a subsequent assessment of the composite capacity. For both Pb^{2+} and Hg^{2+}, the composite shows minimal change in capacity over a total of 4 cycles after saturation and regeneration (Figure 2.3 and Appendix Figure 2.19). While adsorbed Pb^{2+} can be separated completely from the composite, the Hg^{2+} precipitates as solid Hg_2Cl_2, evident by PXRD and XPS (Appendix Figure 2.20-21 and Table S3). However, the solid appears to precipitate outside of the framework leaving the regenerated catechols open for continued reduction/precipitation cycles with Hg^{2+}. We surmise that the catechols on the PDA are likely oxidized to the quinone form, as indicated by a negative Prussian blue test (Appendix Figure 2.12), when reducing Hg^{2+} to Hg^{1+}. This observation is consistent with PDA's known ability to reduce several noble metals such as Au^{3+}, Ag^{1+} and Pt^{3+},[148]. The composites' high capacity and reusability provides an extended lifetime that is needed for long-term use in water purification applications.

The metal ion extraction rates of Fe-BTC and Fe-BTC/PDA-19 were determined from distilled water samples spiked with 1000 ppb Pb^{2+} and Hg^{2+}. We observed that unmodified Fe-BTC reaches a maximum of 18 % heavy metal removal (Figure 2.5) within a minute. Remarkably, when the solutions were treated with the composite, extremely rapid removal and high uptake are recognized. In under a minute, over 99.8 % removal of Hg^{2+} and Pb^{2+} is achieved reducing the concentrations from 1000 ppb to 1.2 ppb and 1.6 ppb, respectively. These values are below the allowable EPA and WHO limits for drinking water. To the best of our knowledge, this composite is the fastest material for the reduction of Hg^{2+} and Pb^{2+} to drinkable concentrations under soaking conditions. The composite achieves impressive uptake capacity without detriment to the fast removal rate observed for the bare Fe-BTC framework. We surmise that this behavior is due to the introduction of extrinsic porosity to the PDA by the MOF template. This phenomenon enhances the heavy metal removal rate and capacity compared to nonporous PDA[153-154]. It should be noted that *Ahmed et al* recently reported a nanoselenium sponge that also removes Hg^{2+} in seconds[43]. However, they use 30 times more material and while the nanoselenium sponge does irreversibly bind mercury allowing for easy disposal if used for in home treatment,[44,45] this characteristic might limit its use in wastewater treatment. For Pb^{2+}, the fastest material observed to date is a porous polymer, mPMF (mesoporous poly-melamine-formaldehyde), that reportedly gets below the EPA limit also in seconds; however, the capacity for this material is extremely low, 0.628 mg Pb^{2+}/g requiring large amounts of sorbent to achieve the same performance as Fe-BTC/PDA (Appendix Table 2.4)[46].

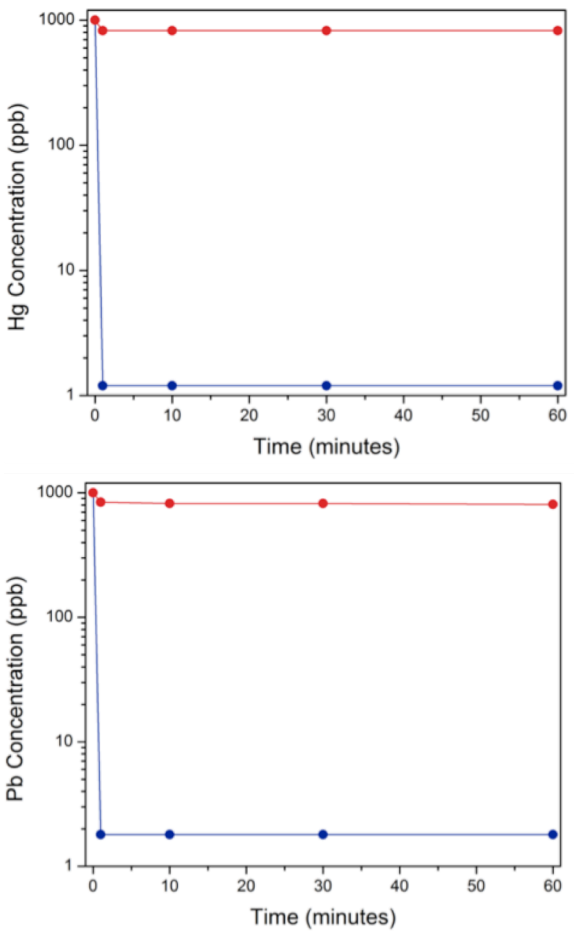

Figure 2.5. Metal ion concentrations after treatment of water spiked with 1 ppm of (Top) Hg^{2+} and (Bottom) Pb^{2+} with Fe-BTC/PDA-19 (blue) or Fe-BTC (red) at different time points.

Selectivity over common organics or inorganics, such as Ca^{2+}, Mg^{2+}, Na^{+}, K^{+} found at high concentrations in waste water or surface water samples, respectively, is the most important factor when evaluating a porous material for water treatment applications. While ions can compete for binding sites, organics can complex metals in solution or block the pores of the adsorbent entirely compromising capacity and/or removal rate. Given this, Fe-BTC/PDA-19 was first tested in Rhone River samples spiked with high concentrations of Hg^{2+} and Pb^{2+}, up to 1000 ppm. (Appendix Figure 2.15). Fe-BTC/PDA's capacities are either increased (for Hg^{2+}) or well maintained (for Pb^{2+}) in the river water, implying the interferents commonly found in surface waters have a minimal effect on composite performance.

The material's ability to competitively maintain efficiencies and rapid extraction rates at sub ppm levels, more typical of exposure cases, is highly desirable[155]. As such, Rhone River and Mediterranean Sea water were first spiked with 850 and 1050 ppb Pb^{2+}, respectively. The concentrations of the ions in the solutions were analyzed before and after treatment with Fe-BTC/PDA-19 (Figure 2.6). The composite is shown to remove over 99.7% of Pb^{2+} from Rhone river water bringing lead concentrations to 2.2 ppb and in the drinkable regime. For the seawater, the final Pb^{2+} concentrations could not be assessed by ICP-MS due to large amounts of Na^{+}; however, the levels are below the detectable limit of the ICP-OES (10 ppb) and hence also in the drinkable regime. Remarkably, within error of the experiment, we see no uptake of any metal ions observed in the two water samples, where interferents such as Na^{+} are up to 14,000 times the

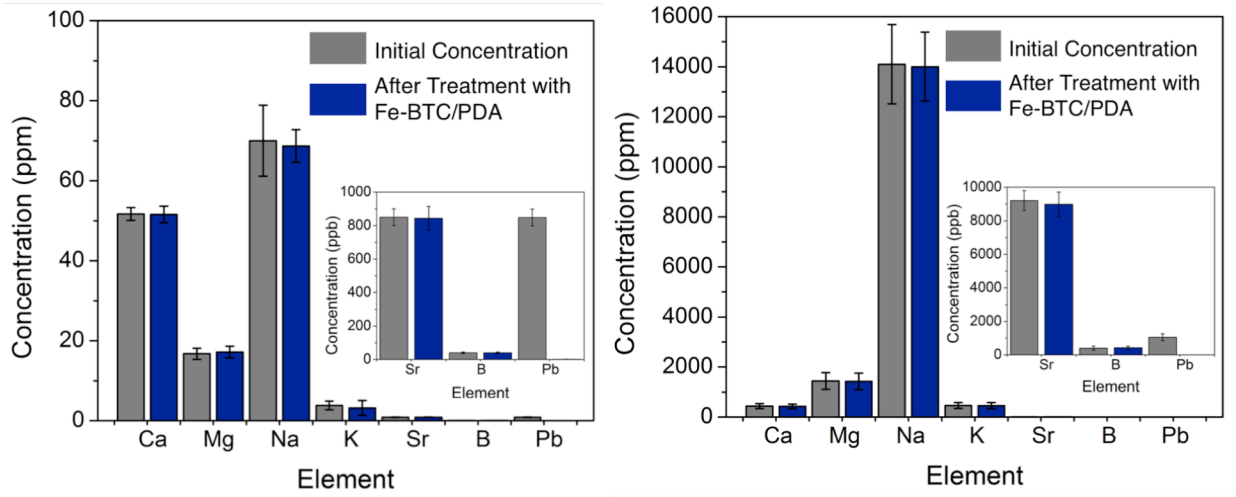

Figure 2.6. Compositions of Real World Samples. (left) Rhone River Water and (right) Mediterranean Sea water were spiked with ~1 ppm of Pb^{2+} and then subsequently treated with Fe-BTC/PDA-19. The concentrations of ions before and after treatment are denoted as grey and blue, respectively.

concentration of Pb^{2+} (Figure 2.6). A similar experiment carried out with 860 ppb Hg^{2+} in Rhone river water reveals final levels of 8 ppb, a value only slightly above the level deemed drinkable (<2 ppb) and an excellent removal efficiency of ~99%. It should be noted that all tests performed in Mediterranean Sea water spiked with Hg^{2+} indicate some competitive interference with removal efficiencies slightly reduced to ~90%. Last, the extraction rates of Pb^{2+} and Hg^{2+} were examined between 1 to 60 minutes in both surface water samples; in all cases the equilibrium is reached in under a minute (Appendix Figure 2.22), implying that the removal rates are not affected by inorganic or organic interferents found in river or seawater samples. To date, we have found no materials in the literature with comparable selectivities or rate for the separation of trace contaminants from real world water samples.

Compared to surface water samples, wastewater is often comprised of fewer competing ions but significantly higher concentrations of organics. Because these organics can readily complex Pb^{2+} ions in solution, we tested the materials performance in a wastewater sample collected from a treatment plant in Switzerland. Given the minimal amount of lead present in the influent stream, the water was spiked with approximately 700 ppb Pb^{2+}. The composite is able to reduce concentrations to drinkable levels, approximately 2 ppb; however, the extraction rate is slowed slightly compared to the surface water samples as expected with high levels of lead complexation. Approximately, 70% removal is observed in the first minute, 90 % is achieved within the first hour, and up to 99.8% is observed in 24 hours. To our knowledge, there are no current studies that evaluate the impact of metal speciation on materials performance in wastewater, and hence is an area we will be required to study for future implementation.

2.3 Conclusion

Fe-BTC/PDA is a novel MOF-polymer composite that has demonstrated the ability to extract large quantities of Pb^{2+} and Hg^{2+} from real-world water samples with unprecedented selectivity and rate. The resulting composite promotes the reduction of trace concentrations of Pb^{2+} ions to drinkable levels in under one minute, even in seawater where interferent concentrations are up to 14,000 times that of Pb^{2+}. These observed properties are derived from introducing extrinsic porosity to an intrinsically non-porous polymer pinned inside of a MOF template. The nanoporous windows of the template not only inhibit leaching of the hydrophilic polymer into the water enabling easy separation and consistent performance with cycling, but they also inhibit the diffusion of large organic interferents into the composite, a phenomenon known to foul most mesoporous adsorbents. Given the demonstrated easy tunability, regeneration, and separation combined with

low-cost, long term stability, and high performance in application relevant conditions, this new material could become highly influential for in-home or waste water treatment technologies, particularly in the event of an impending water crisis. It is envisioned that through judicious selection of MOF and polymer building blocks, this new platform technology could be used to selectively target a wide array of trace contaminates from water and aerial media. Understanding and controlling the properties of highly porous, redox active composites like Fe-BTC/PDA will unlock new useful properties for a variety of applications in host-guest chemistry.

2.4 Synthetic Methods and Procedures

Synthesis of Fe-BTC. Iron(III) chloride hexahydrate (97%) was bought from Alfa Aesar and 1,3,5-benzenetricarboxylic acid (trimesic acid, 98%) was bought from ABCR GmbH and used without further purification. All other metal salts and chemicals were bought from Sigma Aldrich and used without further purification. Fe-BTC[142] was prepared using the following synthetic procedure: 9.72 g of iron(III) chloride hexahydrate, 3.36 g of trimesic acid and 120 mL of distilled water were loaded in a 180 mL Teflon autoclave. The reaction mixture was heated to 130 °C for 72 hours. After the reaction was cooled down to room temperature the orange solid was filtered under vacuum and washed with copious amounts of water and methanol. The resulting powder was loaded into a double thickness whatman cellulose extraction thimble and underwent soxhlet purification with methanol for 24 hours. After solvent exchange, the sample was dried under vacuum overnight. The material was activated under vacuum at 150 °C for 17 hours before nitrogen adsorption and standard characterization.

Elemental Analysis Fe-BTC: C 34.65 % H 2.85 % Fe 21.84 % and yield = 4.2 grams

Free Base Dopamine Synthesis. Dopamine HCl, dry sodium hydride 95% and anhydrous solvents were bought from Sigma Aldrich and used without further purification. In a N_2 purged, a 2-neck round bottom flask was charged with 10 g of Dopamine HCl mixed in 80 mL of anhydrous tetrahydrofuran (THF) and 80 mL of anhydrous methanol. 1.264 g of dry sodium hydride 95% was added slowly in small quantities over a period of approximately 15 minutes. The reaction mixture was allowed to stir for 48 hours under flowing N_2. After the completion of the reaction, the mixture was filtered under vacuum and washed with copious amounts of THF. The white powder was dried and kept under vacuum until further use (Supplementary Fig. S1). ^{1}H NMR (400 MHz, Methanol-d_4): δ = 6.72 (d, J = 8.0 Hz, 1H), 6.67 (d, J = 2.1 Hz, 1H), 6.55 (dd, J = 8.0, 2.1 Hz, 1H), 2.87 (t, J = 7.1 Hz, 2H), 2.65 (t, J = 7.1 Hz, 2H).

Fe-BTC/PDA-19 Synthesis. 2 g of Fe-BTC was activated at 150 °C under vacuum overnight in a 500 mL 2-neck round bottom flask using a schlenk line and an oil pump. After activation, the reaction vessel was cooled to room temperature and then N_2 was flowed over the sample for 10 minutes. Afterwards, the sample was sealed under an inert atmosphere. Then 400 mL 0.02 M anhydrous methanol solution containing the as-prepared free base dopamine, was prepared in a glove box purged with N_2. Using a steel cannula and N_2, the methanol/dopamine solution was transferred to the flask containing the activated Fe-BTC. Over a period of 1 hour, the orange powder turned dark purple indicative of polymerization. The reaction was allowed to stir for 24 hours at room temperature under an inert atmosphere. After completion, the reaction mixture was filtered under vacuum and washed with copious amounts of methanol and water. To remove any excess dopamine, the resulting purple powder was loaded into a double thickness Whatman cellulose extraction thimble, and the composite underwent soxhlet extraction with methanol for 24 hours under N_2. Afterwards, the sample was dried under vacuum at room temperature over night, and then the material was activated under vacuum at 125 °C for 17 hours before nitrogen adsorption and standard characterization was carried out.

Elemental Analysis Fe-BTC/PDA-19: C 39.553% N 1.81% H 2.45% Fe 17.84%

It should be noted that several samples were prepped with various loadings of dopamine. The amount of dopamine loaded into the MOF was altered by varying the concentration of free dopamine in methanol before its addition to an activated Fe-BTC sample. Five Fe-BTC/PDA samples were prepped including, Fe-BTC/PDA-19, Fe-BTC/PDA-28, Fe-BTC/PDA-38 and Fe-BTC/PDA-42. The dopamine concentrations in 400mL of methanol were varied from 12 mM, 24 mM, 36 mM and 47 mM, respectively.

“There’s a thousand ways to be successful and there’s a thousand ways to fail”

CHAPTER 3 - RAPID, SELECTIVE EXTRACTION OF TRACE AMOUNTS OF GOLD FROM COMPLEX WATER MIXTURES WITH A MOF/POLYMER COMPOSITE

With the ever-increasing production of electronics, there is an ensuing need for gold extraction from sources other than virgin mines. Currently, there are no technologies reported to date that can effectively and selectively concentrate ultra-trace amounts of gold from liquid sources. Here, we provide a blueprint for the design of several highly porous composites made up of a metal-organic framework (MOF) template and redox active, polymeric building blocks. One such composite, Fe-BTC/PpPDA, is shown to rapidly extract trace amounts of gold from several complex water mixtures that include waste water, fresh water, ocean water, and solutions used to leach gold from electronic waste and sewage sludge ash. The material has an exceptional removal capacity, 934 mg gold / g of composite, and extracts gold from these complex mixtures at record-breaking rates, in as little as two minutes. Further, due to the high cyclability, we demonstrate that the composite can effectively concentrate gold and yield purities of 23.9 K.

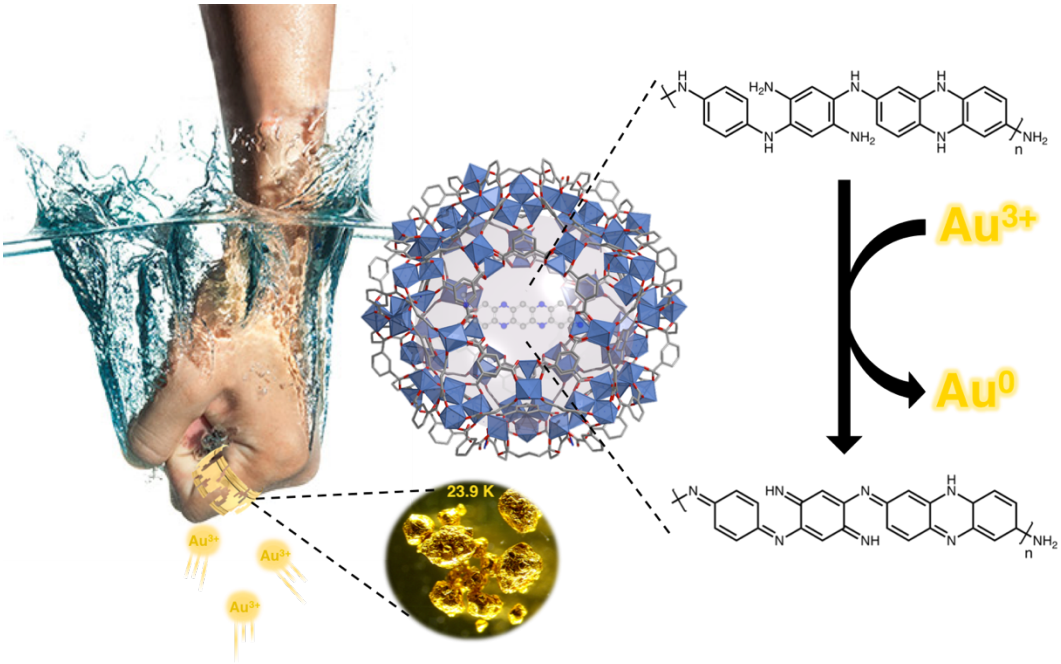

This chapter is based on published work: *Sun et al. J. Am. Chem. Soc.* 2018, 140, 48, 16697-16703

3.1 Introduction

Gold has a high value that stems from its rarity[156]. To date only 190,000 tons have been mined, an amount that readily fits into a box with dimensions of ~20 m on each side[157]. Gold, which is primarily employed in electronics, is irreplaceable due to high electrical conductivity and corrosion resistance. However, limited diminishing supplies and an incessant rise in electronics production have led organizations like the European Union to label this precious metal as a critical resource[158]. When considering as much as a ton of ore is required to mine enough gold for the production of ~40 mobile phones[159], it is no surprise that recent studies suggest that urban mining of metals from electronic waste (e-waste) is becoming more cost effective than the virgin mining of ores[23]. In 2016 alone, 45 million tons of e-waste were generated, and less than 20% went into a recycling scheme. The projected worth of gold in e-waste is ~10 billion euros[54]. Further, with increasing incomes and cheaper electronics the amount of e-waste will certainly soar; current projections estimate a 16% rise before 2021[160].

In addition to ore and e-waste, trace quantities of gold are found in freshwater, seawater, incinerated sludge and the effluent water of treatment plants[161-163]. For instance, ~1.5 million euros of gold go into the Swiss sewage annually[164], and even higher quantities of gold were recently reported in UK sewages[165]. While many scientists question the economic viability of gold extraction from such sources, this doubt stems from the absence of an adequate separation technology able to efficiently concentrate the precious metal while in the presence of large quantities of interferents. For example, in wastewater or freshwater, gold is typically below 10 μg per liter, requiring over 100,000 liters to recover a single gram. This problem is even more difficult when considering seawater sources, where gold concentrations are in the low ppt regime. Despite over 20 million tons of gold in our oceans[166-168], this number is miniscule when compared to the quantity of other competing metal ions. New innovative technologies able to concentrate and recover this commodity are essential for a sustainable future[169]. To the best or our knowledge, there are no materials reported to date that have demonstrated the ability to rapidly extract and concentrate trace amounts of gold (<100 ppb) from such complex solutions. These inadequacies sparked our interest to test metal-organic framework (MOF)/polymer composites for the extraction of gold from these aforementioned sources.

MOFs, a class of porous, crystalline materials, have quickly moved to the forefront of material science due to unprecedented internal surface areas[170], easy chemical tunability[171-172], and extraordinary ability to selectively adsorb large quantities of guests[173-175]. Further, their internal

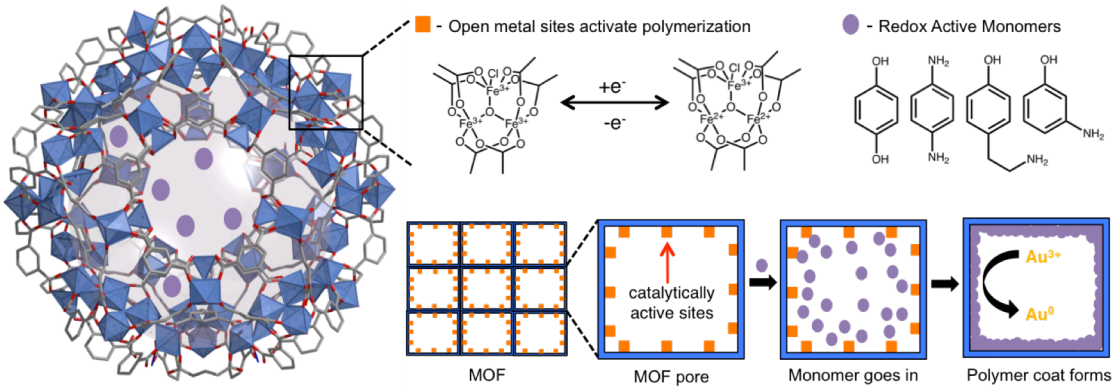

Figure 3.1. Blueprint for the design of novel, redox active composites. (left) A polyhedral view of the large cage found in Fe-BTC. (right) Monomers diffuse into the porous network containing open Fe^{3+} metal sites, which are reduced to Fe^{2+} catalyzing the polymerization process in the MOF pores.

surfaces can be post-synthetically decorated with high densities of strong adsorption sites[136, 176-177]. In our previous work, we used a MOF, Fe-BTC (BTC - 1,3,5-benzenetricarboxylate), as a porous template to introduce extrinsic porosity to an otherwise non-porous polymer, polydopamine[178]. This templation method provides accessibility to the metal extracting functionality on the polymer backbone, lending to exceptional capacities and record-breaking extraction rates of heavy metals, such as Pb^{2+} and Hg^{2+}, from fresh water, sea water, and waste water. Given the observed reduction of Hg^{2+} to Hg^{1+}, it was hypothesized that similar redox-active MOF/polymer composites could be used to rapidly extract precious metals, such as Au^{3+}, from complex mixtures. Here we report a series of new, redox active composites, Fe-BTC/PHQ (PHQ – polyhydroquinone), Fe-BTC/PpPDA (PpPDA – poly-para-phenylenediamine), Fe-BTC/PTA (PTA – polytyramine), Fe-BTC/PmAP (PmAP – poly-meta-aminophenol) and demonstrate their activity in gold extraction. The best performing composite, Fe-BTC/PpPDA, was employed to extract gold from several complex solutions including river, sea, and wastewater as well as solutions obtained from e-waste and sewage ash. The composite has outstanding removal capacities, record-breaking rates, and is regenerable allowing gold concentration with cycling. In a solution of simulated e-waste, the extracted gold is 23.9 K.

3.2 Results and Discussion

3.2.1 Design, Synthesis and Characterization

In this work, Fe-BTC is employed as a template[178], because it is scalable and made from cheap biologically and environmentally benign building blocks[140]. Further, it offers high internal surface

areas (2056 m^2/g) and accessible Fe^{3+} sites (Appendix Figure 3.1). The latter promotes the anaerobic oxidation of guest species for their polymerization inside the MOF pore[142, 145] and can subsequently anchor the polymer inside the MOF. The latter inhibits leaching during metal extraction. Fe-BTC, composed of Fe_3O clusters interlinked by BTC^{3-} ligands, has a porous MTN topology with apertures of 0.5 and 0.8 nm that lead into mesoporous pore cages that are 2.5 and 2.9 nm in diameter. While small analytes can diffuse inside, the unique architecture inhibits large intereferents, such as humic acid, from entering, eliminating the fouling observed for most mesoporous adsorbents[91]. The monomers, including hydroquinone, *p*-phenylenediamine, tyramine or *m*-aminophenol, were selected because they can readily diffuse into the pores of Fe-BTC. Further, they contain chemical moieties, such as amine ($-NH_2$) or hydroxyl (-OH) groups that undergo oxidative transformations, promoting the formation of the redox active polymers (Figure 3.1). It is thought that the polymerization process entails the reduction of Fe^{3+} to Fe^{2+} followed by subsequent oxidation of the amine and/or hydroxyl groups to the imine (=NH) or quinone (=O) (Appendix Scheme 3.1).

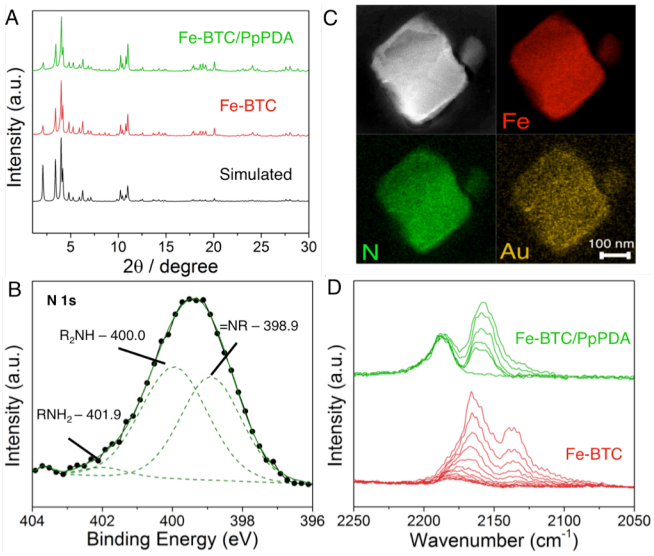

Figure 3.2. Characterization of Fe-BTC and Fe-BTC/PpPDA. Powder X-ray diffraction patterns of Fe-BTC (red) and Fe-BTC/PpPDA (green) compared to the simulated pattern of Fe-BTC (black) (A). N 1s X-ray photoelectron spectrum of Fe-BTC/PpPDA (B). HAADF-STEM images coupled with EDX after ultramicrotome for Fe-BTC/PpPDA (C). In-situ IR with CO at an equilibrium pressure of 67 mbar and then under dynamic vacuum for Fe-BTC (red) and Fe-BTC/PpPDA (green) (D).

Upon polymerization, the orange MOF powder turns dark brown/black due to polymer conjugation (Appendix Table 3.1). Powder X-ray diffraction (PXRD) confirms the structural integrity of Fe-BTC (Figures 3.2A and Appendix Figure 3.1) post polymerization, and nitrogen adsorption reveals that the composites are highly porous with BET surfaces areas above 1000 m^2/g. *In-situ* DRIFTS, obtained from Fe-BTC/PpPDA sparged with CO (Figures 3.2D and Appendix Figure 3.2), provided evidence of Fe^{2+} that results from the polymerization. The peak centered at 2187 cm^{-1}, associated

with the Fe^{2+}-CO stretching mode, does not disappear under vacuum, an observation that is consistent with a previous study of Ferey et al[179]. Next, thermogravimetric analysis was used to estimate the polymer loadings, which ranged from 14 to 20 weight % (Appendix Figure 3.3), and this was further confirmed via combustion analysis (Appendix Table 3.1). Infrared spectroscopy of the composites reveals new peaks associated with the vibrational modes of the added polymer (Appendix Figure 3.4), and scanning electron microscopy (SEM) indicates no polymer formation outside of the MOF crystals (Appendix Figure 3.5).

For the initial evaluation, each composite was soaked in concentrated solutions of Au^{3+} (Appendix Figure 3.6). While the bare framework extracts 136.9 mg of Au^{3+} per gram of MOF, Fe-BTC/PHQ, Fe-BTC/PpPDA, Fe-BTC/PTA and Fe-BTC/PmAP have removal capacities of 631.86, 934.20, 506.23 and 591.83 mg Au^{3+} per gram of composite, respectively. These values are 4 to 6.8 times higher than that of the parent material indicating that the gold scavenging functionality on the polymer backbone significantly enhances extraction. Next, each composites' removal rate was evaluated in river water spiked with 1 ppm Au^{3+} (Appendix Figure 3.7). While all composites reach 99 % removal within 24 hours, Fe-BTC/PHQ and Fe-BTC/PpPDA work in minutes. Since Fe-BTC/PpPDA exhibits the highest removal capacity and the fastest extraction, it became the focus for the remainder of the study.

X-ray photoelectron spectroscopy (XPS) was used to probe the N 1s region of the Fe-BTC/PpPDA spectrum (Figure 3.2B). Peaks corresponding to secondary and tertiary amines, which are not present in the monomer *p*-phenylendiamine, indicate successful polymerization. Subsequent MALDI-TOF-MS measurements, carried out on the digested sample, reveal oligomeric chains made up of 8 monomeric units (Appendix Figure 3.8); this strongly suggests that the MOF pores restrict the propagation of the polymer chains. Next, Fe-BTC/PpPDA was embedded in a resin and serially sectioned in 60 nm thick slices using an ultramicrotome. Energy dispersive X-ray spectroscopy (EDX) in a scanning transmission electron microscope (STEM) provided evidence that nitrogen, the polymer signature, is indeed located throughout the MOF crystal (Figures 3.2C and Appendix Figure 3.9). When soaked in Au^{3+} solutions, the gold is likewise found dispersed inside, and PXRD and XPS confirm the hypothesis that the redox active polymer reduces Au^{3+} to its metallic state (Appendix Figure 3.10 and 3.11). Last, when the composite is soaked in river water for two months, there are no signs of the MOF or polymer leaching, and PXRD reveals long-term structural integrity (Appendix Figure 3.12).

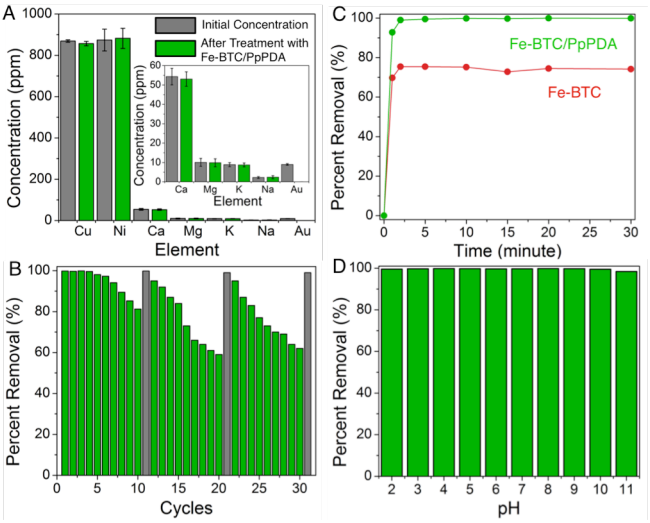

Figure 3.3. Evaluation of gold extraction from river water using Fe- BTC/PpPDA. Concentration of metals before and after treatment of the spiked river water (A). Percent removal of gold after multiple exposures (green bars) and regeneration cycles (grey bars) using ascorbic acid (B). The extraction speed of Fe-BTC (red) and Fe-BTC/PpPDA (green) (C). Percent removal of Au^{3+} at different pH (D) values.

3.2.2 Gold Extraction from Complex Water Mixtures

Increasing numbers of reports evaluate different types of materials for Au^{3+} extraction from water[180-184]. Unfortunately, as outlined in Appendix Table 3.2, most studies do not provide a full evaluation of the materials' performance. Further, to the best of our knowledge, there are no reported materials able to extract and concentrate trace amounts of Au^{3+} in the presence of high concentrations of other interferents, which is of utmost importance given the complexity of the aforementioned solutions. A viable extraction strategy must be scalable, efficient, selective, rapid and recyclable. The as-prepared composite, Fe-BTC/PpPDA, is found to excel in all aforementioned areas.

The composite's ability to extract Au^{3+} from simulated solutions of e-waste was evaluated first. For this, Rhone river water, a matrix containing many competing ions and organics, was spiked with the main components in e-waste including ~870 ppm of Cu^{2+} and Ni^{2+} and ~9 ppm of Au^{3+} (Figure 3.3A)[56, 185]. From this solution, Fe-BTC removes 75 % of the gold, while Fe-BTC/PpPDA removes 99.9% and with minimal uptake of the other ions; the latter is likely due to gold's higher reduction potential combined with higher polarizability and smaller hydration shell relative to other ions in solution. Further, like Fe-BTC, Fe-BTC/PpPDA (Figure 3.3C) reaches equilibrium in less than 2 minutes. This remarkable, rapid extraction rate is attributed to the extrinsic porosity of PpPDA introduced by the MOF template. Next, the composite's extraction efficiency was investigated at varying pH, within the same matrix (Figure 3.3D). Remarkably, >99% removal is achieved for solutions between pH 2-10. At pH 11 gold removal is only slightly reduced to ~98 %, indicating that at these concentrations, pH does not hinder the composite's extraction properties. This initial assessment indicates that the composite has the desirable qualities for various gold extraction processes.

While the material rapidly extracts Au^{3+}, the quantity of gold contained in the composite is quite low (~0.018 mass %), due to low starting concentrations. As such, the material must be able to concentrate gold over time or with regeneration for actual implementation into recovery processes. So, the regenerability of Fe-BTC/PpPDA was tested. For this, 10 river water solutions containing ~10 ppm Au^{3+} were prepared and then treated with Fe-BTC/PpPDA for 5-minute exposures (Figure 3.3B). Figure 3B reveals that the removal efficiency remained at 99 % for four exposures. After cycle 5, the removal efficiency decreases to 98 % and after 10 cycles to 81 %. After this, Fe-BTC/PpPDA, was treated with ascorbic acid to reduce the imine (=NH), generated during Au^{3+} reduction, back to the amine ($-NH_2$), and the process was repeated two more times. It should be noted that after each regeneration with ascorbic acid, 99% removal of Au^{3+} is observed; however, there is a decrease in performance with subsequent exposures, which is likely due to a combination of material loss, decrease in extraction rate, and/or pore clogging as the gold is becoming more concentrated inside. After three regeneration cycles and subsequent sample digestion, the amount of reclaimed gold was calculated to be 0.29 mg of Au^0 per mg of composite, a value that is readily increased with continued cycling. Last, the materials ability to concentrate gold over time was also tested. For this, 10 mg of composite were added to a 10 L solution containing 0.8 ppm Au^{3+}. Although it took 3 weeks, over 99% removal of Au^{3+} is observed. The amount of gold extracted from the 10 L solution is ~8 mg or ~80 mass % of the original composite. This data suggests that a small amount of composite can concentrate trace amounts of Au^{3+} from large quantities of water by simply soaking the material for extended periods of time.

After gold concentration, it is necessary to separate the metal from the materials used for extraction. For this, the gold containing composite that was used to treat the aforementioned river water, was calcined at 900 °C in air and subsequently treated with concentrated hydrochloric acid. The resulting material, inspected under an optical microscope and via PXRD, reveals solid gold particles (Figure 3.4 and 3.13). After dissolution in aqua regia and subsequent elemental analysis, the

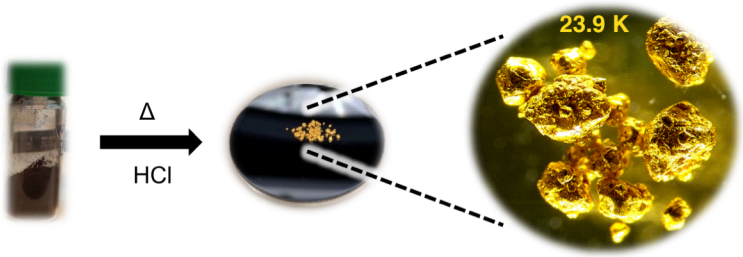

Figure 3.4. Gold removal from the Fe-BTC/PpPDA composite. several saturation and regeneration cycles, the sample was heated and soaked in acid. The resulting gold particles are shown under an optical microscope (right image), and the purity was determined to be 23.9 K.

particles are found to be 99.6 % Au and 0.4 % Fe, a purity of 23.9 K. Despite high concentrations of competing ions, such as Cu^{2+}, Ni^{2+}, etc, no evidence of any other metals is found. To the best of our knowledge, this is the highest purity of gold reported to date for this type of extraction process. This is attributed to the co-adsorption/reduction mechanism for gold extraction. Should the composite take up any of the other ions in solution, this is done through pure adsorption due to their low reduction potentials, and hence, these ions are readily desorbed and returned to solution. The only study found with comparable purities, 23.4 K, employs Zn powder as a reducing agent[56].

Next, gold was extracted from actual solutions obtained from e-waste. For this, metals were mechanically removed from a computer processing unit (CPU) (Figure 3.5), and then leached into a solution. It should be noted that, like ore extraction, gold extraction from e-waste is done using toxic alkali cyanide agents and/or extreme pH conditions[38]. Recently, Yang *et al* reported a facile, method that utilizes an aqueous solution of N-bromosuccinimide (NBS) and pyridine (Py) at near neutral pH levels[56]. This oxidative leaching process is more environmentally benign than the aforementioned methods. As such, the metal obtained from the CPU was soaked in the aqueous NBS/Py mixture. The resulting blue solution had a metal composition of 1470 ppm Cu^{2+}, 95 ppm Ni^{2+} and 7.3 ppm Au^{3+}. After soaking the composite in the resulting solution, there is 86% gold removal in less than two minutes, over 90% in 10 minutes, and 95% removal in 30 minutes (Figure 3.6). The composite is over 662 times more selective for Au^{3+} than Cu^{2+} and Ni^{2+} based on the relevant calculated distribution coefficient, k_d, 1.3 x 10^4 mL/g, 19.13 mL/g, and 5.38 mL/g,

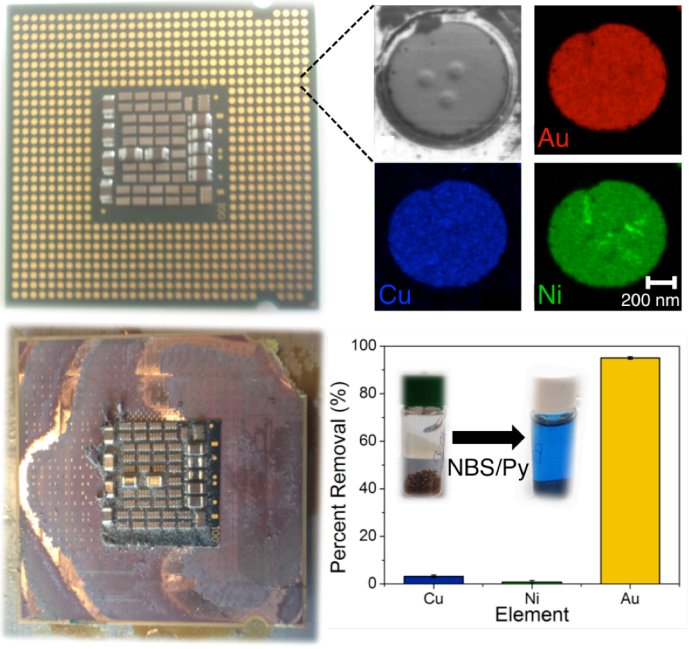

Figure 3.5. Extraction of gold from a CPU. (top) SEM coupled with EDX showing the metal composition in the CPU. (bottom) The metal was mechanically removed from the CPU and then soaked in an NBS/Py leaching solution. The resulting blue solution (bottom, inset) was treated with Fe- BTC/PpPDA and the percent removal of the metals

respectively. With continued cycling and subsequent composite removal, it is expected that the extracted gold will be free of other competing metals, as previously observed in river water. Hence, it is concluded that Fe-BTC/PpPDA has great potential for Au recovery from e-waste.

Given that recent media attention has shed light onto gold lost in the Swiss sewage system, gold-containing wastewater samples were obtained from a waste water treatment plant in Switzerland[161]. The concentration of Au was determined to be approximately 3.7 ppb. The wastewater solutions were then treated with Fe-BTC/PpPDA. In less than 1 minute, 90% of Au^{3+} is extracted from the wastewater, and in under 30 minutes (Figure 3.6) over 99 % of Au is extracted with a final gold concentration of < 10 ppt (Appendix Figure 3.14). This extraction is truly remarkable, particularly considering the high concentrations of organics in wastewater, which often competitively complex metal ions and also often foul mesoporous adsorbents. To our knowledge, there has been no demonstration of any material capable of extracting precious metals from wastewater. The unique architecture, rare adsorption/reduction mechanism, and high porosity make Fe-BTC/PpPDA highly effective for gold separation from such a complex mixture.

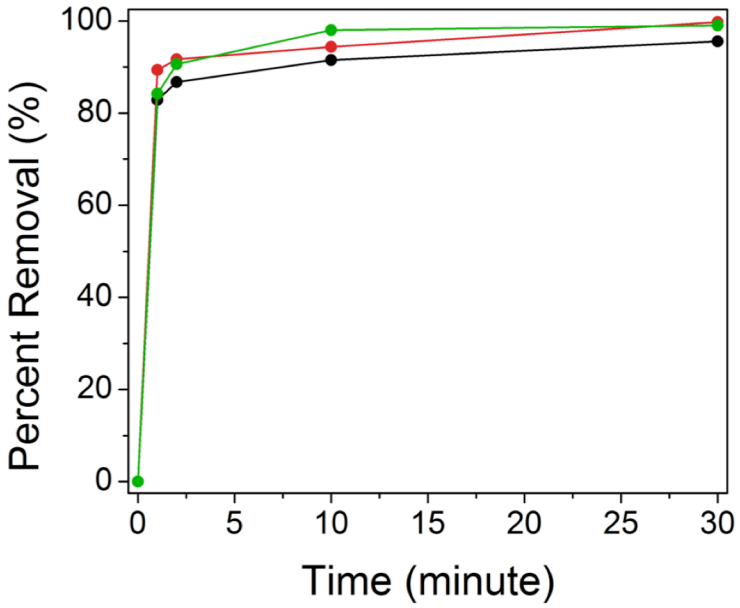

Figure 3.6. Extraction rates of gold from different matrices using Fe-BTC/PpPDA. The matrices are e-waste leaching solution obtained from the CPU (Ci – 7.3 ppm) (black), wastewater (Ci - 3.7 ppb) (red) and river water (Ci – 120 ppb) (green).

In addition to this, gold was extracted from the sewage ash, which is known to contain large concentrations of a variety of metals[163]. For this, we again employed the NBS/Py technique[56]. The resulting solution contained 5.47 ppm Au^{3+} (Appendix Figure 3.15) and many other metals such as Ca^{2+}, Cs^{+}, Mg^{2+}, Na^{+}, Fe^{3+}, Cu^{2+}, K^{+}, B^{3+}, Zn^{2+} and Rb^{+} with concentrations ranging from ~130 ppm to 0.35 ppm. In less than two minutes the composite is able to extract 61 % of the Au^{3+} from the NBS/Py solution and then reaches 90% removal in 24 hours. We also observe little to no uptake of most of the other metal intereferents present. Although the Cu^{2+} concentration is decreased from 1.76 ppm to 0.16 ppm, the removal capacity is

quite low. Further, Cu^{2+} (Figure 3.3) is readily desorbed, and hence will not influence the final gold purity.

Many mining operations near fresh water sources tend to discharge metal ions into the environment. In Alaskan rivers, the gold concentration ranges between 60-120 ppb, 100 times lower than what was tested in the previous experiments. As such, we spiked Rhone river water with 120 ppb Au^{3+} and evaluated the extraction rate after treatment with Fe-BTC/PpPDA (Figure 3.6). Remarkably, in less than 2 minutes we observe 90% Au extraction and then 99% removal in less than 30 minutes, indicating that Fe-BTC/PpPDA could be implemented in mining Au from surface water sources.

Last, one of the most difficult challenges is gold recovery from the sea. It is estimated that the ocean contains gold valued at 720 trillion US dollars. Unfortunately, gold in seawater has an ultra-low concentration, < 20 ppt, and is one of the most complex matrices in the world. For example, competing ions, such as Na^{+} can have concentrations that are 2×10^{9} times higher than that of Au^{3+}. As such, extraction of the precious metal from the sea is conceptually thought to be nearly impossible. Given this challenge, Mediterranean Sea water was spiked with 1 ppm Au^{3+}. Fe-BTC/PpPDA was found to extract 95 % in 20 minutes and then reached > 99 % removal in 30 minutes (Figure 3.16). It should be noted that given the complexity of the solution, we could not obtain the remaining concentration of gold in the seawater; however, we note that it is below 100 ppt based on the detection limit of our ICP-MS method. As this value is approaching the gold concentration in the sea, we daringly attempted to concentrate gold directly from the ocean. For this, 0.5 g of Fe-BTC/PpPDA was soaked in the ocean for 1 week off the coast of Jacksonville Florida, USA. The sample was then recovered, dried and digested in aqua regia to determine if any Au was extracted while soaking. The post-treated sample was found to contain 0.01 wt % Au. While this is a small amount, with much longer soak times and subsequent regeneration, composites like Fe-BTC/PpPDA might bring new found optimism towards even mining gold from the sea.

3.3 Conclusion

Fe-BTC/PpPDA is a novel, redox active MOF-polymer composite with demonstrated ability to rapidly extract and concentrate trace amounts of Au^{3+} from highly complex solutions. The material effectively removes > 90 to 99% of trace amounts of Au from a variety of different matrices that include surface water, wastewater, and those obtained from e-waste and the sewage ash.

Further, due to its high porosity, the material reaches equilibrium in as little as two minutes. With regeneration the composite effectively concentrates gold, and, after subsequent removal of the composite, the remaining gold has the highest reported purity to date of 23.9 K. The latter is due to a combined adsorption/reduction mechanism, which inhibits Cu^{2+}, Ni^{2+}, and many other competing ions from being reclaimed from the solutions. These remarkable properties result from the introduction of extrinsic porosity to redox active polymers. The reported results indicate that this material can be highly influential in gold recovery processes, and through judicious selection of MOF and polymer building blocks, it is envisioned that this new platform technology can be used to selectively recover many other high value commodities or contaminates from liquid or air.

3.4 Synthetic Methods and Procedures

Synthesis of Fe-BTC. In a 180 mL teflon autoclave, 9.72 g of iron(III) chloride hexahydrate, 3.36 g of trimesic acid and 120 mL of distilled water were mixed together. The reaction mixture was heated to 130 °C for 3 days. After the reaction was cooled down to room temperature the orange solid was centrifuged at 7200 rpms and washed with copious amounts methanol. The orange powder was loaded into a double thickness whatman cellulose extraction thimble and underwent soxhlet purification with methanol for 24 hours. After purification, the sample was dried under vacuum overnight. The material was activated under vacuum at 125 °C overnight before nitrogen adsorption and standard characterization.

Elemental Analysis: C: 34.85 % **H:** 2.15 % **Fe:** 21.44 % **and BET Surface Area:** 2056 m^2/g

Synthesis of Fe-BTC/PpPDA. 1 g of Fe-BTC was activated in a two neck 500 mL round bottom flask overnight using a schlenk line and an oil pump. After activation the reaction vessel was allowed to cool to room temperature and then was flushed with nitrogen. In the dry box purged with nitrogen, 1.2 g of p-phenylenediamine and 200 mL of anhydrous ethanol were loaded in a 250 mL round bottom flask and capped with a septum. The ethanol solution was then transferred air free via a steel canula and nitrogen. The reaction mixture was allowed to stir at 420 rpms for one hour. The reaction was then exposed to air and heated to 50 °C for 24 hours. The resulting brown powder was filtered via vacuum filtration and underwent soxhlet purification with ethanol for 24 hours. After purification, the sample was dried under vacuum overnight. The composite was activated under vacuum at 125°C overnight before nitrogen adsorption and standard characterization.

Elemental Analysis: C: 43.53 % **H:** 3.05 % **N:** 5.06 % **Fe:** 17.26 % **and BET Surface Area:**

1032 m^2/g

Fe-BTC/PHQ. 1 g of Fe-BTC was activated in a two neck 500 mL round bottom flask overnight using a schlenk line and an oil pump. After activation the reaction vessel was allowed to cool to room temperature and then was flushed with nitrogen. In the dry box purged with nitrogen, 1.3 g of hydroquinone and 200 mL of anhydrous ethanol (0.05M) were loaded in a 250 mL round bottom flask and capped with a septum. The ethanol solution was then transferred air free via a steel canula and nitrogen. The reaction mixture was allowed to stir at 420 rpms for one hour. After expected complete diffusion of the monomer, 1.8 mL of ammonia (25%) in water was added to the reaction mixture and the powder turned dark purple. The reaction was then exposed to air and heated to 50 °C for 24 hours. The resulting dark purple powder was filtered via vacuum filtration and underwent soxhlet purification with ethanol for 24 hours. After purification, the sample was dried under vacuum overnight. The resulting composite was activated under vacuum at 125 °C overnight before nitrogen adsorption and standard characterization.

Elemental Analysis: C: 40.06 % **H:** 2.57 % **Fe:** 17.86 % **and BET Surface Area: 1**665 m^2/g

Fe-BTC/PTA. 1 g of Fe-BTC was activated in a two neck 500 mL round bottom flask overnight using a schlenk line and an oil pump. After activation the reaction vessel was allowed to cool to room temperature and then was flushed with nitrogen. In the dry box purged with nitrogen, 1.62 g of tyramine and 200 mL of anhydrous ethanol were loaded in a 250 mL round bottom flask and capped with a septum. The ethanol solution was then transferred air free via a steel canula and nitrogen. The reaction mixture was allowed to stir at 420 rpms for one hour. The reaction was then exposed to air and heated to 50 °C for 24 hours. The resulting dark purple powder was filtered via vacuum filtration and underwent soxhlet purification with ethanol for 24 hours. After purification, the sample was dried under vacuum overnight. The composite was activated under vacuum at 125°C overnight before nitrogen adsorption and standard characterization.

Elemental Analysis: C: 38.75 % **H:** 2.76 % **N:** 1.44 % **Fe:** 17.66 % **and BET Surface Area:** 1776 m^2/g

Fe-BTC/PmAP. 1 g of Fe-BTC was activated in a two neck 500 mL round bottom flask overnight using a schlenk line and an oil pump. After activation the reaction vessel was allowed to cool to room temperature and then was flushed with nitrogen. In the dry box purged with nitrogen, 1.72 g of m-aminophenol and 200 mL of anhydrous ethanol (0.05M) were loaded in a 250 mL round bottom flask and capped with a septum. The ethanol solution was then transferred air free via a

steel canula and nitrogen. The reaction mixture was allowed to stir at 420 rpms for one hour. After expected complete diffusion of the monomer, 1.3 mL of ammonia (25%) in water was added to the reaction mixture and the powder turned dark purple. The reaction was then exposed to air and heated to 50 °C for 24 hours. The resulting dark purple powder was filtered via vacuum filtration and underwent soxhlet purification with ethanol for 24 hours. After purification, the sample was dried under vacuum overnight. The resulting composite was activated under vacuum at 125 °C overnight before nitrogen adsorption and standard characterization.

Elemental Analysis: C: 40.35 % **H:** 2.78 % **N:** 2.12 % **Fe:** 17.32 % **and BET Surface Area:** 1358 m^2/g

“The mind is everything. What you think you become”

CHAPTER 4 – CLEAN WATER INITIATIVE – NEX GEN FILTER DEVICES

Continuous flow through operations is the most widely used adsorption configuration in industry. Under batch configuration adsorption experiments, Fe-BTC/PDA and Fe-BTC/PpPDA excel in the capture of Pb^{2+}, Hg^{2+} and Au^{3+} from complex water mixtures, respectively. The materials must now be considered in a fixed-bed column or filter device under dynamic continuous flow through conditions for possible industrial implementation. The progress for the scale up of the MOF/Polymer composites, structuring, construction of a continuous flow through apparatus and a preliminary continuous fixed-bed column experiment are shown in this chapter.

4.1 Introduction

In order to design and develop any adsorption process, adequate selection of an adsorbent is an important first step. Thus, several characteristics of the adsorbent such as capacity, selectivity, kinetics, chemical and thermal stability, cost, and reusability must be evaluated and considered before large scale implementation.[186] Two materials, Fe-BTC/PDA and Fe-BTC/PpPDA, products of this thesis have been evaluated in the aforementioned arenas and excel in all of these metrics.[89-90] Next, is to now consider the MOF/Polymer composites for large-scale implementation. Unfortunately, information from these lab scale batch experiments is not enough for the prediction of an adsorbent's performance in more practical modern processes. Several other adsorption configurations do exist and are employed more than batch adsorption operations[89] such as continuous fixed-bed adsorption,[187] fluidized bed adsorption[188] and continuous stirred-tank reactor (CSTR)[189] for water and wastewater streams. However, the continuous fixed-bed operation is the most widely used configuration in industrial processes. As such, this configuration is mainly employed by researchers to investigate the relevant performance of adsorbents for modern industrial practices.[186] For potential industrial implementation, these materials must now be considered in a dynamic continuous flow through operation.

Although batch adsorption experiments can provide information to initially assess adsorbents, continuous fixed-bed adsorption experiments must be conducted to obtain other crucial information such as breakthrough time, length of mass transfer zone and maximum capacity of the column under those dynamic conditions. Modeling of the fixed-bed adsorber and validation of that model with experimental data obtained will help facilitate the design of a large-scale prototype. The key objectives related to studying the materials of the previous chapters in a continuous flow through operation are: 1) the construction of a custom continuous flow through apparatus, 2) cost-effective scaling up of the MOF/Polymer composites' synthetic protocols, 3) optimally structuring the MOF/Polymer composites and 4) optimization and modeling of dynamic continuous flow through experiments.

Scaling up the synthesis of the MOF/Polymer materials is needed to allow for multiple gram large-scale flow-through experiments. Afterwards, the fine powders must be structured before implementation into a filter device to prevent pressure drops or gradients along the fixed-bed column. How a fine powder is structured and what additives are employed can either help or hinder a material's performance. Dynamic continuous flow experiments will then be conducted on

the newly constructed filter devices. Parameters such as column bed length, column bed diameter, adsorbent mass, flow rate and analyte concentration will affect a filter device's performance. As such, once the most effective structuring methodology has been determined, flow through experiments will be executed with these parameters being varied systematically for simulated and real-world water samples. This data will allow for the validation of different models commonly used for filter devices to determine selectivity, metal ion capacity, kinetics/diffusion coefficients and overall performance. Models will then be validated incrementally by gradually increasing the filter size until the most cost-effective filter device is realized. The current state of each of these endeavors is described in this chapter.

4.2 Results and Discussion

4.2.1 Scale up of MOF, MOF/Polymer Composites and Structuring

In comparison with the typical synthesis of Fe-BTC mentioned in the previous chapters, the type of reactor was changed from a Teflon autoclave to glass bottles. As such, several large-scale reactions were performed in parallel for optimization purposes. A decrease in the temperature of the reaction was achieved from 130 °C to 110 °C. The amount of chemicals, which were used for different volume of reactor, are listed in Table 4.1. First, $FeCl_3.6H_2O$ is simply added to the specified amount of water and mixed while stirring until a homogenous solution reached. Then, BTC (Table 4.1) was added to the solution and was mixed for a very short amount of time (less than a minute) to obtain homogenous solid-liquid suspension (BTC is not soluble). Finally, the reactor was put in oven and was kept for 72 hours at 110 °C. After the reactor was cooled down to room temperature in the oven, the solids were separated from the mother liquor by centrifuging and washed two times with water to remove unreacted $FeCl_3$ and two times with methanol to remove unreacted ligand. The average surface area of the synthesized Fe-BTC is greater than 1800 m^2/g with high crystallinity (Appendix Figure 4.1). Currently, the largest reactor size performed is 10 L producing up to 412 g of Fe-BTC. It was found that the work up step, i.e. the washing of the material greatly influences the BET surface area. The mother liquor, which can contain up to 8000 ppm of non-reacted $FeCl_3.6H_2O$, can also be reused for future Fe-BTC synthesis reducing the production of waste. It was demonstrated up to four cycles of reusing the mother liquor to produce new Fe-BTC powder with consistent porosity and crystallinity (Appendix Figure 4.1). The intention is to gradually increase the batch size of the reaction to 25 L to yield 1 kg of Fe-BTC.

Material & condition	Reactor volume			
	100 mL	**250 mL**	**2000 mL**	**10000 mL**
$FeCl_3.6H_2O$	6.48 g	16.2 g	129.6 g	518.4 g
BTC	2.24 g	5.6 g	44.8 g	179.2 g
H_2O	80 ml	200 ml	1600 ml	8000 mL
Temperature	110 °C	110 °C	110 °C	110 °C
Duration	72 h	72 h	72 h	72 h
Mass of product	2.9 g	6.8 g	55-60 g	350-412 g

Table 4.1. Recipes and yields for the scaling up of Fe-BTC up to 10 L batch reactions.

The final *in-situ* polymerization step can also be performed using batch reactors. Currently, 5 g of Fe-BTC/PDA and 10 g of Fe-BTC/PpPDA per batch can be achieved. Although batch methodologies can be sufficient, kg scale reactions will require greater than 50 L batch reactors with the current recipe. As such, continued optimization on the protocol must be done. High quality of Fe-BTC/PpPDA material could also be synthesized by this scale up methodology. The material is highly crystalline and exhibits similar gold extraction properties from a material made using batch methodologies in Chapter 3 (Appendix Figure 4.2). We also intend to scale up the synthesis of Fe-BTC/PDA using a similar methodology. Last, Fe-BTC/PpPDA was then pelletized by compressing the fine powder with 0.5 tons of pressure using a press producing 1 mm cylindrical pellets.

4.2.2 Design of 1st Generation Continuous Flow Through Apparatus

The apparatus and devices shown in this chapter were designed and constructed in the EPFL Valais Electric and Mechanical Work Shop. Figure 5.2 shows an overall schematic of the custom built continuous flow through apparatus. This fixed bed adsorption set up is widely used in various studies for heavy metal removal.[186-187] It starts with two large 20 L reservoirs. The reservoirs are connected to a ¼ inch wide line that is connected to an adjustable speed peristaltic water pump

with 2-way Swagelok valves in between. The output of the pump is connected to another ¼ inch wide line that is then connected to a 3-way Swagelok valve. One direction of the valve is used to sample the water mixture before treatment and another direction is connected to the filter device. After the water passes through the fix-bed column or filter device, it is brought to an auto-sampling robot. The robot can then be programed in customizable ways to sample the water at different time points or volumes. For instance, it can be programed to dispose of 1 L of the water mixture post treatment, sample 10 mL into a test tube and repeat this process. The sampled water is then taken to the ICP-OES to measure the concentration of the metal ions present post-treatment. A picture of the finished apparatus is shown in figure 5.3.

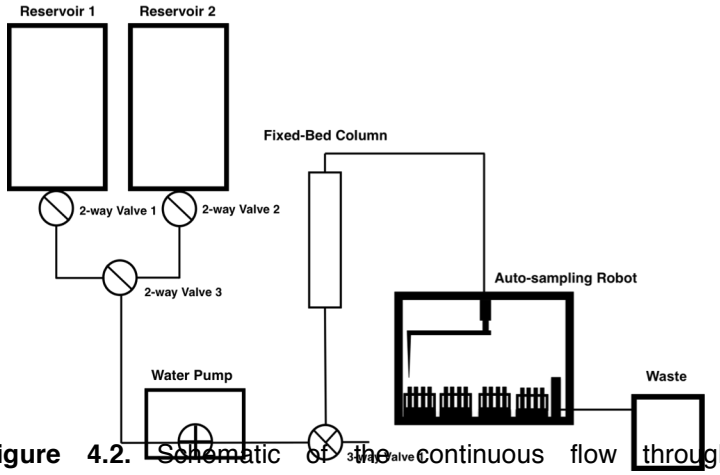

Figure 4.2. Schematic of the continuous flow through apparatus for fixed-bed column experiments.

4.2.3 Continuous Fix-Bed Column Experiments and Preliminary Results

The main purpose of a continuous fixed bed column (filter device) experiment is to obtain the parameters such as breakthrough time, length of mass transfer zone, removal percentage and maximum capacity of the column under dynamic conditions. Typically, the column, with a specified height and diameter, is packed with a certain amount of adsorbent between two layers of glass wool or beads (Figure 4.3). The contaminated liquid feed containing different metal ions, named as the influent, is pumped into the adsorption column at the desired flow rate. The outlet stream, named as the effluent, is collected in different time intervals in order to obtain the breakthrough curve as aforementioned. During the continuous flow experiment, by changing the parameters such as initial metal ion concentration, flow rate and/or height of the adsorbent layer i.e. the column, the performance of the filter device can be evaluated in varying conditions.

The breakthrough time and saturation time are defined as the time when the concentration of the metal ion in the outlet stream is 5% and 95% of the inlet stream, respectively. The shape of the breakthrough curve is also an important characteristic of adsorption column under continuous flow conditions shedding light on the mass transfer occurring. The adsorption capacity, q (mg/g), in the fixed bed column can be calculated using the following equation:

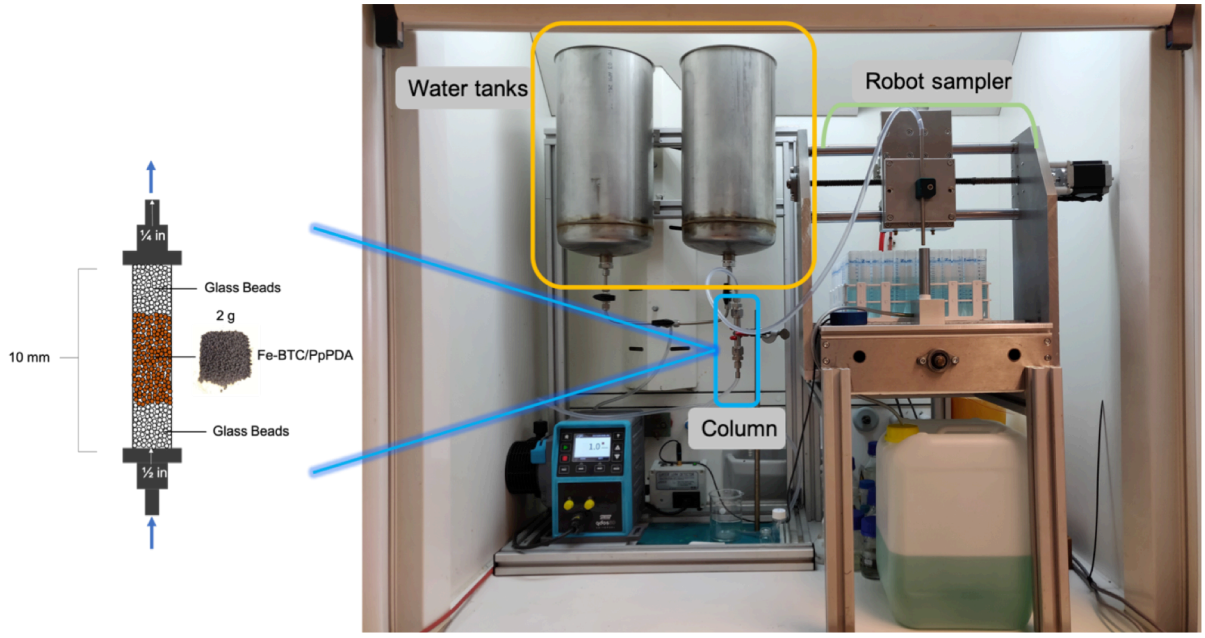

Figure 4.3. Photo of the custom-built continuous flow through apparatus.

$$q = \frac{Q \int_0^t (C_0 - C_e) dt}{M}$$

where Q is the flow rate (L/min), M is the mass of the adsorbent in the column (g), C_0 and C_e(mg/L) are the influent and effluent metal ion concentrations, respectively. Also, t (min) could be t_{sat} or t_b that represent the saturation time or the breakthrough time, respectively.

The total amount of metal ions (m_{total}) injected to the adsorption column can be calculated as follows:

$$m_{total} = C_0 Q t_{total}$$

where t_{total} is the total time of the experiment.

Further, the removal percentage of metal ions can be calculated as follows:

$$\text{Percent Removal } \% = \frac{\text{q}}{\text{m}_{\text{total}}} \times 100$$

In order to analyze the breakthrough results from the lab scale experiments and predict the performance of a large-scale column, finding the right mathematical models, which accurately predict the experimental data for practical size columns, is required. Thus, several models have been developed by researchers for the prediction of the breakthrough curves in a continuous fixed-bed column set up. Cruz-Olivares et all highlight several of these models for Pb^{2+} adsorption in their fixed-bed column experiments.[187] Three models are highlighted in this chapter for the intended use once high quality breakthrough curves are obtained.

For instance, the Thomas Model[190] has been employed since 1944 and is widely used to describe a columns performance and predict breakthrough curves. It utilizes the Langmuir kinetics of adsorption and assumes negligible axial dispersion in the column. It is described in the equation below:

$$\frac{C}{C_o} = \frac{1}{1 + \exp\left[\left(\frac{k_{Th}}{Q}\right)(q_o X - C_o Q t)\right]}$$

where, C is the concentration (ppm), C_o is the initial concentration (ppm), k_{Th} is the Thomas rate constant (mL/min mg), X is the total mass of the adsorbent in the column (g), Q is the flow rate (mL/min) and q_o is the maximum concentration of the analyte in the solid phase (mg/g).

The Bed Depth Service Time (BDST) model, described by Hutchins, is also widely employed for metal ion adsorption in a fixed bed column. It is useful to predict the relationship between the depth and service time in terms of process concentration and adsorption parameters. It ignores external film and intraparticle mass transfer resistance and is primarily based on measuring the capacity of the bed at different breakthrough values. It is described in the equation below:

$$\frac{C}{C_o} = \frac{1}{1 + \exp\left[k_{BDST} C_o \left(\frac{N_o}{C_o v} L - t\right)\right]}$$

where, C is the concentration (ppm), C_o is the initial concentration (ppm), k_{BDST} is the adsorption rate constant that describes the mass transfer from the liquid to the solid phase (L/mg min), L is the bed height (cm), N_o is the biosorption capacity of the bed (mg/L) and v is the linear flow velocity of the metal solution through the bed (cm/min).

Transport parameters can be obtained using a model based on the mass transfer that takes place in the filter device. The model assumes: 1) the diffusion occurs in the axial directions, 2) mass diffusivity does not depend on the concentration of the metal ions, 3) temperature, velocity and density are constant, and 4) no intraparticle diffusion occurs. It is applied for a differential mass balance below:

$$\frac{\partial C}{\partial t} = \frac{D}{\varepsilon}\frac{\partial^2}{\partial z^2} - \frac{u}{\varepsilon}\frac{\partial C}{\partial z} - \frac{(1-\varepsilon)}{\varepsilon} k_c a (C - C_e)$$

where, D is the coefficient of the dispersed metal ions, a is the specific area of the particles, ε is the porosity of the column bed, k_c is the mass transfer coefficient, t is time, z is the axial distance in the column, u is the speed surface of the liquid, C is the concentration of the metal ion in the

liquid and C_e is the equilibrium concentration obtained from isotherms obtained from batch experiments. K_c is estimated by a correlation factor based on J_D dimensionless Reynolds (N_{Re}) and Schmidt (N_{Sc}) numbers seen below:

$$J_D = \frac{0.25}{\varepsilon} N_{Re}^{-0.31}$$

where, $J_D = \frac{k_c N_{Sc}^{2/3}}{u}$

Once high-quality breakthrough curves are obtained the date will be modeled, first using these previous equations.

For the first continuous flow through experiment, 2 g of Fe-BTC/PpPDA that was compressed at 0.5 tons to produce 1 mm pellets was loaded into a ½ inch wide column. The column is 10 mm long in length with 1 mm glass beads at each end of the column and is connected to ¼ in lines on each side that are then connected to the water pump and the autosampling robot. The reservoirs were filled with a river water mixture containing metal ions at concentrations of approximately 10 ppm of Au^{3+}, 800 ppm of Cu^{2+}, 800 ppm of Ni^{+}, 50 ppm of Ca^{2+}, 12 ppm of Na^{+} and 2 ppm of K^{+} to simulate the inorganic components found in electronic waste. So far, 10 L of the complex water mixture was pumped through the fix-bed column at a flow rate of 1 mL/min (Figure 4.4). Within the first minutes, Ca^{2+}, Mg^{2+}, K^{+}, Na^{+} and Ni^{2+} break through immediately. 70% of the Cu^{2+} influent is observed in the effluent initially. It completely breaks through after 2 L of influent has passed through the column. This is expected, as there is minor uptake for Cu^{2+} observed in the batch adsorption experiments in Chapter 3. Au^{3+} however, does not break through after 10 L of influent has passed. This demonstrates that the gold is concentrating inside the filter device. Although still more than 95 %

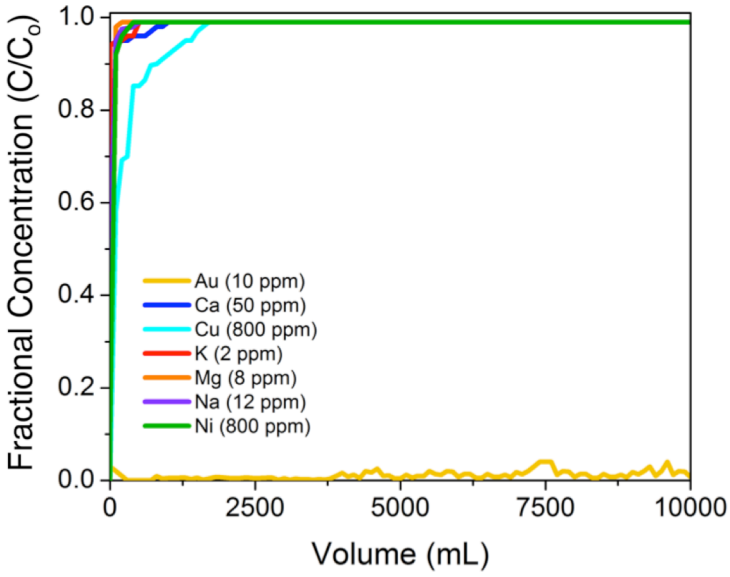

Figure 4.4. Breakthrough curve after 10 L of a complex water mixture containing trace amounts of gold continuously passed through a fix-bed column containing Fe-BTC/PpPDA.

of the gold is concentrating, after 4 L is treated, fluctuations in the effluent's gold concentration is observed. The change in liquid volume from ¼ inch line to a ½ inch fixed-bed column and back to a ¼ inch line could cause turbulent flow, which we surmise results in these fluctuation in gold concentration. Now experiments with the configuration of a ¼ inch line to a ¼ inch fix-bed column to a ¼ inch line will be conducted to minimize this problem.

4.3 Conclusion

In this chapter, the progress for each objective mentioned in the introduction is shown. A custom continuous flow through apparatus to test filter devices has been constructed. High quality Fe-BTC and Fe-BTC/PpPDA have been produced using a 10 L batch and a continuous flow through reactors, respectively. Unfortunately, one drawback in the scaled-up protocol that is encountered, is the separation of the material from the reaction solution. The current methodology utilizes centrifugation due to the small particle size of the material (< 0.5 μm). As such the centrifugation of large volumes of liquid can be time consuming and tedious depending on the centrifugation volume capacity. The problem can be alleviated by of a large-scale filtration apparatus for a rapid and effective separation of micron-sized powder from solution. More optimization experiments will be performed regarding the scale up. Fe-BTC/PpPDA is then structured into 1 mm cylindrical pellets with pressure and loaded into a column. Using the custom-built continuous flow through apparatus, the selective extraction and concentration of trace amounts of gold is demonstrated in a fixed-bed column or filter device. Although the preliminary results presented in this chapter are promising, much more work must be done for large-scale industrial implementation.

“It’s going to be bigger than you thought,
it’s going to happen quicker than you imagined and,
it’s going to be more rewarding than you ever dreamed of.”

Summary

The majority of this work described in this thesis is focused on the construction and characterization of MOF/Polymer composites for metal ion capture with a water purification and economic relevance. The general aim was to design a set of new porous materials using a bottom up approach to give synergy between the building blocks and evaluate their heavy and precious metal ion extraction performance. The strategy used throughout the thesis was to facilitate the *in-situ* polymerization of redox active monomers via electron transfer events with the open metal sites along the MOF's pore surface. The open metal sites not only act as catalytic active sites to facilitate the polymerization reactions, but also provide a way for the polymer to append to the pore surface. This methodology gives extrinsic porosity to intrinsically non-porous polymers.

- In chapter 2, we illustrate this novel platform technology that introduces extrinsic porosity to intrinsically nonporous polymers using highly porous metal-organic frameworks as a template. For proof of concept, a MOF named Fe-BTC, was treated with dopamine, which subsequently polymerizes to polydopamine (PDA). The heavy metal scavenging PDA, now pinned on the internal MOF surface results in a material that binds up to 1634 mg Hg^{2+} and 394 mg Pb^{2+} per gram of composite and removes over 99.8 % of these contaminants from a 1 ppm solution at record-breaking rates, yielding drinkable levels in seconds. Further, Fe-BTC/PDA's properties are well-maintained in river water, waste water (obtained from Swiss industry) and sea water spiked with only trace amounts of lead and mercury; this illustrates unprecedented selectivity. The material is further shown to be resistant to fouling due to its unique pore architecture and is fully regenerable over many cycles.
- In chapter 3, it was discovered that the underlying mechanism for the extraction of mercury with Fe-BTC/PDA was an electron transfer event between Hg^{2+} and the polymer that lines the MOF pore walls. As such, we surmised that we could selectively target precious metals like gold, which also has a high reduction potential, from liquid sources as currently there were no technologies reported to date that can selectively concentrate ultra-trace amounts of gold from liquid sources effectively. We demonstrate that changing the redox-active polymer building block in the MOF will result in a new material, Fe-BTC/PpPDA, that is able to selectively and rapidly extract trace amounts of gold from several complex water mixtures that include waste water, fresh water, ocean water, and solutions used to leach gold from electronic waste and incinerated sewage sludge. The material has an

exceptional removal capacity, 934 mg gold per g of composite, and extracts gold from these complex mixtures also at record-breaking rates. Further, due to the high cyclability, we demonstrate that the composite can effectively concentrate gold and yield purities up to 23.9 K.

- In chapter 4, we consider the materials mentioned in the previous chapters for large-scale implementation. For potential industrial implementation, continuous fixed-bed adsorption experiments must be conducted to obtain information to help design, model and predict a large-scale prototype in a continuous flow operation. The schematic and construction of a custom-built continuous flow through apparatus is provided. The current progress for scaling up the synthesis of high-quality Fe-BTC, Fe-BTC/PDA and Fe-BTC/PpPDA, structuring of the fine powder into 1 mm pellets via compression and incorporation into a filter device for continuous fixed-bed column experiments is shown. For the first experiment, a complex water mixture containing trace amounts of gold and high concentrations of inorganic interferents is passed through the filter device. We show that almost immediately all inorganic interferents breakthrough completely while the concentration of gold in the effluent is nonexistent. This illustrates that gold is concentrating into the filter device. More work is underway to obtain the information needed to design, model and predict a large-scale prototype with these materials for industrial-scale operations.

Several examples throughout this thesis demonstrate how to incorporate high densities of specific types of functionality into the highly porous and rigid systems of MOFs. Utilizing the pore and pore surface chemistry of MOFs, we are able to introduce extrinsic porosity to intrinsically non-porous polymers via an *in-situ* polymerization process. The infinite number of MOF and polymer building blocks in this platform allows for the rationale design of competitive and interesting new materials. Through judicious selection of MOF and multiple polymer building blocks, it is envisioned that this new platform technology will influence the next generation of porous materials used for the selective extraction of high value commodities and contaminants from liquid or air.

“I can do all things….”

EXPERIMENTAL PART

General Methods for Synthesis

Air Free Synthesis of MOF/Polymer Composites. Initially, MOF/Polymer composites were constructed under air free conditions to reduce variables that could affect the performance of the resulting material. First, MOFs were activated under vacuum in a 2-neck round bottom flask connected to a schlenk line and a rough oil pump at a temperature higher than the boiling point of water or solvent. This increases monomer diffusion into the porous netoworks and removes any solvent or water bound to open metal sites so that they may be used to facilitate the *in-situ* polymerization of the monomers. After activation, usually overnight, the reaction vessel is filled with an inert gas like argon or nitrogen. Next, in a dry box the monomer is mixed with anhydrous alcohol, stirred until dissolved and sealed. Using a steel canula and an inert gas, the solution is transferred to the reaction vessel containing the activated MOF and allowed to stir at room temperature under an inert atmosphere until the polymerization has finished again usually overnight. It should be noted that if the reaction mixture is exposed to air and temperatures are elevated then the polymer wt. percent will increase in the system. Likely, this is due to oxygen oxidizing and regenerating the catalytic open metal site to push the *in-situ* polymerization reaction forward. After reaction completion, the powder now a darker color is separated with centrifugation or vacuum filtration and washed with the solvent used in the reaction. The powder is loaded into a cellulose whatman thimble and undergoes soxhlet purification overnight with the solvent of choice. After purification, the powder is dried under vacuum and is activated at the desired temperature before standard characterization.

Double Solvent Method. This method can be utilize if MOFs do not have unsaturated open metal sites that facilitate the *in-situ* polymerization reaction, but also works with MOFs that do have open metal sites. First, a MOF with hydrophilic pores in activated under vacuum in a two-neck round bottom flask using a schlenk line and rough oil pump to remove any polar solvent like water. After dosing an inert gas into the system, anhydrous non-polar hexane is added to the reaction mixture and allowed to stir until complete diffusion usually in less than 30 minutes. The monomer is then dissolved into the most minimal amount of water as possible. This aqueous solution is then syringed into the reaction mixture. Over time, the hydrophilic MOF will mix will the water and work its way to the bottom of the reaction vessel. Once this is achieved, the anhydrous hexane is then decanted out. Now a pH swing is conducted to facilitate the *in-situ* polymerization

reaction. An alcohol solution containing a base like ammonia (NH_3) is added to the reaction and allowed to stir until reaction completion usually over night. The solids now a darker color is separated from the solvent either by centrifugation or vacuum filtration and is washed with fresh solvent that is used in the reaction. The powder is loaded into a cellulose whatman thimble and undergoes soxhlet purification over night. After purification, the powder is dried and activated before standard characterization.

Material Characterization

Powder X-ray Diffraction. Lab Source powder X-ray diffraction was performed on a Bruker D8 Discover system with a Cu Kα source (1.54056 Å) at 40 kV and 40 mA. The primary optics slit and secondary optics slit were set to 12 mm and 9 mm respectively with a NiO filter. The powder samples were ground with a mortor and pestle and then loaded onto a 1 mm deep sample holder. The scanning range was set from 1-80° over 2760 steps with 1 second exposure time per step. Simulated powder patterns were generated using Mercury 3.6 crystallography software.

Nitrogen Adsorption Measurements. All adsorption measurements were performed on a Micromeretics 3Flex. Samples between 50-100 mg were activated at 125 °C under vacuum overnight. After activation, the samples were cooled to room temperature, back filled with argon, and transferred to the 3Flex adsorption analyzer. Nitrogen adsorption isotherms were collected at 77 K with nitrogen and helium 99.999% purity gas. After the isotherms were generated the surface areas (m^2/g) were calculated using the BET (Brunaer-Emmet-Teller) method from the software.

X-ray Photoelectron Spectroscopy. X-ray photoelectron spectroscopy measurements were carried out using a Physical Instruments AG PHI VersaProbe II scanning XPS microprobe. Experiments were performed with a beam size of 100 μm using a monochromatic Al Kα X-ray source of 24.8 W power. The spherical capacitor analyzer was set at 45° take-off angle with respect to the sample surface. The pass energy was 46.95 eV yielding a full width at half maximum of 0.91 eV for the Ag 3d 5/2 peak. The data was analyzed using the CasaXPS software.

***In-situ* FT-IR with Carbon Monoxide.** *In-situ* IR data was collected in transmission mode on sampled mounted on a self-supported wafer using a custom-built infrared cell and a Harrick Scientific Praying Mantis on a PerkinElmer Frontier Spectrometer at -123 °C. Before measurements, the samples were activated overnight at 125 °C while under dynamic vacuum. After cooling down the sample cell was purged with argon for 30 minutes and then cooled to -123

°C with liquid nitrogen. The background was collected and CO was then introduced into the sample cell. The background subtracted *in-situ* DRIFTS spectra were collected for Fe-BTC and Fe-BTC/PpPDA at a CO equilibrium pressure of 67 mbar. After the peaks were observed vacuum was then pulled on the sample while simultaneous collecting spectra.

Scanning and Transmission Electron Microscopy with Microtomy. Scanning Electron Microscopy (SEM) images were taken using a FEI Teneo. Samples were sputter-coated with iridium (~ 7 nm thick) in a Quorum-Q150 to minimize electron charging effects. SEM images were acquired using an in-column (Trinity) detector at an accelerating voltage of 1.0 kV . SEM-EDX data were acquired using an X-Flash silicon drift detector (Bruker) at an accelerating voltage of 20 kV.

High-angle annular dark-field scanning transmission electron microscopy (HAADF-STEM) imaging and corresponding STEM-EDX spectroscopy were performed on a FEI Titan Themis 60-300 operated in scanning mode at an accelerating voltage of 200 kV. This microscope is equipped with a high brightness X-FEG gun and four silicon drift Super-X EDX detectors...Sample preparation for STEM measurements was done using ultramicrotomy. A resin-embedded composite was serially sectioned in ~60 nm thick slices that were deposited on a TEM grid with an ultrathin carbon support film.

Attenuated Total Reflection Infrared Spectroscopy. ATR-IR spectra were collected using a Perkin-Elmer Frontier MIR/FIR spectrometer equipped with a Quest ATR attachment. The sample was pressed on a diamond window and the spectra were recorded between 4000 and 400 cm^{-1} at a resolution of 4 cm^{-1}.

Thermogravimetric Analysis. The thermogravimetric analysis curve was obtained using a TA Q-Series TGA Q500. Samples were loaded onto a tared platinum pan. The balance flow rate was at 10 mL/min with nitrogen and the sample flow rate was at 25 mL/min with air heating at a rate of 5 °C per minute.

Matrix-assisted Laser Deposition/Ionization Time of Flight Spectroscopy. For polymer characterization matrix-assisted laser desorption/ionization time of flight mass spectrometry (MALDI-TOF-MS) analysis was performed using a Bruker Microflex. Composites were digested in a 15 mL 4M HCl solution with 2:1 water to methanol ratio. A 10 mg/ml DHB (2,5-dihydroxybenzoic acid) matrix consisting of H_2O/acetonitrile/trifluoroacetic acid with a 49.9/50/0.1 ratio was mixed with the solution of the digested composite, previously diluted 100 times, at a 1 to 1 ratio. 2 uL

was drop casted onto a sample plate and allowed to dry in air completely. The mode was set to linear with a positive polarity and scanning range of 400-1500 m/z.

General Metal Ion Capture Experiments

Metal concentrations in aqueous solutions were determined using an Agilent 5110 synchronous vertical dual view ICP-OES or a Perkin-Elmer NexIon 350 D ICP-MS for ultra low concentrations. All samples were acidified to either a 2% HCl solution for Au or a 2% HNO_3 solution for all other metals before analysis. Up to five wavelengths were chosen for ICP-OES analysis and averaged. All ICP standards were bought from Roth. Rhone river water was collected in Sion, Switzerland (Latitude: 46.228332, Longitude: 7.369975) and Mediterranean Sea water was collected in Nice, France (Latitude: 43.694937, Longitude: 7.27655).

Batch Heavy Metal Removal Experiments. Removal capacities were compared at varying concentrations. Different concentrations of the desired metal salts were prepared using distilled water, water from the Rhone river and water from the Mediterranean Sea. About 10 mg of MOF/Polymer sample were added to 20 mL of the solution and the vials were placed in a Thermo Scientific MaxQ4450 Orbital Shaker for 24 hours at 200 rpms and held at a constant temperature of 28 °C. The samples were filtered using a 25 mm hydrophilic PTFE membrane syringe filter with 0.22 µm pores to remove any solids and elemental analysis was carried out on the remaining aqueous media. After the analysis, Q_e, the amount of metal removed per gram of composite (mg/g), was calculated using the following equation:

$$Q_e = \frac{C_o V - C_e V}{m}$$

where, C_o is the initial concentration, C_e is the end concentration, V is the volume of the simulated contaminated water, and m is the mass of the composite.

For the pH study, the pH was adjusted using 0.02M aqueous solutions of HCl or NaOH. 10 mg of MOF/Polymer sample was added after a desired pH was reached and the pH was remeasured. Samples were also placed in a thermo scientific maxQ4450 orbital shaker at 420 rpms and held at a constant temperature of 28 °C. All samples were allowed to shake for 24 hours to allow equilibrium. Afterwards the solutions were filtered using a 25 mm hydrophilic PTFE membrane syringe filter with 0.22 µm pores to remove any solids for subsequent elemental analysis.

Rate of Removal. Various vials containing 20 mL of a specific concentration of the desired metal ion were treated with ~10 mg of MOF/Polymer sample. At each time point, the samples were filtered using a 25 mm hydrophilic PTFE membrane syringe filter with 0.22 µm pores to remove any solids for elemental analysis of the aqueous media. After analysis, the percent removal was calculated using the following equation:

$$Percent\ Removal\ \% = \frac{C_o - C_e}{C_o} x100$$

where, C_o is the initial concentration and C_e is the end concentration.

Regeneration. Regeneration of the materials was investigated using reagents such as EDTA (ethylenediaminetetraacetic acid) $^{+}$ and ascorbic acid. For this experiment, 0.500 g of Fe-BTC/PDA-19 was added to a concentrated solution of the desired metal ion to saturate the samples. After 24 hours, the samples were filtered, dried, and weighed. The metal concentrations in the aqueous media were analyzed and the values were used to calculate the capacity value Q_e (mg/g). The samples were added to 0.001M solutions of EDTA and Ascorbic acid and allowed to shake at 200 rpms for 4 hours. The samples were filtered, washed with methanol, dried and weighed. The EDTA regeneration solution was made into a 2 % HNO_3 solution for analysis to obtain the metal concentration to calculate the % recovery of metal. The regenerated materials were then added to 1000 ppm solutions of desired metal ion. This procedure was repeated 3 more times to obtain the capacity Q_e (mg/g) for each of the 4 cycles.

***k_d,* Distribution Coefficient.** We obtained the k_d values by immersing the MOF/Polymer composite in aqueous media with a specific metal concentration at 200 rpms and at a temperature of 28 °C for 24 hours. The samples were filtered using a 25 mm hydrophilic PTFE membrane syringe filter with 0.22 µm pores to remove any solids for elemental analysis of the aqueous media. After the analysis, k_d, the distribution coefficient was calculated using the follow equation:

$$\boldsymbol{k_d = \frac{C_o - C_e}{C_e}\left(\frac{V}{m}\right)}$$

where, C_o is the initial concentration, C_e is the end concentration, V (mL) is the volume of the solution and m (g) is the mass of the composite.

Gold Concentration. Regeneration of the composite was investigated using ascorbic acid for the reduction of imines to amines. For this experiment 50 mg of MOF/Polymer was exposed to 20 mL of a Rhone river water solution spiked with 10 ppm of Au^{3+} for 5 minutes. After exposure the sample was centrifuged and the solution was filtered using a 25 mm hydrophilic PTFE membrane syringe filter with 0.22 um pores. This process was repeated for 10 batches. After a clear reduction in removal efficiency the composite was soaked in 50 mL of a 0.002M solution of ascorbic acid for 4 hours, washed with ethanol and then was exposed to another 10 batches. This protocol was repeated for a total of 31 batch exposures.

Gold Extraction from Electronic Waste and Incinerated Ash. Electronic waste was obtained from the EPFL IT department and incinerated ash from sludge was obtained from the Swiss Federal Institute of Aquatic and Science Technology. The CPU, which contains Cu, Ni and Au confirmed by SEM-EDX was separated from the motherboard and the surface was scratched using a Fehlmann Picomax 20 table drill to obtain metal scraps. Au was then leached from the resulting metal powder using a facile method that has been previous reported. The leaching solution was prepared by mixing 119.034 mL of distilled water with 0.966 µL of pyridine (100 mM) and 0.750 g of NBS (35 mM). 0.30 g of the electronic waste or incinerated ash were then added to the leaching solutions and allowed to sit for 24 hours. Within hours the leeching solution changed from clear to a blue solution and was acidified for subsequent elemental analysis. After the metal concentrations of Cu, Ni and Au were determined 0.030 g of Fe-BTC/PpPDA was added to 20 mL of the leaching solution and until equilibrated. The blue solution was filtered using a 25 mm hydrophilic PTFE membrane syringe filter with 0.22 µm pores to remove any solids for subsequent elemental analysis.

Gold Purification. The MOF/Polymer sample was soaked in a highly concentrated simulated electronic waste leaching solution until equilibrated and the resulting powder underwent PXRD to confirm the presence of neutral state Au. The mother liquor was filtered using a 25 mm hydrophilic PTFE membrane syringe filter with 0.22 µm pores to remove any solids for subsequent elemental analysis to determine how much gold was extracted. 50 mg of the resulting composite/Au powder was then loaded in an MTI OTF-1200X tube furnace and heated to 900 °C at a ramp of 30 °C per minute in air. The temperature was held for 2 hours and then allowed to cool to room temperature. The brown powder was transferred to a vial and 10 mL of concentrated HCl was added. The vial

was loaded into a thermo scientific maxQ4450 orbital shaker at 420 rpms and held at a constant temperature of 28 °C for 24 hours. The Au particles were separated from the yellow acidic solution, soaked in a fresh batch of concentrated HCl. The sample was allowed to shake at 420 rpms at a constant temperature of 28 °C for another 12 hours. The Au particles were then separated from the clear acidic solution and washed with distilled water 3 times. PXRD was performed to confirm neutral state gold. The purified Au was then dissolved in aqua regia and underwent subsequent elemental analysis to determine the purity.

“I don’t know why... but sometimes... I find myself wishing this journey could go on forever… and at the same time I know that can never happen.”

APPENDIX to Chapter 2

H[1] NMR of Free Base Dopamine

Free base dopamine was dissolved in deuterated methanol and analyzed using a Bruker AVDHD 400 MHz 9.5 T NMR and a 5 mm BBFO liquid probe. After 128 scans, the proton NMR spectrum was integrated using Maestro NMR analysis software[191].

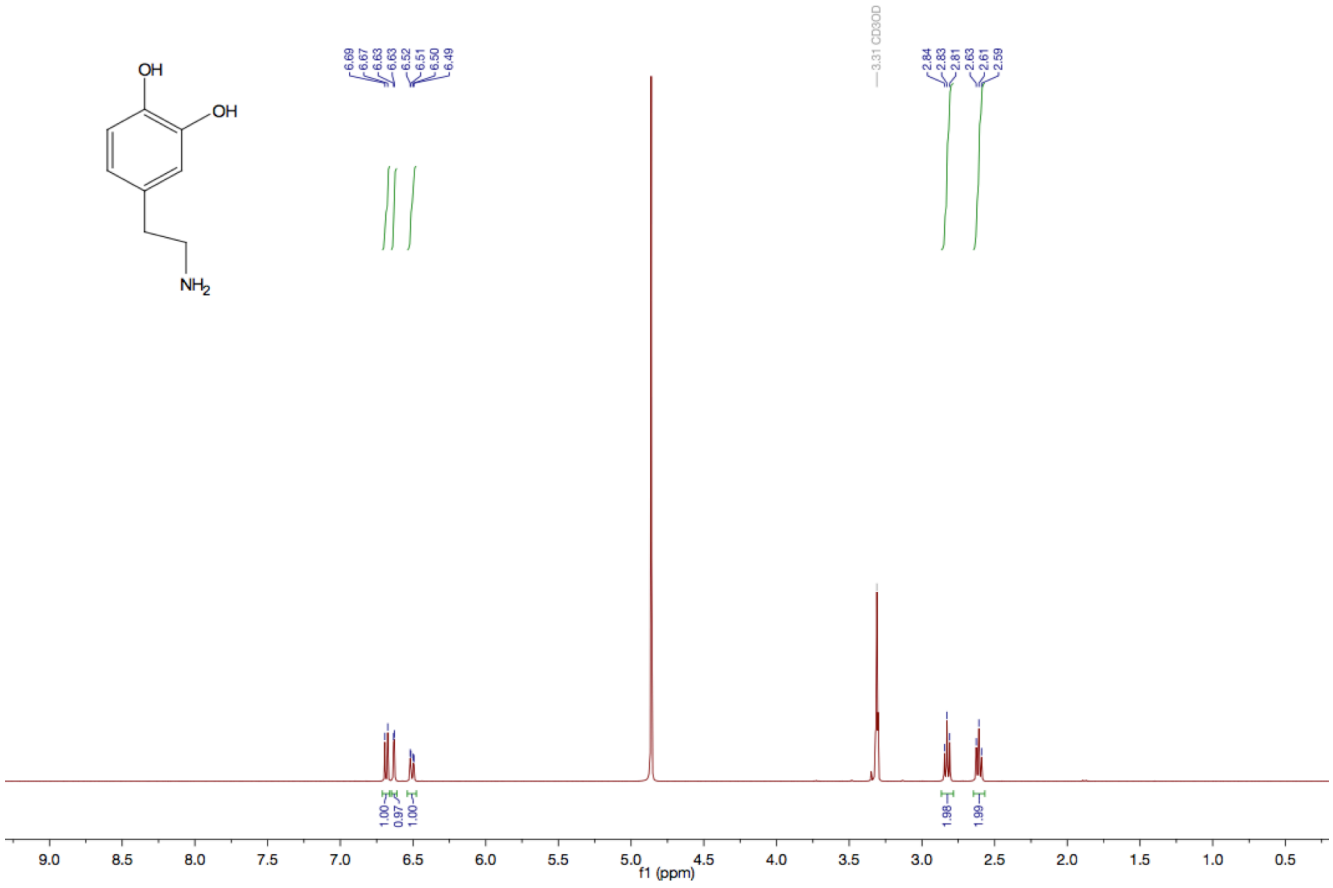

Figure 2.1. [1]H NMR spectrum of the as synthesized free base dopamine.

In-Situ FT-IR with CO

In-situ IR data was collected in transmission mode on samples mounted on a self-supported wafer using a custom-built infrared cell and a Harrick Scientific Praying Mantis on a PerkinElmer Frontier Spectrometer at -123 °C. Before measurements, the samples of Fe-BTC and Fe-BTC/PDA were activated overnight at 150 °C and 125 °C, respectively, while all under dynamic vacuum. After cooling down, the sample cell was purged with Argon for half an hour and then cooled to -123 °C. The background was collected and CO was then charged into the sample cell. The background subtracted *in-situ* DRIFTS spectra were collected for Fe-BTC/PDA-42, Fe-BTC/PDA-38, Fe-BTC/PDA-28, Fe-BTC/PDA-19, and Fe-BTC at -123 °C (with a CO equilibrium pressure of 125, 46, 173, 103, and 650 mbar respectively). The observed changes in intensity with increased dopamine loading imply that the metal sites are being blocked by polymer.

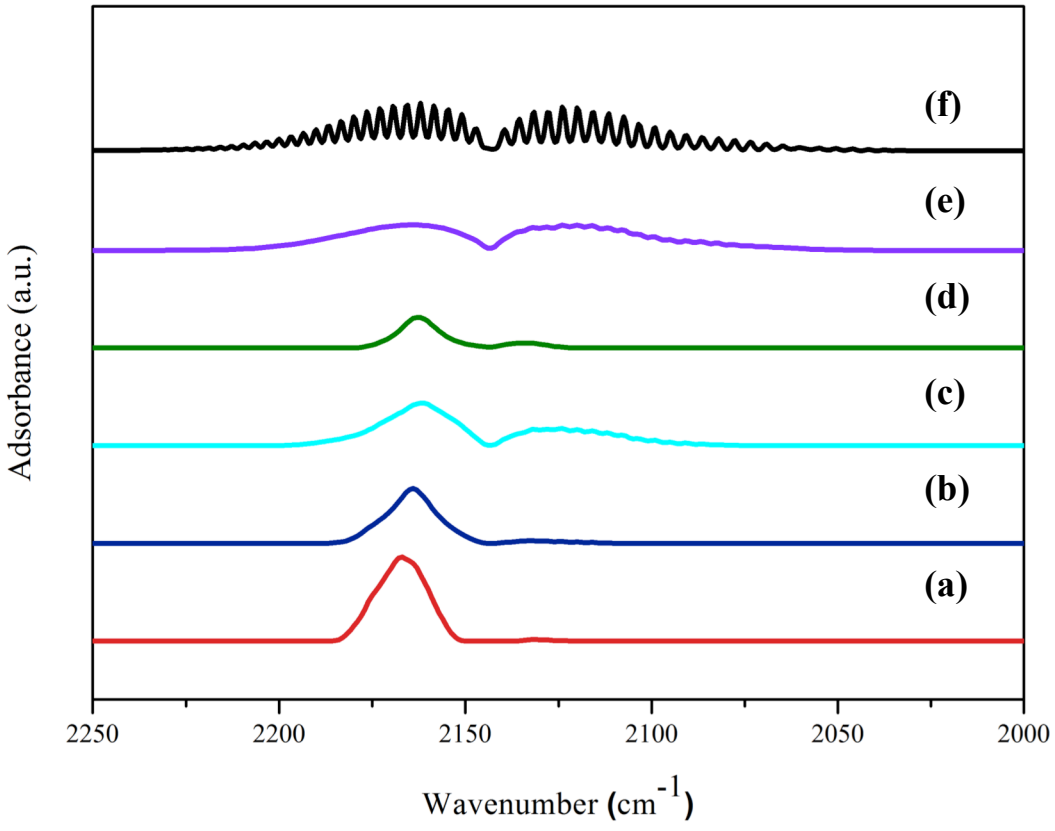

Figure 2.2. *In-situ* FT-IR drift with CO. (a) Fe-BTC (b) Fe-BTC/PDA-19 (c) Fe-BTC/PDA-28 (d) Fe-BTC/PDA-38 (e) Fe-BTC/PDA-42 (f) Free CO

Long-term stability of Fe-BTC/ PDA

Stability of Fe-BTC/PDA was assessed using synchrotron powder x-ray diffraction, MALDI and ICP-OES. Samples were first soaked in water from the Rhone River with and without lead and mercury contamination (approximate concentration = 1 and 1000 ppm) for 8 weeks at room temperature. The solutions were centrifuged at 7000 rpms and the isolated solids were dried overnight under vacuum. MALDI (see Fig. S6 for methods) analysis was done on the Rhone river water and Rhone river water with Fe-BTC/PDA to see if any polymer was leaching into solution. The MALDI spectra show no evidence of PDA in Rhone River water.

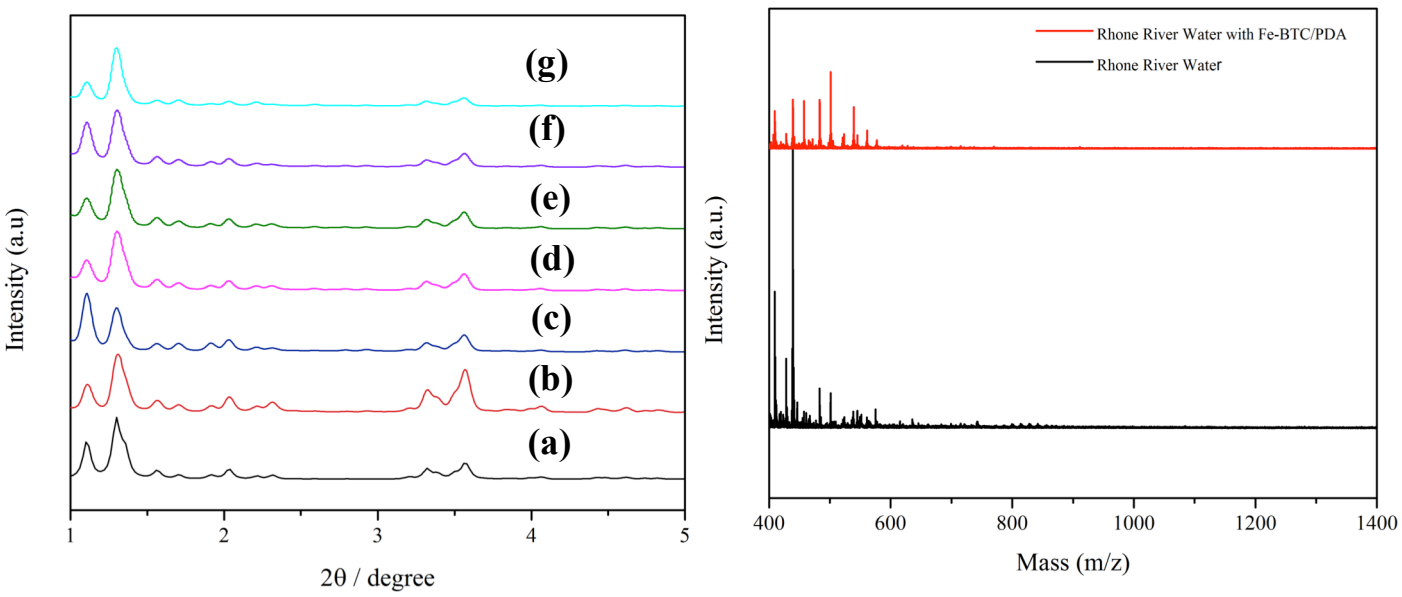

Figure 2.3. (left) Powder X-ray diffraction of (a) simulated, (b) Fe-BTC/PDA-19, (c) Fe-BTC/PDA-19 in river water, (d) Fe-BTC/PDA-19 in a 1 ppm Hg^{2+} solution, (e) Fe-BTC/PDA-19 in a 1 ppm Pb^{2+} solution, (f) Fe-BTC/PDA-19 in a 1000 ppm Hg^{2+} solution and (g) Fe-BTC/PDA-19 in a 1000 ppm Pb^{2+} solution. MALDI spectra (right) of Rhone River water (black) and Rhone River water with Fe-BTC/PDA soaked for 8 weeks illustrating no polymer leaching.

Attenuated Total Reflection Infrared Spectroscopy

ATR-IR spectra were collected using a Perkin-Elmer Frontier MIR/FIR spectrometer equipped with a Quest ATR attachment. The sample was pressed on a diamond window and the spectra were recorded between 4000 and 400 cm^{-1} at a resolution of 4 cm^{-1}. Three new peaks are observed for Fe-BTC/PDA compared to Fe-BTC. These signature stretches emerge at 1273 cm^{-1}, 806 cm^{-1} and 570 cm^{-1} and represent the C–O, C–N and O–H stretching modes in the polymer, respectively

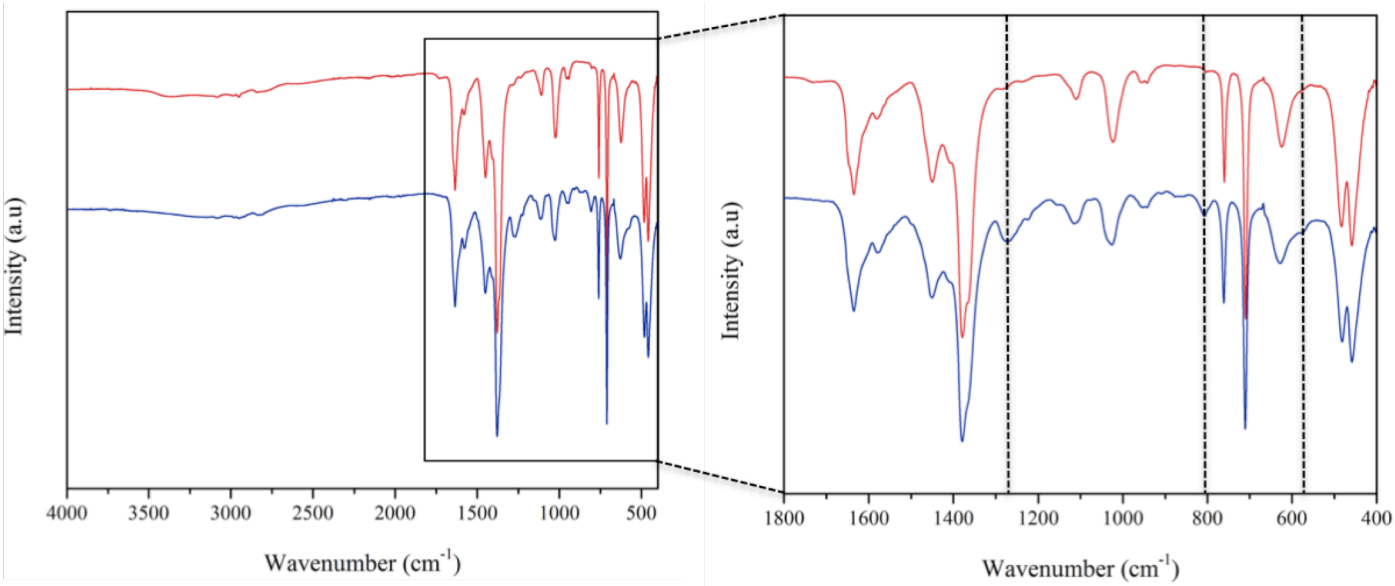

Figure 2.4. ATR spectrum of Fe-BTC (red) and Fe-BTC/PDA-19 (blue).

Thermogravimetric Analysis

The thermogravimetric analysis curve was obtained using a TA Q-Series TGA Q500. Samples were loaded onto a tared platinum pan. The balance flow rate was at 10 mL/min with nitrogen and the sample flow rate was at 25 mL/min with air heating at a rate of 1 °C per minute. The TGA for Fe-BTC/PDA illustrates a similar curve compared to Fe-BTC as well. The composite starts degrading at 250 °C and we observed a higher weight lost on the final transition indicating that we have added more organics to the system.

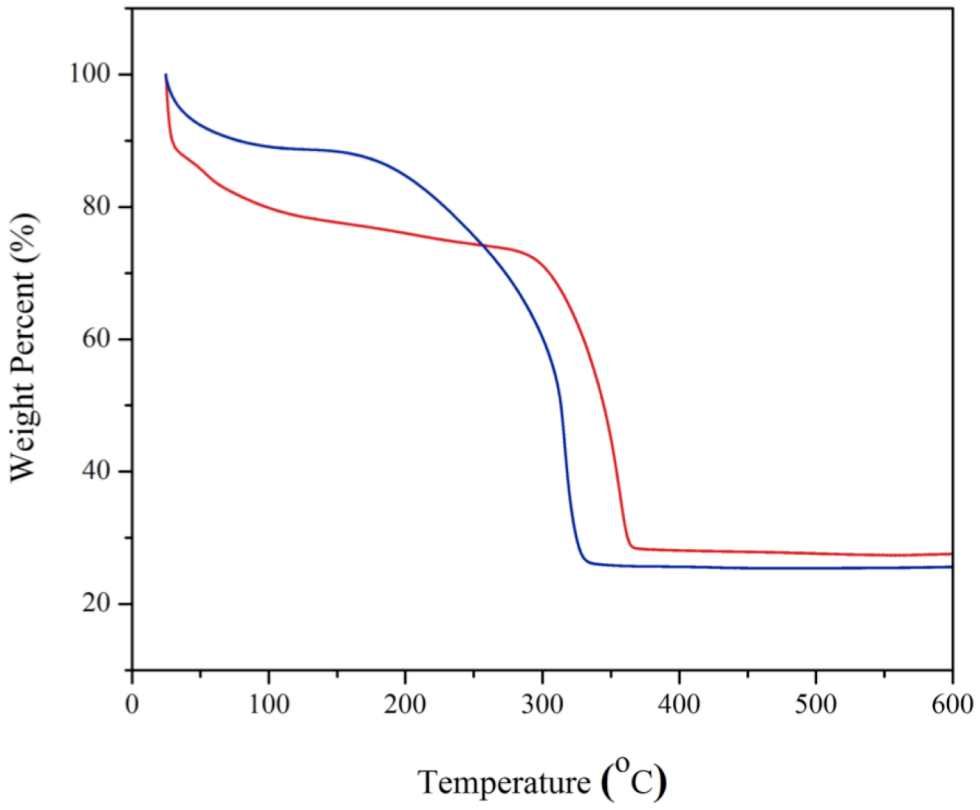

Figure 2.5. Thermogravimetric analysis curve of Fe-BTC (red) and Fe-BTC/PDA-19 (blue). The ramp rate was 1 °C per minute.

Polymer Characterization

Matrix-assisted laser desorption/ionization time of flight mass spectrometry (MALDI-TOF-MS) analysis was performed using a Bruker Microflex. 50 mg of Fe-BTC, Fe-BTC/PDA-19 and Fe-BTC/PDA-42 were soaked in 4M HCl solution (15 mL) and then 5 mL of methanol were added to the solution to dissolve the ligand. Then 1uL of the solutions were mixed with the following matrix: 1 uL of 2,5-dihydroxybenzoic acid H_2O/Acetonitrile/Trifluoroacetic acid (49.9/50/.1), and then the solutions were dried on a sample plate. The mode was set to linear with a positive polarity. The MALDI spectra of Fe-BTC/PDA-19 and Fe-BTC/PDA-42 illustrate the presence of PDA in solution that consists of as many as 7 monomeric units.

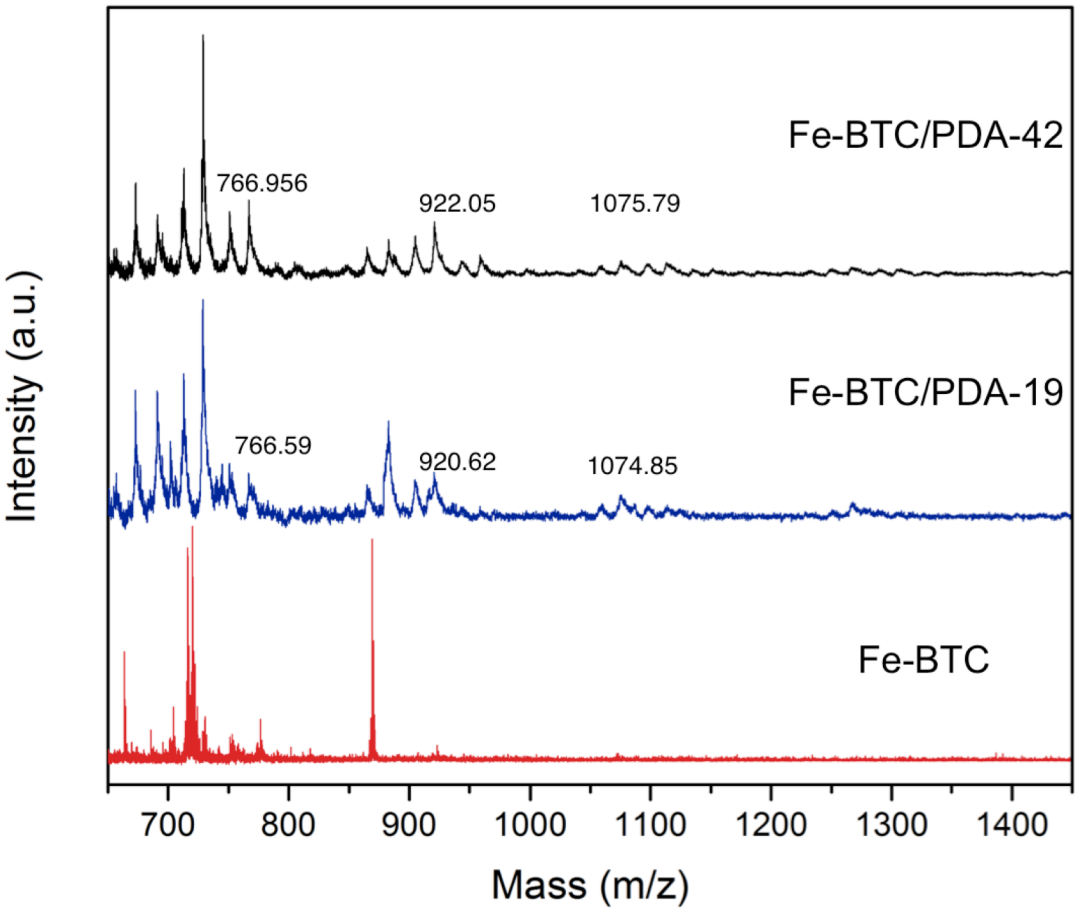

Figure 2.6. MALDL-TOF-MS spectra of Fe-BTC, Fe-BTC/PDA-19 and Fe-BTC/PDA-42 after destroying the materials in 4M HCl. The results indicate the polymerization of dopamine.

Scanning Electron Microscopy

Scanning Electron Microscopy (SEM) analysis was performed on a FEI Teneo at an accelerating voltage of 1.0 kV using a beam current of 13 pA. SEM images were acquired with an in-column (Trinity) detector. To minimize electron-charging effects, samples were sputter-coated with iridium (~ 7 nm thick) in a Quorum-Q150.

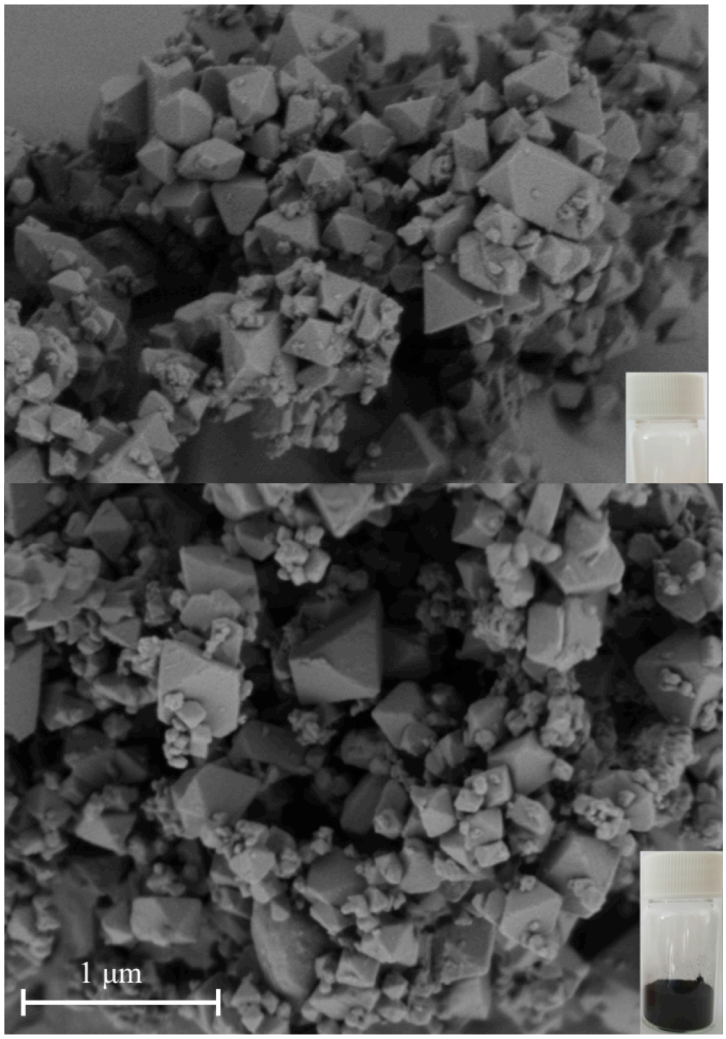

Figure 2.7. SEM images of Fe-BTC (top) and Fe-BTC/PDA-19 (bottom).

STEM-Electron-Dispersive X-ray Specytoscopy

Fe-BTC/PDA-19 was embedded in an epoxy resin and serially cut into 100 nm slices and deposited onto a TEM grid (see Methods) for elemental analysis using EDX.

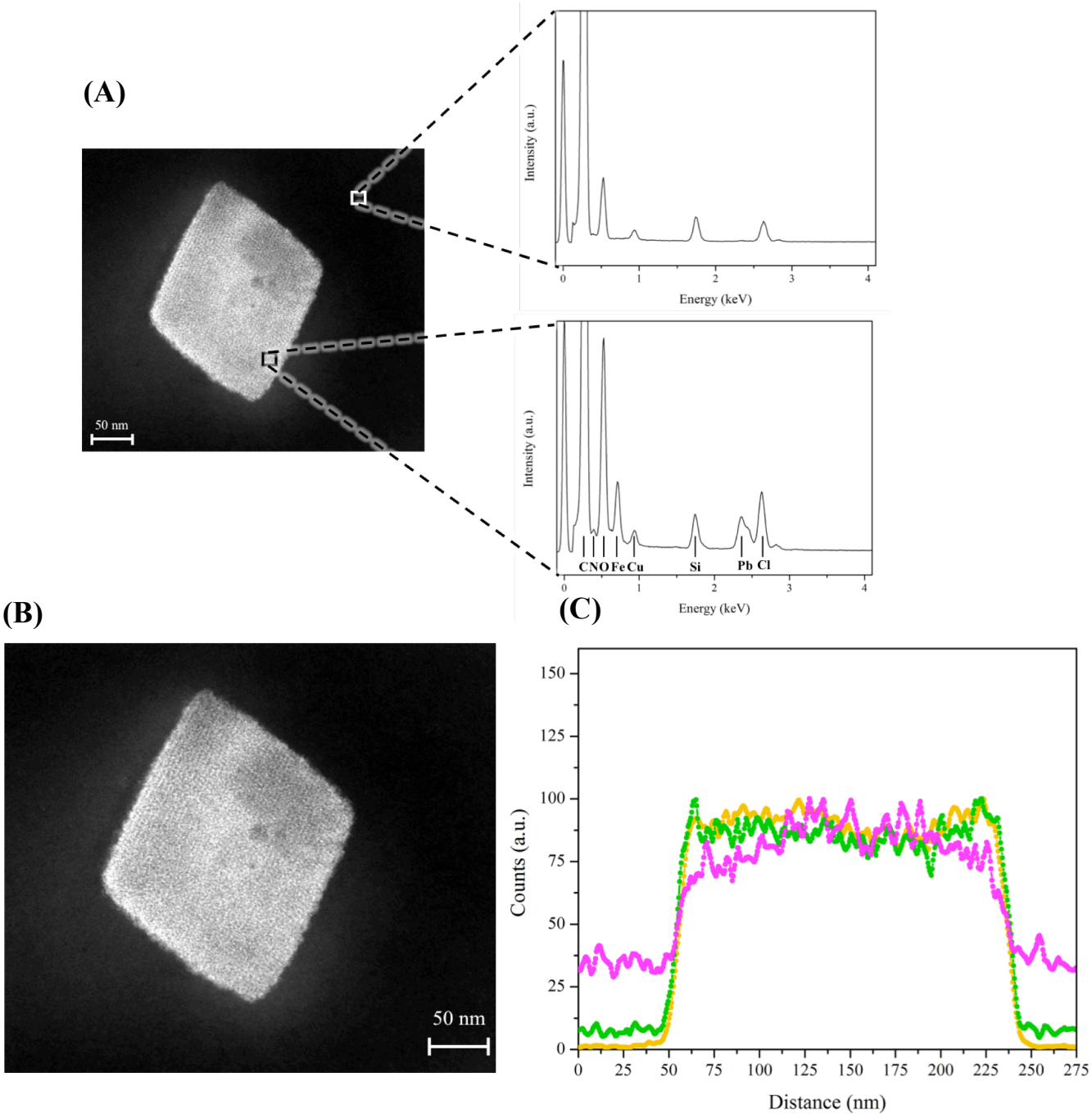

Figure 2.8. (a) HAADF-STEM image coupled with EDX spectra of the substrate and an Fe-BTC/PDA-19 crystallite. (b) Scanning transmission electron microscopy images coupled with energy-dispersive X-ray spectroscopy (collected for 1 hour) reveals the presence of Fe (yellow), N (purple) and Pb (green) along a 275 nm line across the Fe-BTC/PDA-19 crystallite.

STEM– Electron Energy Loss Spectroscopy

STEM-EELS measurements were done with a beam current of ~ 250 pA and mapping was performed using the "ultrafast" spectrum imaging mode over a region of 126 x 80 pixels and with a dwell time of 0.25 ms per pixel.

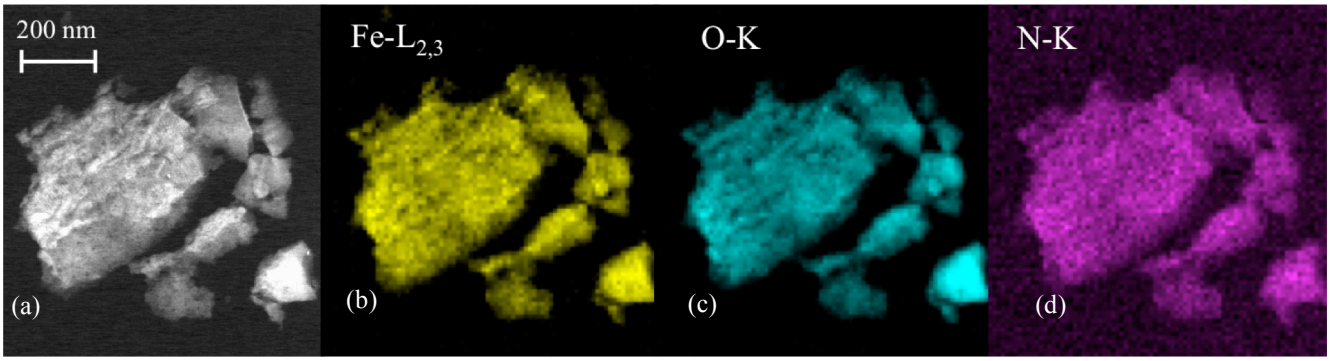

Figure 2.9. (a) HAADF-STEM image and corresponding EELS color-coded element mapping of (b) Fe, (c) O, and (d) N in selected Fe-BTC/PDA-19 particles.

Density Functional Theory Calculations

Density functional theory (DFT) calculations were used to elucidate the interactions between Fe-BTC and polydopamine. Since the unit cell of Fe-BTC is excessively large for periodic DFT calculations, we performed the calculations on a fragmented cluster of the MOF (Fig. S10). The structure of PDA is still under debate[192-193], therefore we chose a representative set of all possible structures (monomers) of PDA to investigate the feasible binding configurations of the polymer to the MOF internal surface (Table S2). In principle, the confined ligand environment alongside the Fe(III) open metal site can restrict the polymer confirmation. Consequently, for each structure in the set, additional aromatic unit(s) were appended to the PDA structure to mimic the steric effects of bulky polymer inside the confined pore. The energies were calculated using a plane wave basis set and projector augmented wave (PAW) pseudopotential as implemented in the Quantum-ESPRESSO package with PBEsol exchange-correlation functional and DFT-D2 corrections[194-195], which have shown good accuracy for metal-organic frameworks[196-198]. The simulation box size was set to $30\ \text{Å}$ ensuring isolated molecule simulation. In all calculations, the electronic structures were optimized using spin-polarized calculation at gamma point only and using a kinetic energy cutoff of 500eV or higher. Spin polarized calculations were performed optimizing the total magnetization of the system. The cluster of Fe-BTC and the PDA structures were optimized separately to calculate the ground state total energy of each derivative. Afterwards, each PDA structure was placed inside the simulation box together with the MOF cluster. The initial configuration illustrates that the binding site of the PDA structure is attracted to one of the open metal sites (Fig. S10). The Fe-BTC SBU's atoms were kept fixed from the previous optimized step whilst the PDA derivative was relaxed. In all structural optimizations, the quasi-Newtonian relaxation algorithm was used to reach convergence threshold for the total forces and energies lower than 0.5 kcal/mol.Å and 0.1 kcal/mol, respectively. The binding energies of each configuration were determined as the difference between the energy of later step and former one, as shown in the equation below.

$$\Delta E_{binding} = E_{MOF+PDA} - E_{MOF} - E_{PDA}$$

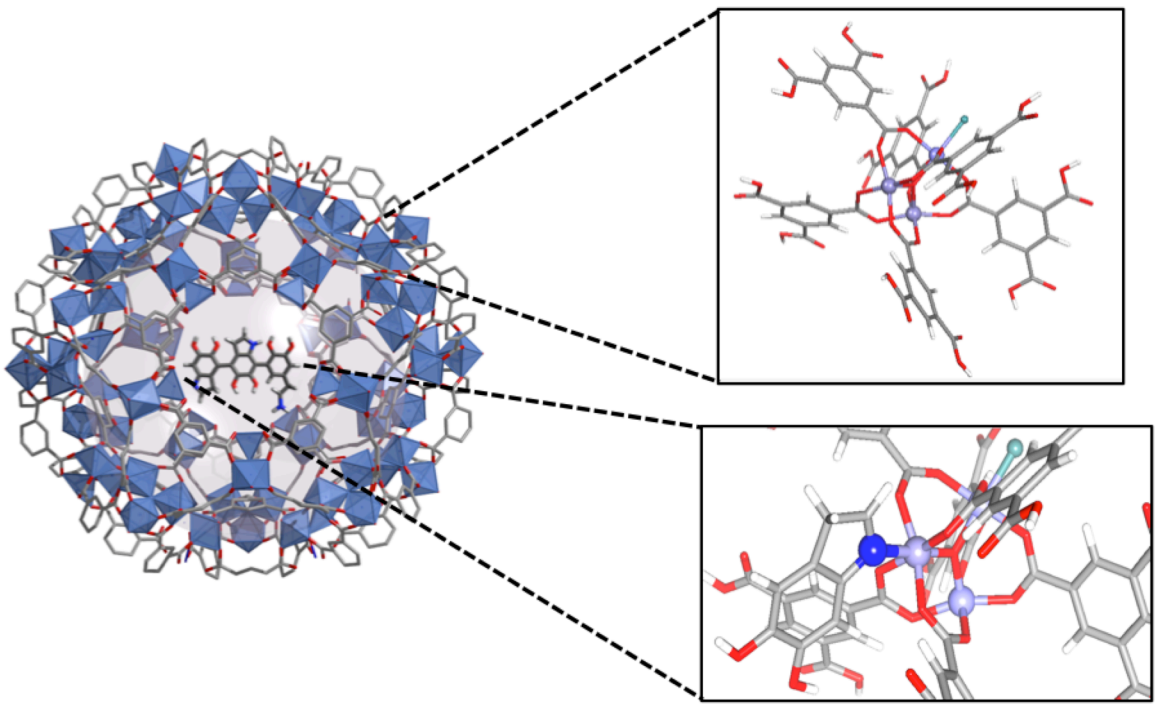

Figure 2.10. DFT calculations were carried out on a fragmented cluster of the MOF (top box). The binding energies and bond distances were calculated for various possible polydopamine structures. The values are represented in Table S2.

Raman and ATR-IR

ATR-IR was performed using the methods mentioned above. Raman spectroscopy was carried out using a Renishaw microscope, where the focused excitation light is collected in a back scattering configuration. The powder sample is loaded onto a translational stage of a Leica microscope equipped with a 50x objective, and the excitation is a laser diode of 633 nm at 1% power (115 mW) to prevent degradation of the sample. The spectra were collected from 400 cm^{-1} to 900 cm^{-1} with a 25 second acquisition time. All experiments were conducted at room temperature and in air. Peaks associated with the polymer interacting with the Fe^{3+} along the pore surface are observed in both spectroscopy experiments shown below.

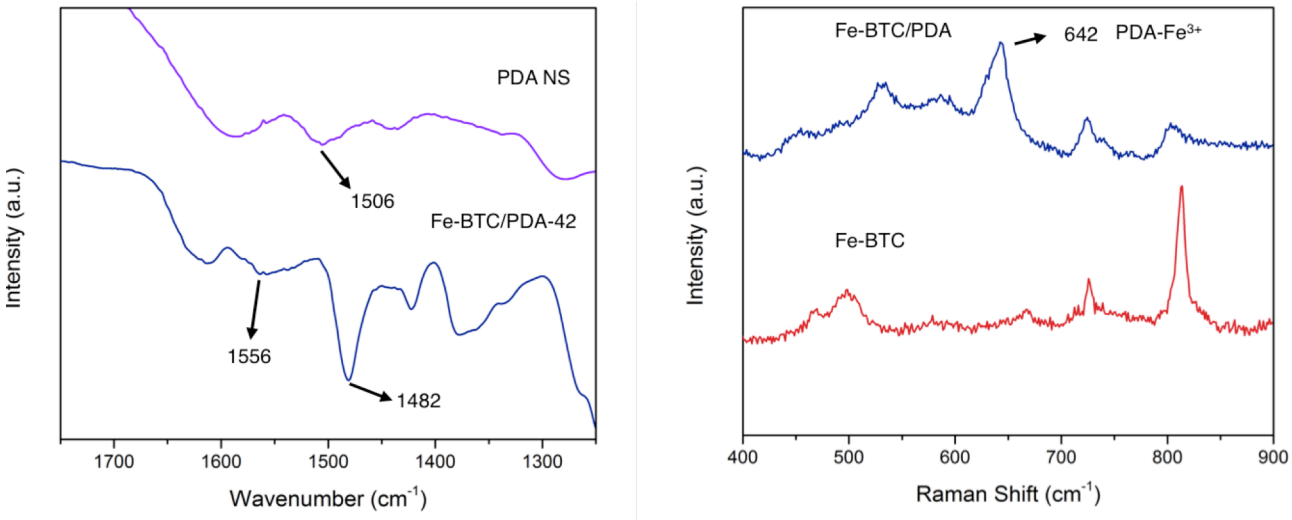

Figure 2.11. ATR-IR spectra (left) of PDA nanospheres (purple) and FeBTC/PDA-42 (blue) and Raman Spectra (right) of Fe-BTC (red) and Fe-BTC/PDA-42 (blue).

Prussian Blue Test

Colorimetric Prussian blue tests were performed on the bare framework and the composite (Fig. S10). The a 10 mL aqueous solution was created by mixing 1 mg of $FeCl_3$ and 2 mg of $K_3Fe(CN)_6$ giving a yellow liquid. Roughly 5 mg of Fe-BTC and Fe-BTC/PDA-19 were added to separate 1 mL solutions with Fe-BTC/PDA-19 solution turning blue instantly indicative of free catechols present. Fe-BTC and Fe-BTC/PDA soaked in a Hg^{2+} solution gave negative results.

Figure 2.12. Prussian blue test of Fe-BTC (left) and Fe-BTC/PDA-19 (middle) and FeBTC/PDA-19 soaked in a Hg solution (right). The change in color from yellow to blue illustrates free catechols throughout the composite.

Initial Screening for Removal of Hg, Pb, As, Cr, and Cd

Fe-BTC and Fe-BTC/PDA-19 were screened in water solutions containing the nefarious five (Hg, Pb, As, Cr, Cd). First, 1 ppm solutions were prepared for each of the metal salts. Next, ~10 mg of Fe-BTC or Fe-BTC/PDA-19 were added to 20 mL of the aforementioned solutions. The vials were placed in a Thermo Scientific MaxQ4450 Orbital Shaker for 24 hours at 200 rpms and held at a constant temperature of 28°C. The samples were filtered to remove any solid for subsequent elemental analysis of the aqueous media. Fe-BTC/PDA-19 illustrates a significance increase in capacities for all cases except hexavalent chromium and reduces the concentration of Hg^{2+} and Pb^{2+} to drinkable levels below the EPA limit respectively. As such, Hg^{2+} and Pb^{2+} were chosen for further investigation.

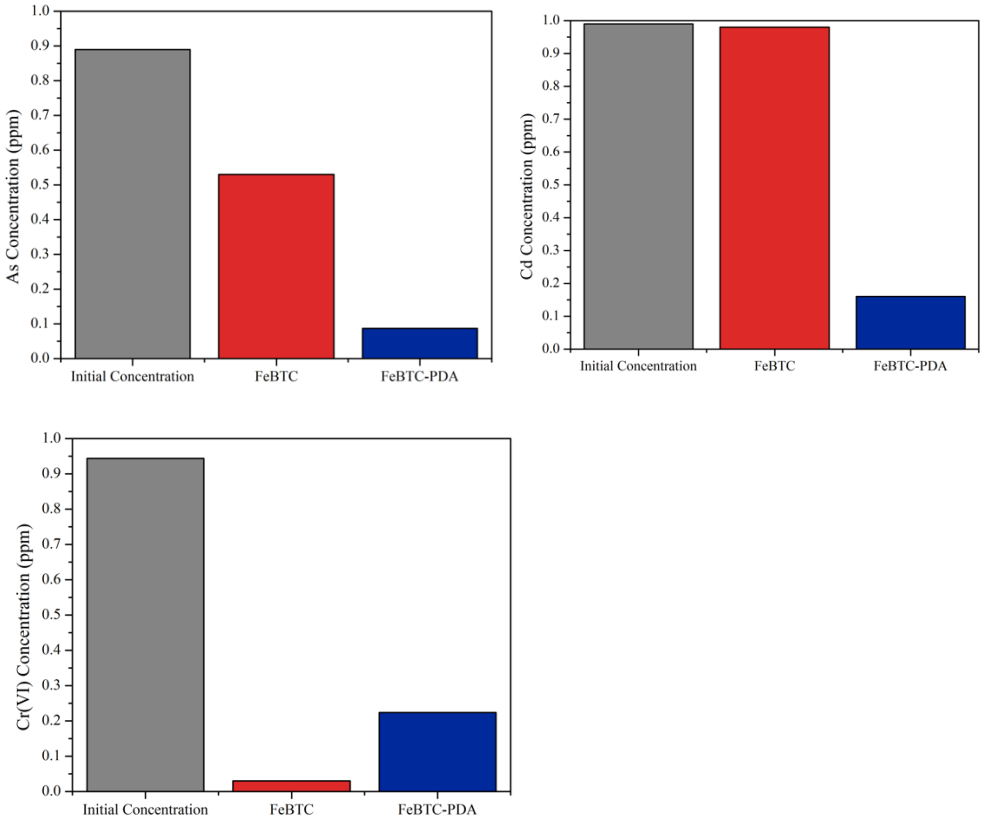

Figure 2.13. Screening of the nefarious five, (top, left) As, (top, right) Cd, or (bottom, left) Cr. Approximately 1 ppm solutions were treated with Fe-BTC (red) and Fe-BTC/PDA-19 (blue). The concentrations were measured before (grey) and after treatment with the bare framework and the composite.

Kinetic Model

Various vials containing 20 mL of 1.8 ppm millipore water solutions of Pb^{2+} were treated with ~20 mg of Fe-BTC/PDA between 0 and 60 seconds. At each time point, the samples were filtered using a 25 mm hydrophilic PTFE membrane syringe filter with 0.22 µm pores to remove any solids for elemental analysis of the aqueous media. Experimental data was fitted with a pseudo-second-order kinetic model[138] shown below.

$$\frac{t}{q_t} = \frac{1}{k_2 q_e^2} + \frac{t}{q_e}$$

where, k_2 (g mg^{-1} min^{-1}) is the rate constant, q_t (mg/g) is the amount adsorbed at time (min) and q_e (mg/g) is the amount adsorbed at equilibrium). The R^2 value of 0.99998 was obtained. The rate constant k_2 was calculated to be 216.7 g mg^{-1} min^{-1}.

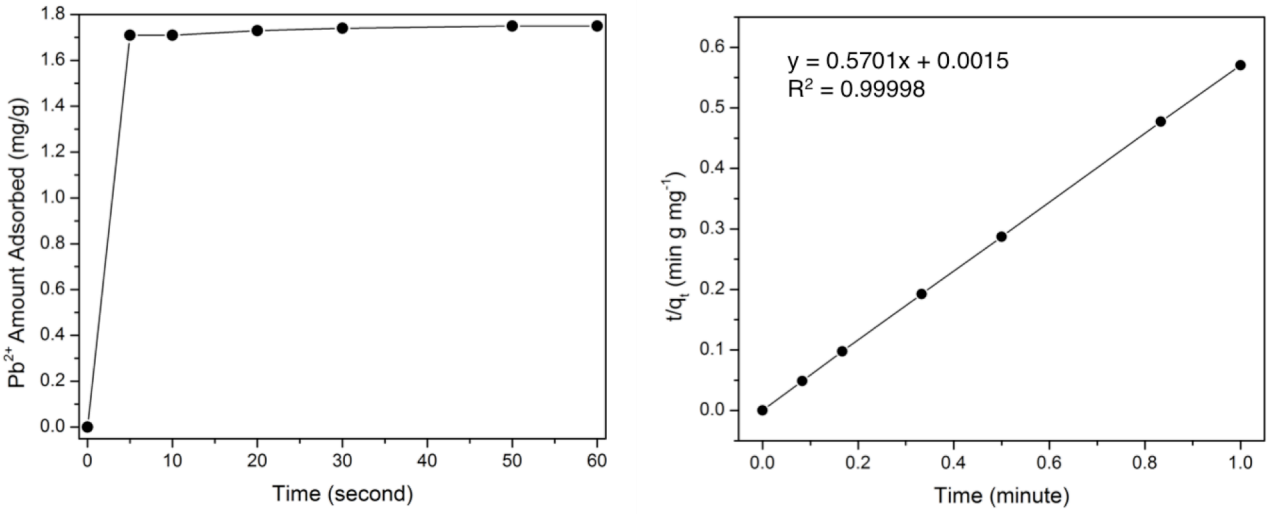

Figure 2.14. Adsorption kinetics of Pb^{2+} between 0 and 60 seconds (left) obtained from a starting concentration of 1.8 ppm. The data was fit using a pseudo-second-order kinetic model (right).

Batch Adsorption Experiments

Fe-BTC and Fe-BTC/PDA were soaked in distilled water and Rhone River water spiked with varying concentrations of Hg^{2+} and Pb^{2+} (See methods for experimental details). We observe an enhancement for Fe-BTC/PDA's ability to reduce the concentration of heavy metals compared to Fe-BTC.

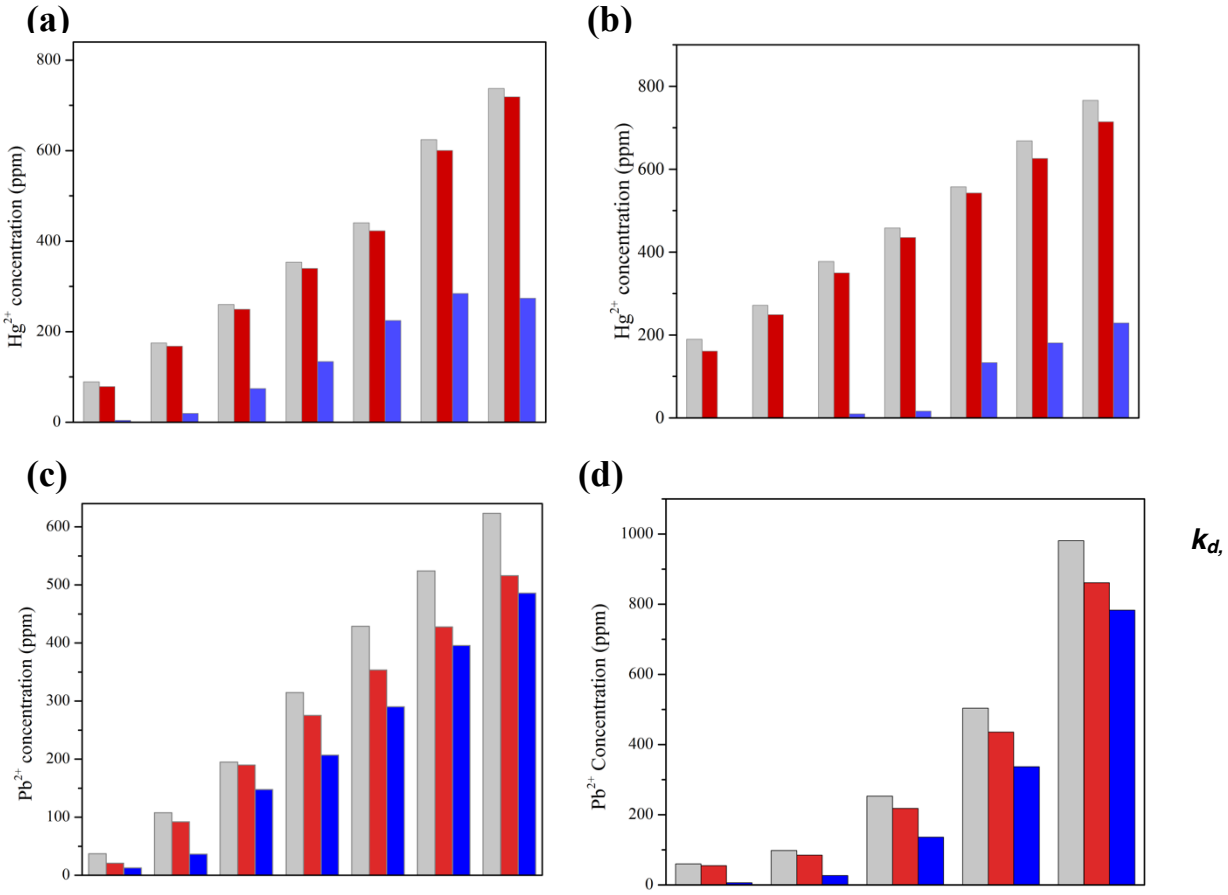

Figure 2.15. Batch capacity experiments illustrating the removal of Hg^{2+} from (a) distilled water and (b) Rhone River water and Pb^{2+} from (c) distilled water using FeBTC (red) and Fe-BTC/PDA-19 (blue). Batch capacity experiments illustrating the removal of Pb^{2+} from (d) distilled water using Fe-BTC (red) and Fe-BTC/PDA-42 (blue). The grey bars represent the starting concentration of mercury or lead.

Distribution Coefficient

We obtained the k_d values by immersing and shaking 10 to 45 mg of Fe-BTC/PDA-19 in 1 ppm 1000 mL and 500 mL aqueous solutions of Pb^{2+} and Hg^{2+} at 200 rpms and at a temperature of 28 °C for 24 hours. The samples were filtered using a 25 mm hydrophilic PTFE membrane syringe filter with 0.22 µm pores to remove any solids for elemental analysis of the aqueous media. After the analysis, k_d, the distribution coefficient was calculated using the follow equation:

$$k_d = \frac{C_o - C_e}{C_e}\left(\frac{V}{m}\right)$$

where, C_o is the initial concentration, C_e is the end concentration, V (mL) is the volume of the solution and m (g) is the mass of the composite.

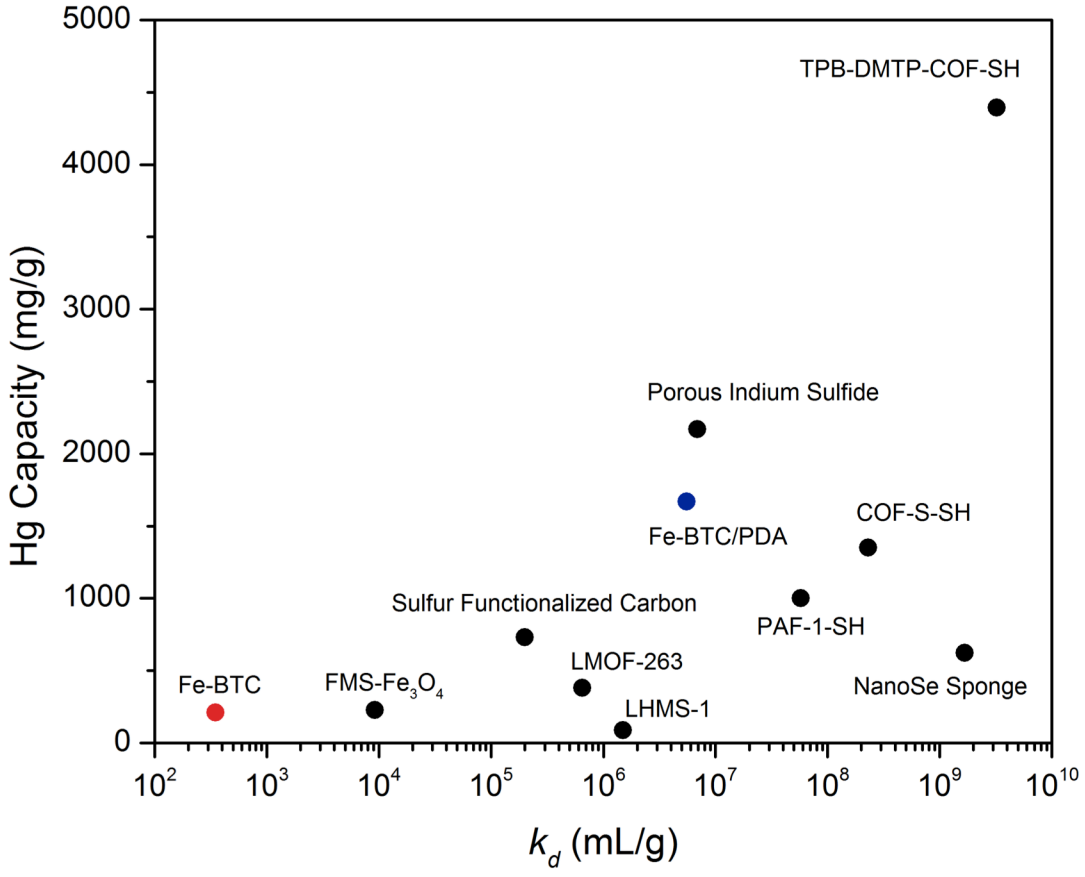

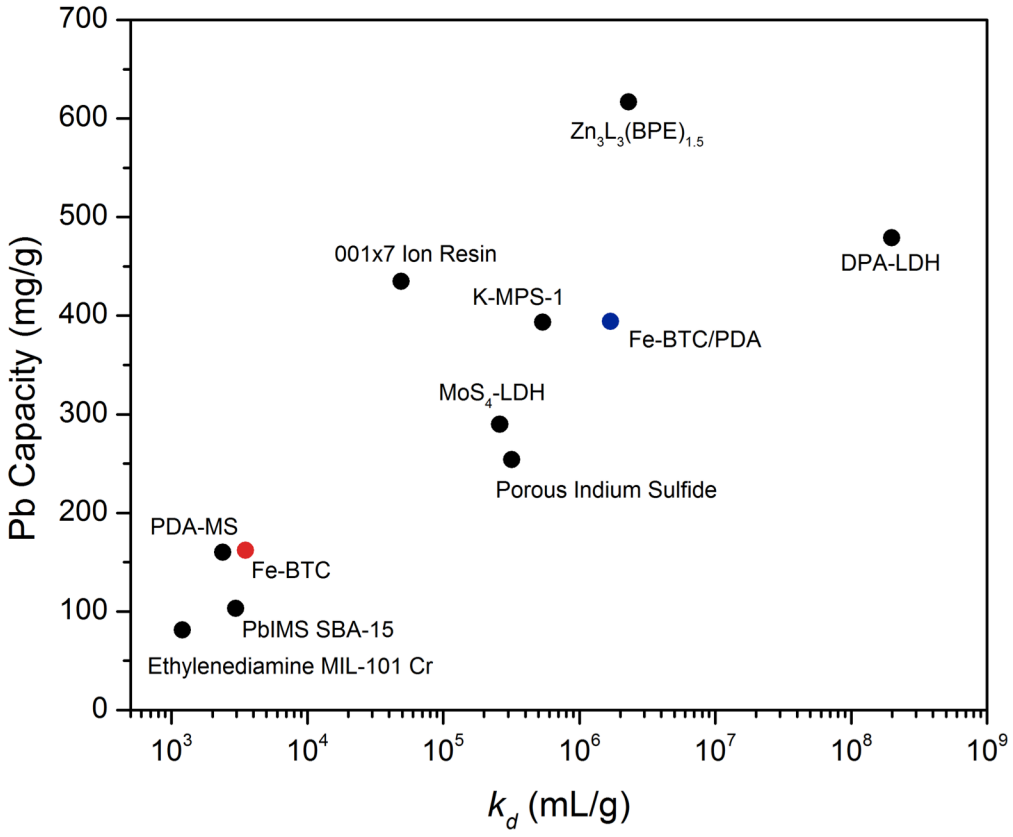

Figure 2.16. The calculated distribution coefficient value, k_d and removal capacities of Fe-BTC/PDA in (top) Hg^{2+} and (bottom) Pb^{2+} solutions are compared to those of other benchmark materials[5-22].

Heavy Metal Removal Experiments with humic acid

The quality of the material was tested in the presence of a common organic interferent, humic acid. Solutions with Pb^{2+} and Hg^{2+} concentrations ranging from 200 to 900 ppm and approximately 100 ppm of humic acid were prepared using distilled water. About 10 mg of Fe-BTC/PDA-19 or Fe-BTC/PDA-42 were added to 20 mL of the solution and the vials were placed in a Thermo Scientific MaxQ4450 Orbital Shaker for 24 hours at 200 rpms and held at a constant temperature of 28 °C. The samples were filtered using a 25 mm hydrophilic PTFE membrane syringe filter with 0.22 µm pores to remove any solids for elemental analysis of the aqueous media.

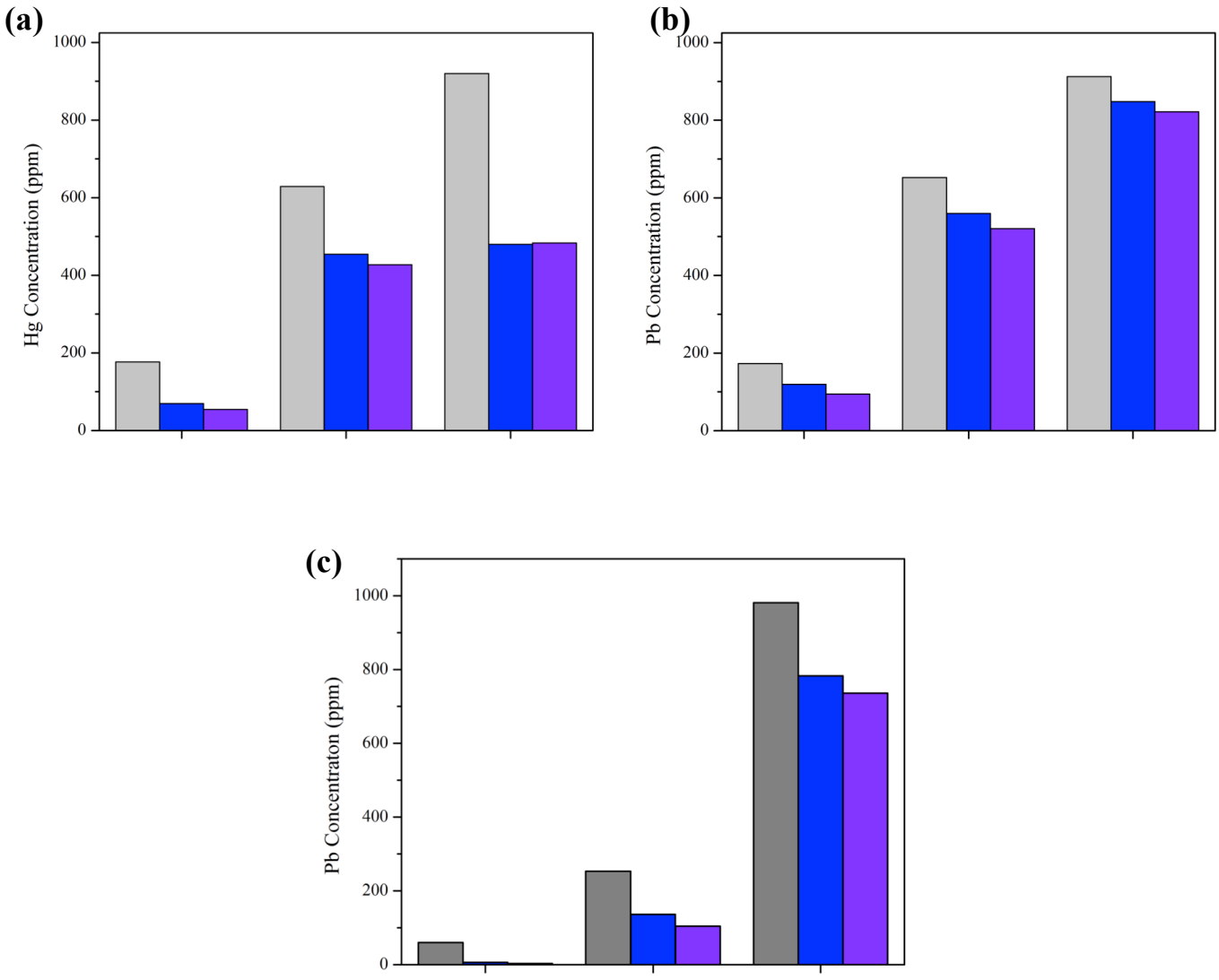

Figure 2.17. Bar plots showing (a) Hg^{2+} and (b-c) Pb^{2+} removal from distilled water and distilled water spiked with 100 ppm humic acid. Plots (a) and (b) were treated with Fe-BTC/PDA-19 while plot (c) is treated with Fe-BTC/PDA-42. The initial metal concentration is shown in grey and the final concentration after treatment with composite in distilled water and distilled water spiked with 100 ppm humic acid, is shown in blue and purple, respectively. No decrease in capacities is observed indicating no fouling.

pH Study

The elevated capacities observed in the Rhone river compared to distilled water is likely due to elevated pH in the fresh water source. Therefore, the effect of pH on the capacities of the material was evaluated. The pH was measured using a Hanna instruments Edge Multiparamter HI2020 pH meter. Solutions with concentrations of randing from 10 to 1000 ppm Hg^{2+} and Pb^{2+} were prepared and the pH was adjusted using 0.02M aqueous solutions of HCl and NaOH. About 10 mg of Fe-BTC/PDA-19 were added after a desired pH was reached and the pH was remeasured. The vials were placed in a Thermo Scientific MaxQ4450 Orbital Shaker for 24 hours at 200 rpms and held at a constant temperature of 28 °C. The samples were filtered using a 25 mm hydrophilic PTFE membrane syringe filter with 0.22 µm pores to remove any solids for elemental analysis of the aqueous media. It was observed that a higher initial pH will increase the capacities for both Hg^{2+} and Pb^{2+}. It should be noted that pH values below 3 lead to a decomposition of the MOF and at pH values above 8 to a precipitation of the metal salts. As such, the activity was only probed between 3 -7 for both Pb^{2+}, and Hg^{2+}.

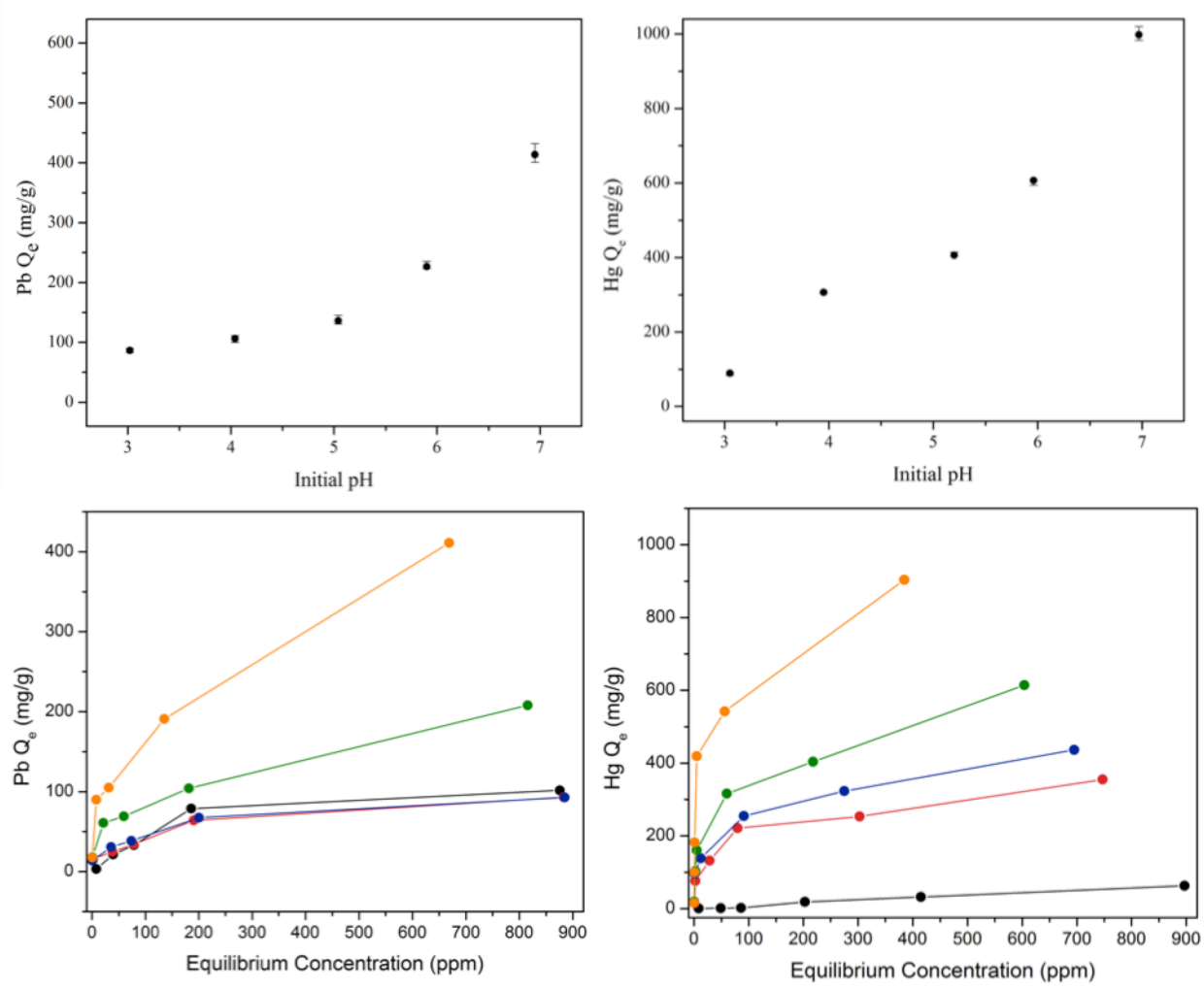

Figure 2.18. Scatter plots showing Pb^{2+} (left) and Hg^{2+} (right) capacities (Q_e, mg/g) at pH values 3 (black), 4 (red), 5 (blue), 6 (green) and 7 (orange).

Recovery of Lead

Regeneration of the composite for Pb^{2+} was achieved using the reagent EDTA (ethylenediaminetetraacetic acid). For this experiment, 0.500 g of Fe-BTC/PDA-19 was added to 1000 ppm 1 liter aqueous solutions of Pb^{2+} to saturated the samples. After 24 hours, the samples were filtered, dried, and weighed. The Pb^{2+} concentrations in the aqueous media were analyzed and the values were used to calculate the capacity value Q_e (mg/g). The samples were added to 0.001 M solutions of EDTA acid and allowed to shake at 200 rpms for 4 hours. The samples were filtered, washed with methanol, dried and weighed. The EDTA regeneration solution was made into a 2 % HNO_3 solution for analysis to obtain the Pb^{2+} concentration to calculate the % recovery of Pb^{2+}. The regenerated materials were then added to 1000 ppm solutions of Pb^{2+} $^{+}$. This procedure was repeated 3 more times to obtain the Pb^{2+} percent recovery for each of the 4 cycles.

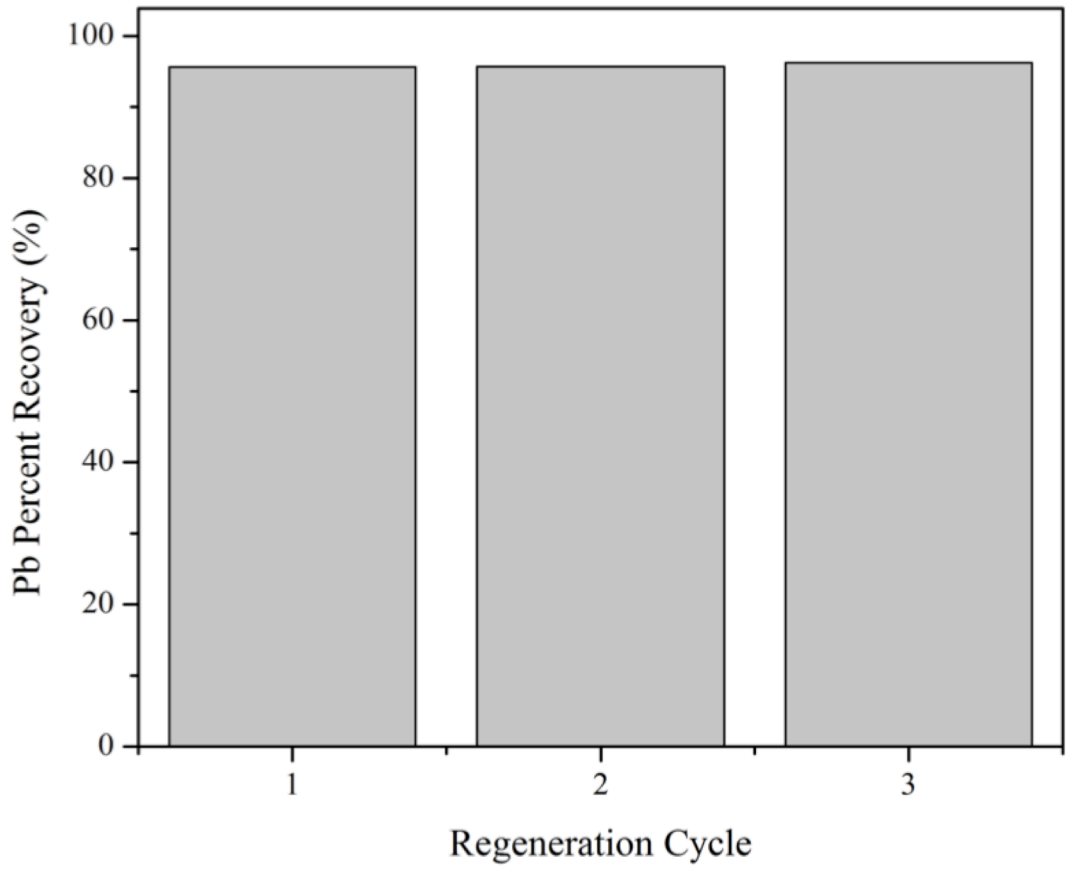

Figure 2.19. After each regeneration cycle >95% of Pb^{2+} was recovered from the composite using EDTA.

Powder X-ray Diffraction pattern supporting the Reduction of Hg^{2+} to Hg^{1+}

After soaking Fe-BTC/PDA in a concentrated Hg^{2+} solution we performed powder x-ray diffraction on the resulting powder. We observe peaks that correlate to Hg_2Cl_2, which is the reduced form of $HgCl_2$. We surmise that the polymer's functional groups are reducing Hg from the 2+ to 1+ oxidation state.

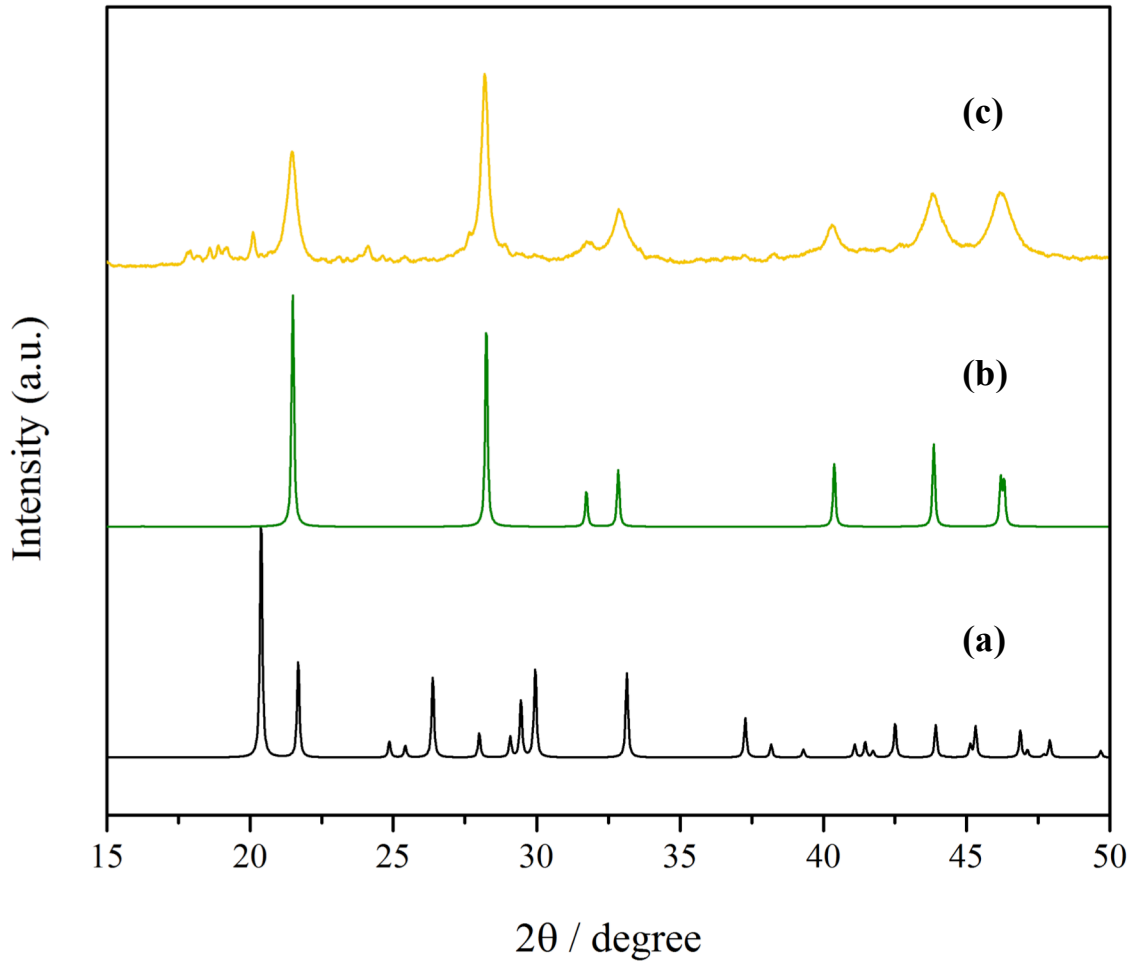

Figure 2.20. Powder X-ray diffraction pattern of Fe-BTC/PDA-19 after being soaked in 1000 ppm solution of $HgCl_2$. (a) simulated pattern of $HgCl_2$ (b) simulated pattern of Hg_2Cl_2 and (c) experimental pattern of Fe-BTC/PDA-19 soaked in $HgCl_2$.

X-ray Photoelectron Spectroscopy

The C1 X-ray photoelectron spectrum for Fe-BTC-/PDA-19 fit for O-C=O, C-O, C-N, CH_x and C-NH_2 functional groups, which are present in MOF-Polymer composite and the O1 spectra fit for the functional groups O-C and HO-C. After soaking Fe-BTC/PDA in highly concentrated solutions of Hg^{2+} and Pb^{2+}, we looked to XPS to elucidate the electronic structure. We observe two signature peaks that fit the data for $HgCl_2$ and Hg_2Cl_2 or HgO. We surmise that the polymer is reducing the Hg^{2+} to Hg^{1+}. For Pb^{2+}, we also observe two signature peaks that fit the data for $Pb(OAc)_2$ and $Pb(OH)_2$. Curve fitting was performed using CasaXPS software[199].

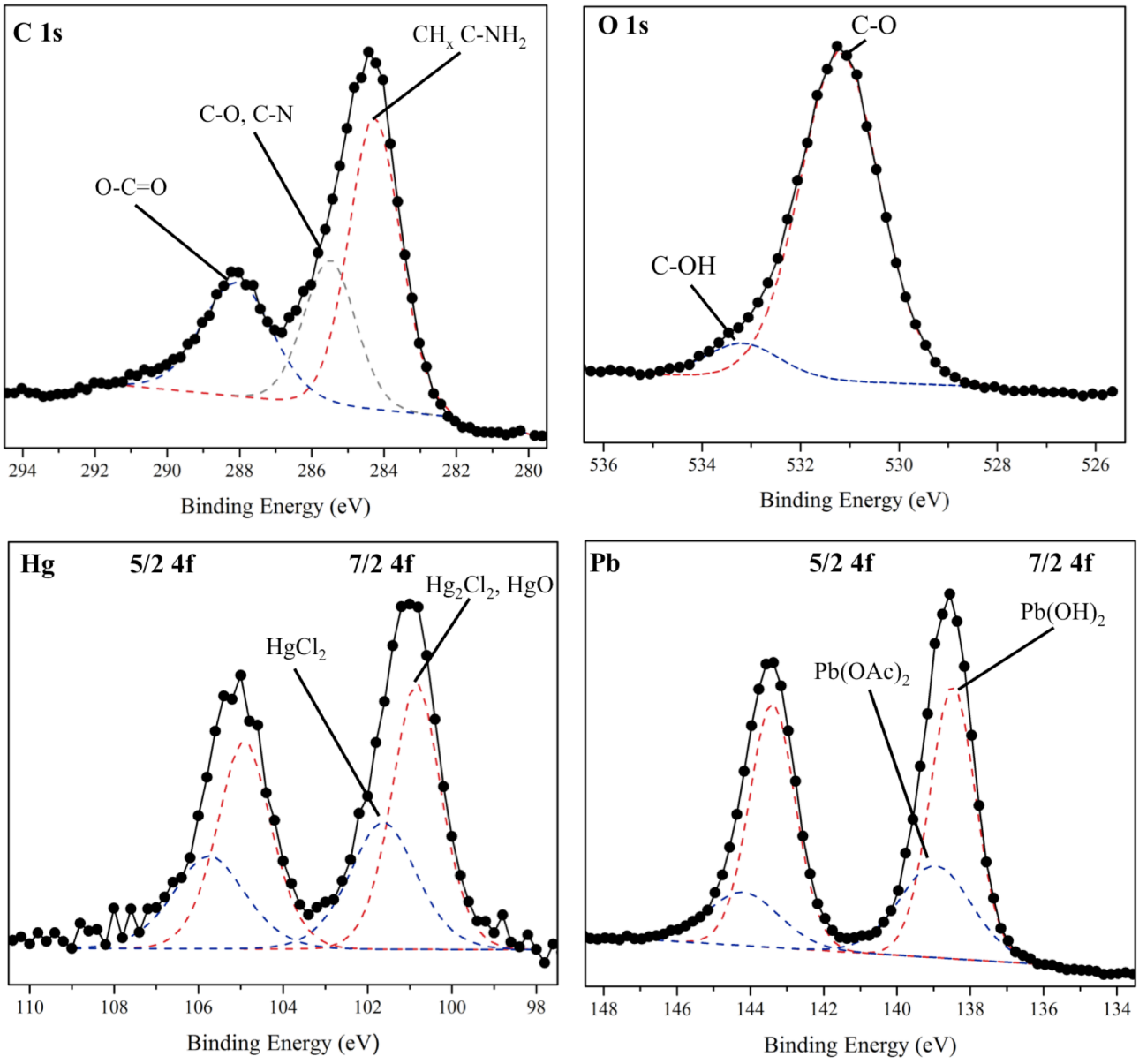

Figure 2.21. X-ray photoelectron spectra of Fe-BTC/PDA-19 after soaking in Hg^{2+} or Pb^{2+} solutions. Values are specified in Table S3.

Performance in Real World Samples

Removal rate was measured in real world samples spiked with Pb^{2+} and Hg^{2+}. Common interferents such as Ca^{2+}, Na^{+} or organics can hinder the composite's removal efficiency and rate. Various vials containing 20 mL of Rhone River water , Mediterranean Sea and wastewater spiked with Pb^{2+} and Hg^{2+} were treated with 10 mg of Fe-BTC or Fe-BTC/PDA. At each time point, the samples were filtered using a 25 mm hydrophilic PTFE membrane syringe filter with 0.22 µm pores to remove any solids for elemental analysis of the aqueous media.

In a second experiment, a syringe was filled with 0.250 gram of Fe-BTC/PDA and 20 mL of ~0.8 ppm Pb^{2+} in Rhone river water or ~0.55 ppm of Pb^{2+} in Mediterranean Sea water was syringed through the samples. In all experiments Fe-BTC/PDA is able to reduce the concentration of Pb to drinkable levels illustrating the composites applicability to be used in real world applications.

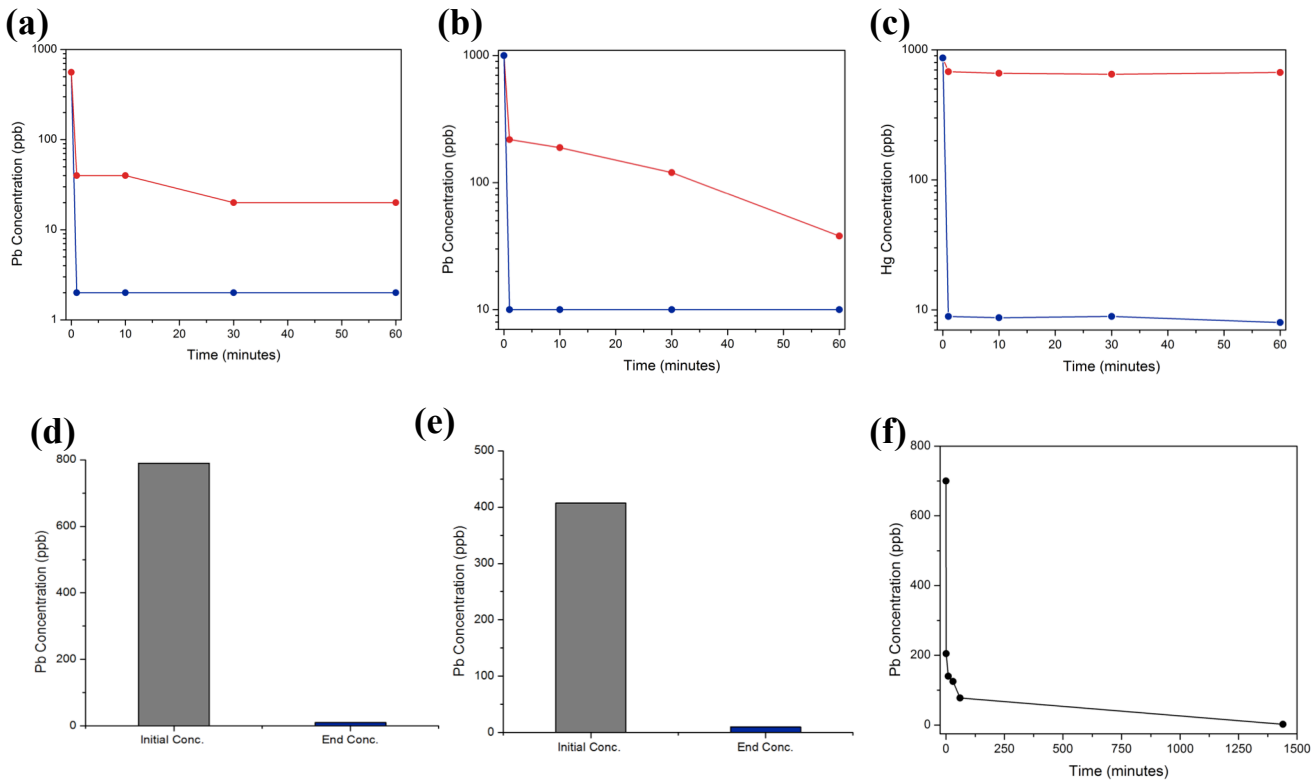

Figure 2.22. Metal ion concentrations after treating Rhone River (a,c) and Mediterranean Sea (b) water contaminated with Pb^{2+} and Hg^{2+} with Fe-BTC/PDA-19 (blue) and Fe-BTC (red) at different time points. Equilibrium of the composite is reached by 1 minute. The initial and final concentration of Pb^{2+} in (d) Rhone River water and (e) Mediterranean Sea water after the contaminated solution is pushed through a syringe containing Fe-BTC/PDA, illustrating heavy metal removal in seconds and (f) the removal rate of Fe-BTC/PDA in wastewater from a treatment facility spiked with Pb^{2+}.

Heavy Metal Removal with Increasing PDA Loading

Composites containing various amount of PDA, ranging from 19 to 42 mass %, were added to concentrated solutions of Hg^{2+} (1000 ppm) to assess the effect of the polymer loading on heavy metal removal, Q_e (mg/g). The mixtures were transferred to a Thermo Scientific MaxQ4450 Orbital Shaker for 24 hours at 200 rpms and held at a constant temperature of 28 °C. The samples were filtered using a 25 mm hydrophilic PTFE membrane syringe filter with 0.22 µm pores to remove any solids for elemental analysis of the aqueous media. After the analysis, Q_e, the amount of metal removed per gram of composite (mg/g), was calculated using the equation above.

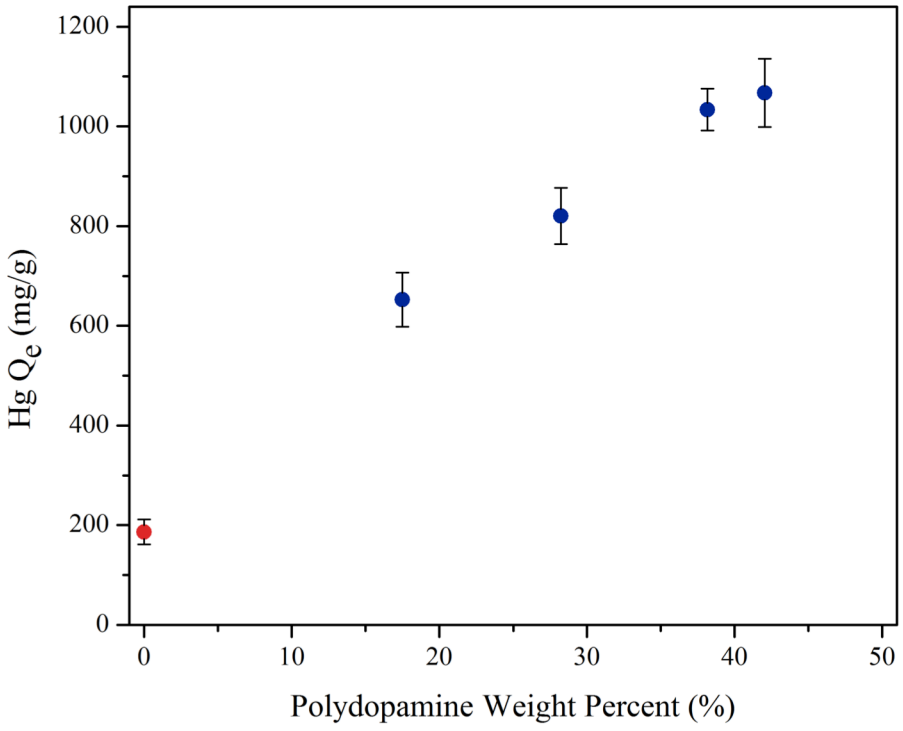

Figure 2.23. Hg^{2+} capacities in distilled water plotted against polydopamine loading in Fe-BTC. For the experiments the MOF was loaded with various amounts of polydopamine ranging from 0 to ~45 mass percent.

Performance of Different Composites in Real World Samples

Different composites were evaluated for Pb^{2+} removal from Rhone River water. 50 mg of composite was loaded into a syringe with a 25 mm hydrophilic PTFE membrane syringe filter of 0.22 µm pores. 10 mL of the of the contaminated river water was passed through and the solution was analyzed to measure the Pb^{2+} concentration.

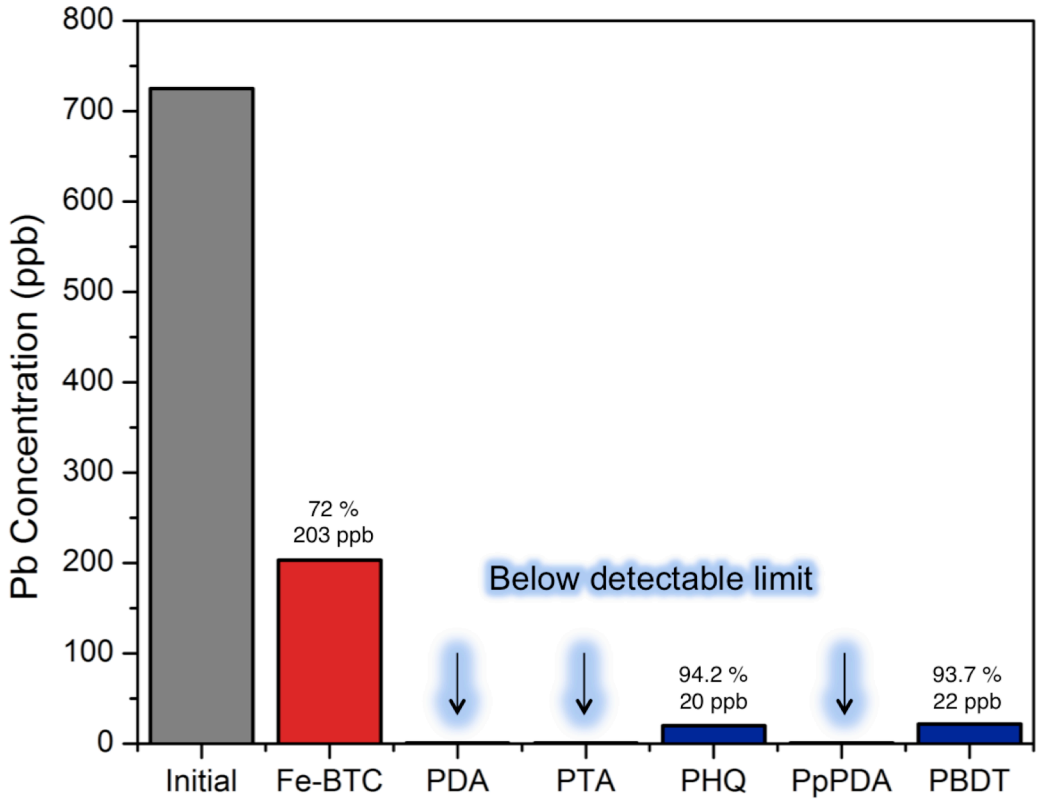

Figure 2.24. Pb^{2+} concentrations after treating Rhone River water with different composites.

Table 2.1.
The dopamine equivalence and concentrations with its C H N % values from the combustion analysis. The polydopamine mass % was calculated based on the N %.

Dopamine:Fe_3	Dopamine Concentration (mM)	C%	H%	N%	PDA% (based on N%)	BET Surface Area (m^2/g)
2.5	12	39.55	2.45	1.81	19.05	1134
5.0	24	42.55	2.98	3.01	28.21	757
7.5	36	47.97	3.86	4.73	38.15	488
10	47	49.67	4.39	5.57	42.05	165

Table 2.2.
The binding energies (kcal/mol) and binding distances (Å) for the functional groups of possible polydopamine derivatives to the Fe metal site on the SBUs (secondary building unit)

ID	PDA structure	Binding site	Binding energy ($\frac{kcal}{mol}$)	Binding distance (Å)
1		N	-29.4	2.3
		O	-20.4	2.1
2	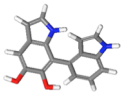	N	-26.3	3.1
		O	-28.4	2.2
4		N	-23.3	3.6
5		N	-40.2	1.9
		O	-18.8	2.3
6	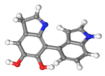	N	-36.6	2.1
		O	-27.2	2.2
7		O	-29.0	2.0
		N	-28.2	2.3
8	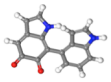	O	-33.7	2.0
		N	-27.7	3.2
9		O1	-23	2.0
		O2	-17.3	2.2
		N	-21.8	2.7
10	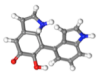	O1	-18.2	2.3
		N	-25.8	3.2
11		O2	-26.5	2.0
12		N	-39.3	2.1
13		O	-33.8	2.0
14		O	-23.1	2.2
		N	-41.97	2.1
15		O	-24.0	2.2

Table 2.3.
The binding energy values from the XPS for each functional group present within the composite.

Functional Group	Binding Energy (eV)
Hg_2Cl_2, HgO	100.8
$HgCl_2$	101.6
$Pb(OH)_2$	138.4
$Pb(OAc)_2$	138.9
CH_x, C-NH_2	284.4
C-O, C-N	285.4
O-C=O	288.3
C=N-C	399.4
C_2NH	400.4
C-NH_2	402.0
O-C	531.2
HO-C	533.2

Table 2.4. Top performing materials for Lead removal

Material	Surface Area (m^2/g)	Mechanism	Reach EPA of ~10 ppb with soaking?	Speed to EPA limit (min.)	Pb^{2+} Capacity (mg/g)	k_d (mL/g)	Regenera-tion	Organic Interferent Test	Selective over Na^+, Ca^{2+}, Mg^{2+}	Ref.
Fe-BTC	2300	Adsorption	✗[a]	✗	162	3.5×10^2	N.R.[b]	✔[a]	N.R.	This work
Fe-BTC/PDA	1134	Adsorption	✔	< 1	394	1.7×10^6	✔	✔	✔	This work
DPA-LDH[c]	168.3	Adsorption	✔	~ 40	479	1.99×10^8	N.R.	N.R.	N.R.	6
MoS_4-LDH[d]	N.R.	Adsorption	✔	> 30	290	2.6×10^5	N.R.	N.R.	N.R.	5
$Zn_3L_3(BPE)_{1.5}$[e]	82.5	Adsorption	✗	✗	616.6	2.3×10^6	✔	N.R.	✔	7
mPMF[f]	1099	Adsorption	✔	1	0.628	N.R.	✔	N.R.	✔	24
PDA-Ms[g]	N.R.	Adsorption	✔	N.R.	160	2.39×10^3	✔	N.R.	✔	9
68W[h]	18.1	Adsorption	✗	✗	254.1	3.17×10^5	N.R.	N.R.	N.R.	11
chitosan/PEI[i]	N.R.	Adsorption	✔	~ 40	341	N.R.	✔	N.R.	✔	25
PbIMS[j]	762	Adsorption	✗	✗	160	2.97×10^3	✔	N.R.	✔	8
ED-MIL-101-Cr[k]	347	Adsorption	✗	✗	81.09	1.18×10^3	✔	N.R.	N.R.	28
MgO@N-biochar[l]	83.2	Ion-exchange	✗	✗	893	N.R.	✔	✔	✔	30
MgO Flower[m]	72	Ion-exchange	✔	> 60	1980	N.R.	N.R.	N.R.	N.R.	32
001x7[n]	N.R.	Ion exchange	✔	N.R.	434.7	4.9×10^4	N.R.	N.R.	✔	9
K-MPS-1[o]	N.R.	Ion-exchange	✔	> 720	393.5	5.36×10^5	N.R.	N.R.	✔	10

highlighted boxes (in yellow) represent excellent performance for a specific metric.

a. **x** implies it was not achieved under the conditions tested. ✔ indicates this parameter was tested and shows reasonable performance.
b. N. R. implies that the parameter is not reported and could not be calculated from the presented data.
c. DPA-LDH is a Ni/Cr Layered double hydroxide with diphenylamine-4-sulfonate intercalated within the layers. While the material reaches the EPA limit in DI water, it takes ~ 40 minutes to reach this. Further, selectivity tests for mixtures containing equivalent amounts of Pb^{2+} Cd^{2+}, Cu^{2+}, and Zn^{2+}, were carried out. Despite that the material adsorbs all 4 metals, it still manages to get to the EPA limit for Pb^{2+}, but it takes 60 minutes. No tests were performed against other important interferents like Na^+, Mg^{2+}, or Ca^{2+} found in real world water samples.
d. MoS_4-LDH is a layered double hydroxide with MoS_4^{2-} anions intercalated in between the layers. While selectivity tests are carried out with equivalent amounts of several ions including Ni^{2+}, Co^{2+}, Cu^{2+}, Zn^{2+}, Ag^+, Pb^{2+}, Cd^{2+}, and Hg^{2+}, it is shown to absorb significant amounts of all metals except Co^{2+}, Ni^{2+}, Zn^{2+}, and Cd^{2+}, Further, it does not get anywhere close to reaching the EPA limit for Pb^{2+} under these conditions within a 3 hour window (reaches only ~ 650 ppb). No tests were done to see how the materials perform in natural water samples with large amounts of Na^+, Ca^{2+}, or Mg^{2+} nor is there any information pertaining to recyclability.
e. $Zn_3L_3(BPE)_{1.5}$ is a Zn-containing MOF (where L^{2-} = 4,4'-azoxydibenzate and BPE = bis(4-pyridyl)ethylene). While the material has a higher capacity, it is not able to get to the EPA limit under the reported conditions listed. From 10 ppm Pb^{2+} concentration reaches approximately 35 ppb in an hour, which is the equilibration time. The material equilibrium is quite slow compared to Fe-BTC/PDA, likely due to the structural transformation it undergoes. The material is not tested in real world water samples, but does show high selectivity for Pb^{2+} over Na^+, Ca^{2+}, and Mg^{2+}, having ratios up to 1:50 (10 ppm Pb : 500 ppm mixed ions). The materials stability is only tested for 300 minutes. Last, the material is cycleable but shows a drop by 10 to 15 % in cycles 3 and 4.
f. MPMF is a mesoporous poly-melamine-formaldehyde polymer: Until Fe-BTC/PDA, this polymer is the fastest reported to date to the EPA limit, but it has extremely low capacities. As such, large amounts of material is required and it only operates well when the concentrations of the solutions are already well into the ppb regime, 50 to 100 ppb of Pb^{2+}.
g. PDM-Ms are polydopamine microspheres. It is expected that these should perform similarly to Fe-BTC/PDA, however it can be seen that the k_d is much higher for our composite and this material is not shown to get below the EPA limit; however, the equilibrium time is on the order of a minute.
h. Porous Indium Sulfide (68W) was generated using an In-MOF known as MIL-68 or In(BDC)OH treated with Na_2S in water. No information is given with regard to testing the selectivity of the material in sources contaminated with other metals. It also is not reported that it reaches the EPA limit and no information is given with regard to equilibrium times.
i. This polymer is a magnetic gelatin that consists of chitosan grafted PEI (polyethylene imine). The cationic polymer can only reach the EPA limit from extremely low concentrations, ~200 ppb. Further, it is regenerable in 0.1 mmol/L Acetic Acid; however, the removal efficiency drops to 89% over 5 cycles. Last, the cationic polymer adsorbs most cations and anions found in drinking water, which decrease the efficiency, particularly Ca^{2+}. Last, it should be noted that the capacity is determined by fitting adsorption isotherms, actually capacities above 66 mg/g for Pb^{2+}were never measured.
j. PbIMS is an periodic ion imprinted silica, SBA-15. Despite that equilibrium is reached in short times, approximately 7 minutes at low concentrations, they do not show under the conditions tested that the material is capable of getting below the EPA limit. While they show the material is selective for various ions such as Na^+, K^+, Ca^{2+}, Mg^{2+}, Cu^{2+}, and Cd^{2+}, they also show that the material is still adsorbing a significant amount of some of these ions from solution, particularly K^+.
k. ED-MIL-101 is an ethylene diamine grafted to the metal sites in the MOF. It has a capacity that drops off by 50% after 4 cycles, likely indicating loss of the amines.
l. MgO@Nbiochar is not shown to get below the EPA limit but removal efficiencies approach 99% in 10 minutes.

m. MgO Flower: Despite high capacities, no selectivity is illustrated. Further, the material reaches the EPA limit, but it can only be done from very low starting concentrations of 200 ppb and very long equilibrium times that are longer than 60 minutes.
n. 001x7[h] is a commercial ion exchange resin.
o. K-MPS-1 is a potassium intercalated layered metal thiophosphate, with the formula $K_{0.48}Mn_{0.76}PS_3 \cdot H_2O$. It is reported to get below the EPA limit but only at very low starting concentrations and long soak times compared to Fe-BTC/PDA. Full equilibration times are reported to be on the order of 2 days. Last, while they tested to see if the Pb^{2+} could be removed, they have not shown that the materials properties

Table 2.5. Top performing materials for mercury removal

Material	Surace Area (m^2/g)	Mechanism	Reach EPA of ~10 ppb with soaking?	Speed to EPA limit (min.)	Hg^{2+} Capacity (mg/g)	K_d (mL/g)	Regenera-tion	Organic Interferent Test	Selective over Na^+, Ca^{2+}, Mg^{2+}	Ref.
Fe-BTC	2300	Adsorption	✗[a]	✗	210	3.5×10^2	N.R.[b]	✔[a]	N.R.	This work
Fe-BTC/PDA	1134	Adsorption	✔	< 1	1670	5.5×10^6	✔	✔	✔	This work
68W[c]	18.1	Adsorption	✗	✗	2170	6.9×10^6	N.R.	N.R.	N.R.	11
TPB-DMTP-COF-SH[d]	291	Adsorption	✔	~10	4395	3.23×10^9	✔	N.R.	✔	21
NanoSe Sponge[e]	N.R.	Adsorption	✔	~10	624	1.67×10^9	✗	N.R.	✔	20
COF-S-SH[f]	496	Adsorption	✔	~20	1350	2.3×10^9	✔	N.R.	✔	22
PAF-1-SH[g]	3274	Adsorption	✔	~30	1000	5.76×10^7	✔	N.R.	✔	17
BioMOF[h]	N.R.	Adsorption	✗	✗	900	N.R.	N.R.	N.R.	✔	18
S-FMC-900[i]	1400	Adsorption	✗	✗	732	5.13×10^5	N.R.	N.R.	N.R.	13
Zr-DMBD[j]	513	Adsorption	✗	✗	140.6	N.R.	N.R.	N.R.	N.R.	16
LMOF-263[k]	1004	Adsorption	✗	✗	380	6.45×10^5	N.R.	N.R.	✔	19
DMS-Fe_3O_4[l]	114	Adsorption	✗	✗	227	2.8×10^5	N.R.	N.R.	✔	14
LHMS-1[m]	N.R.	Ion Exchange	✔	~2	87	6.41×10^6	✔	N.R.	N.R.	15

highlighted boxes (in yellow) represent excellent performance for a specific metric.

a. x implies it was not achieved under the conditions tested. ✔ indicates this parameter was tested and shows reasonable performance.
b. N. R. implies that the parameter is not reported and could not be calculated from the presented data.
c. Porous Indium Sulfide (68W) was generated using an indium-MOF known as MIL-68 or In(BDC)OH treated with Na_2S in water. No information is given with regard to testing the selectivity of the material in sources contaminated with other common metals. It also is not reported that it reaches the EPA limit and no information is given with regard to equilibrium times. Further, it should be noted that indium is not only toxic, but also highly expensive.
d. TPB-DMTP-COF-SH is a covalent organic framework functionalized with pendant thiol groups. While the material performs well in DI water, its removal efficiency is reduced by over 20% when in the presence of common inorganics like, Ca^{2+}, Na^+, and Mg^{2+}. It should be noted that the materials can reportedly get to the EPA limit but 20 mg of sample is placed in 1 mL of solution 10 ppm solution. This test is rather unrealistic. Comparatively, FeBTC/PDA can do the same job with significantly less sample and at least ten times faster.
e. The nano selenium sponge is one of the best materials reported for Hg removal. The Hg^{2+} concentration is reduced to the ppt regime in seconds. However, this is only done under pressure, and the authors do not report what is the length of time that they wait for the water to diffuse into the sponge. Further, they use 30 times more material and are unable to reach the EPA limit within a 10 minute window when just soaking the material in water, as done in our experiments. Also, the material is not reversible. While this is good for in home treatment, it can be seen as a big disadvantage for wastewater treatment.
f. COF-S-SH is a covalent organic framework. While the material is shown to be selective in the presence of Mg^{2+} and Ca^{2+}, there is no report of Na^+. Further, significant amounts of the common ions are shown to adsorb and the manuscript gives no indication of the actual concentrations to show that these materials selectively bind Hg^{2+} at low concentrations while in the presence of high concentrations of these other inorganics.
g. PAF-1-SH, also referred to as the mercury nanotrap, is a porous organic polymer. It can be regenerated with only about a 10% loss in removal efficiency in 3 cycles. They show that in the presence of Ca^{2+}, Na^+, and Mg^2that the material maintains Hg^{2+} capacity; however, they do not report on the removal rate with these other ions and they also do not test in high concentrations of the other ions. They start with 3 ppm Hg^2+ and 0.61, 0.36, and 8.22 ppm of Ca^{2+}, Mg^{2+}, and Na^+ respectively. It should be noted that the concentrations of the competing ions should be significantly higher, (and low concentrations of Hg^{2+}) as expected for wastewater, to truly test selectivity.
h. BioMOF is a MOF with the formula $CaCu_6[(S,S)\text{-methox}]_3(OH)_2(H_2O)\} \cdot 16H_2O$ that is decorated with thioalkyl chains. The material is reported to be selective for $Hg2^+$ over Na^+, K^+, Ca^{2+}, and Mg^{2+}; however, it should be noted that the solutions contained 10 ppm of all ions. They were not tested in high concentrations of these ions with low concetrnations of Hg^{2+}, which is more realistic for wastewater. Further, there are no other experimental procedures that describe whether the other ions are adsorbed nor if the same removal efficiency is achieved with Hg^{2+} in their presence.
i. S-FMC is a sulfur-functionalized mesoporous carbon.
j. Zr-DMBD is a thiol-laced MOF (where $DMBD^{2-}$ = 2,5-dimercapto-1,4-benzenedicarboxyate)

k. L-MOF-263 is a luminescent metal−organic framework with the chemical formula, $Zn_2(dbtdcO_2)_2(tppe)$ where ($dbtdcO_2$) = [dibenzo[b,d]thiophene-3,7-dicarboxylate 5,5-dioxide] and tppe = 1,1,2,2-tetrakis(4-(pyridine-4-yl)phenyl)ethane. For selectivity, L-MOF was only tested in the presence of Mg^{2+} and Ca^{2+}, not Na^{+}. Further, the concentrations were equivalent, (10 ppm for all M^{2+}) rather than low concentrations of Hg and high concentrations of these competing ions. While they report the luminescent properties are reproducible with cycling, they do not actually show that the material can be fully regenerated and cycled.
l. DMS-Fe_3O_4 contains Fe_3O_4 nanoparticles functionalized with dimercaptosuccinic acid (DMSA).
m. LHMS-1 is a layered hydrogen metal sulfide with the chemical formula $H_{2x}Mn_xSn_{3-x}S_6$ (x ¼ 0.11–0.25). It should be noted that while the material works in 2 minutes, it is only tested in 67 ppb solutions. Further, 1 gram of LHMS is used per 1L of water. For Fe-BTC/PDA, half as much material is employed, and it was able to reduced 1000 ppb to drinkable conditions in less than a minute.

Table 2.6.
BET surface areas and polymer loadings of different composites

Composite	Polymer Building Unit	BET Surface Area (m^2/g)	Polymer Mass %
Fe-BTC/PTA	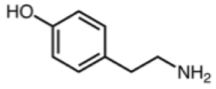	1665	14.31
Fe-BTC/PHQ	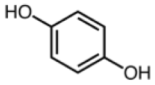	1767	19.69
Fe-BTC/PpPDA	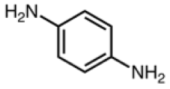	1032	21.1
Fe-BTC/PmAP	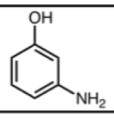	1488	16.54
Fe-BTC/PBDT	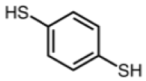	683	10.21
Cu-TDPAT/PDA	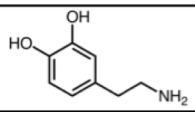	434	24.11

APPENDIX to Chapter 3

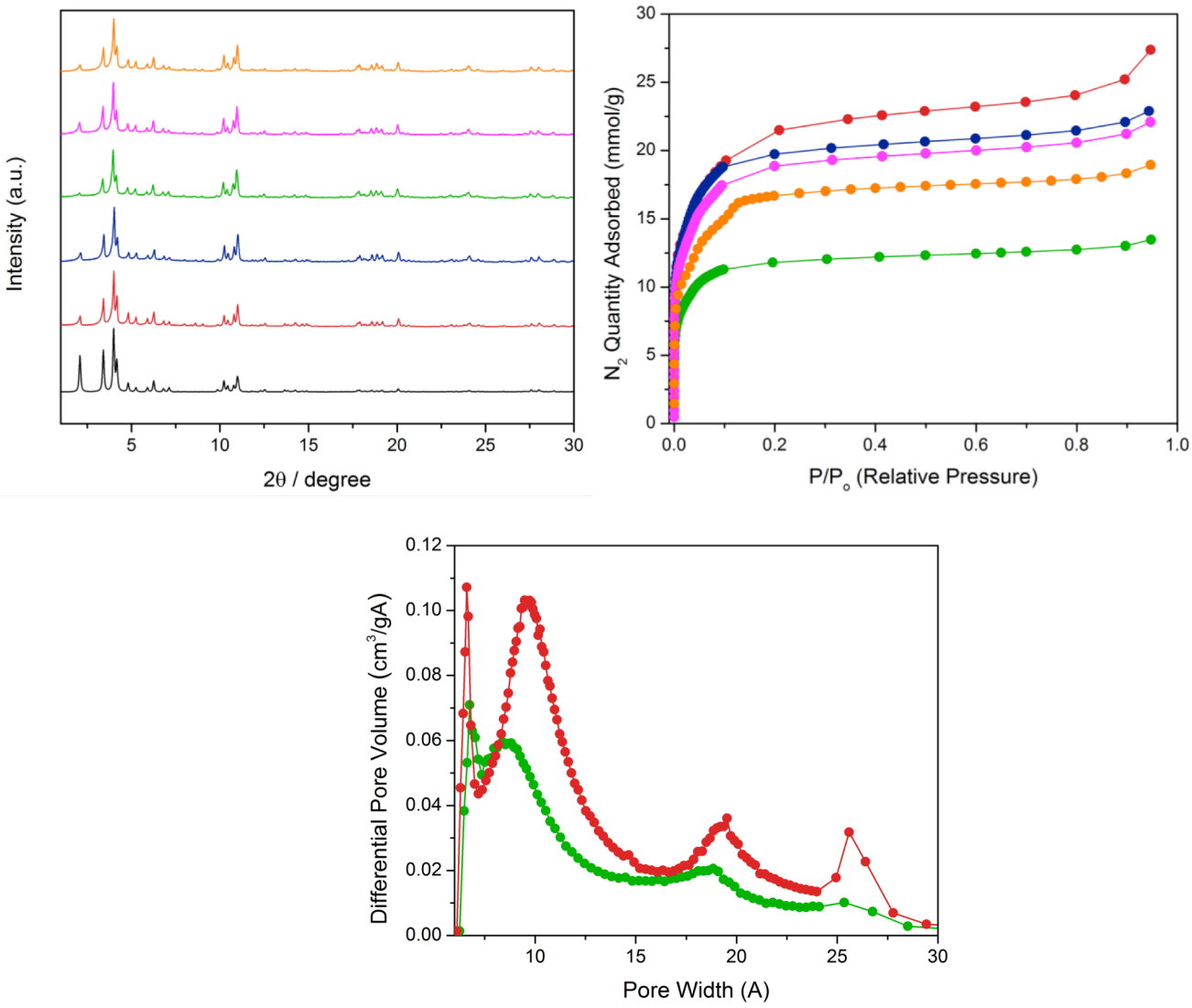

Figure 3.1
Powder X-ray diffraction patterns (top, left) and N_2 adsorption isotherms (top,right). Simulated powder pattern of Fe-BTC (black), Fe-BTC (red), Fe-BTC/PHQ (blue), Fe-BTC/PpPDA (green), Fe-BTC/PTA (pink) and Fe-BTC/PmAP (orange). Horvath-Kawazoe pore distribution for Fe-BTC (red) and Fe-BTC/PpPDA (green).

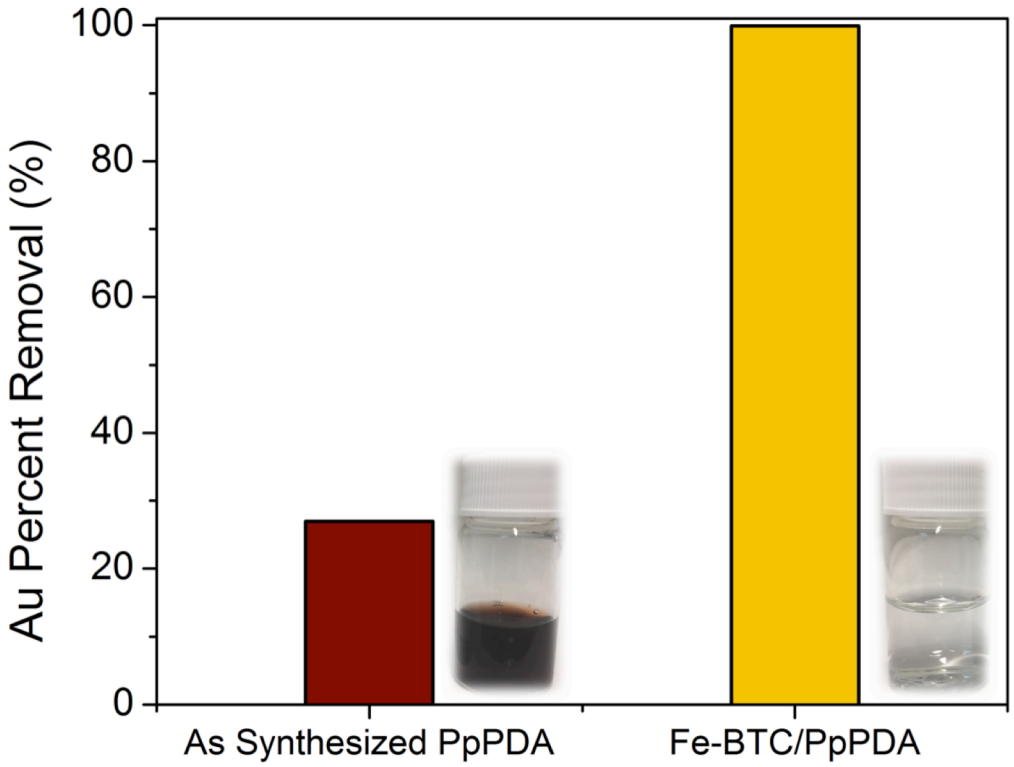

Figure 3.2
Percent removal (%) of Au^{3+} from a 10 ppm Au^{3+} solution after treatment with as synthesized PpPDA and the composite Fe-BTC/PpPDA. Pictures of the water solution after treatment with the pure polymer (left) and the MOF composite (right).

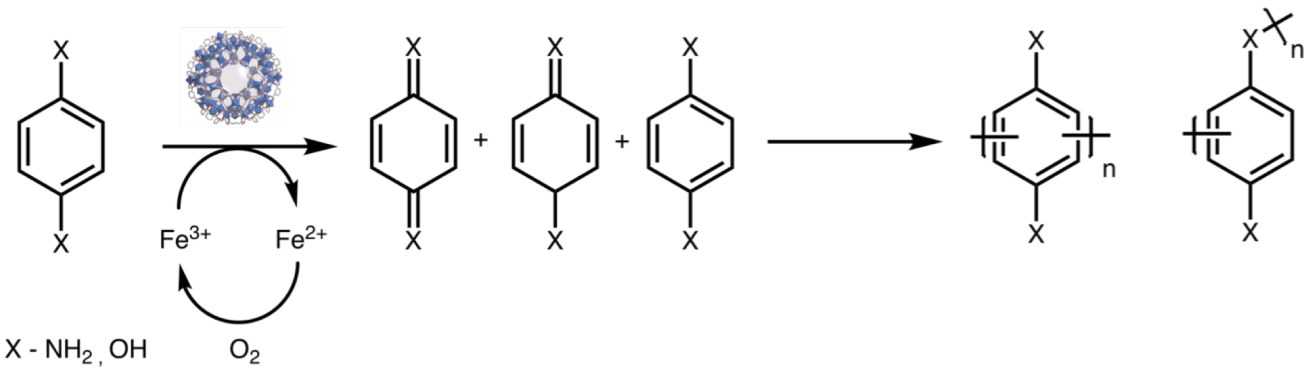

Scheme 3.1
Proposed mechanism for in-situ polymerization.

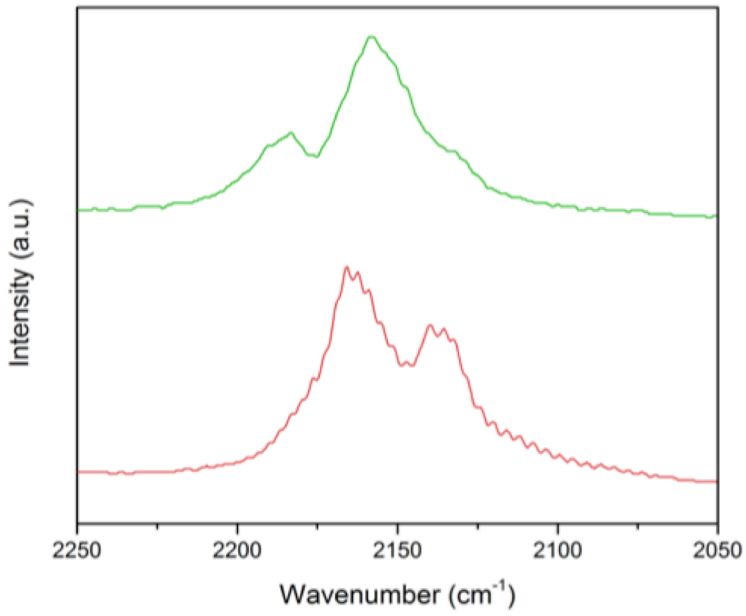

Figure 3.3
In-situ IR with CO for Fe-BTC (red) and Fe-BTC/PpPDA (green). Samples were activated at 125 °C and sparged with CO at an equilibrium pressure of 67 mbar.

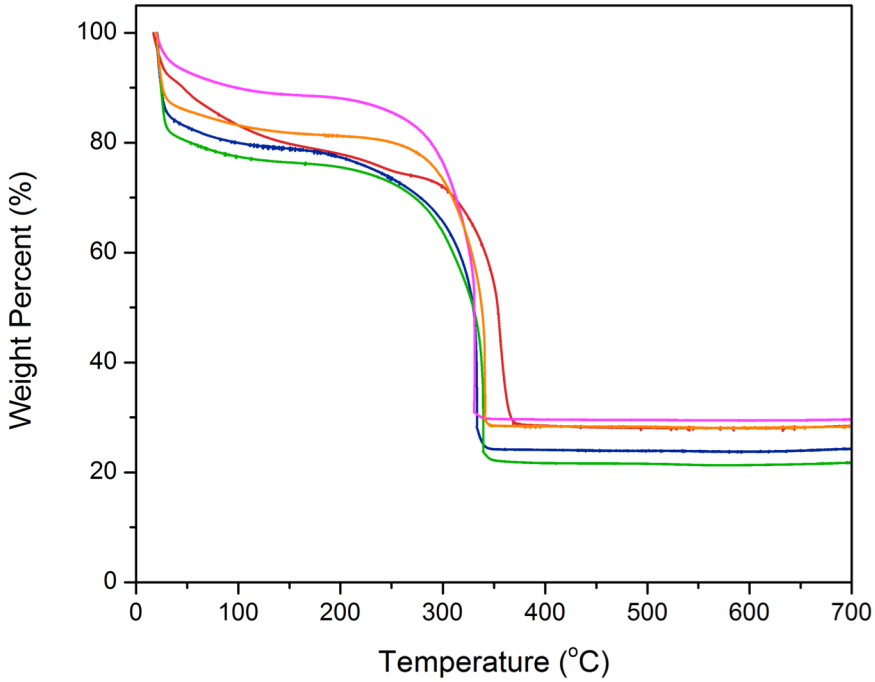

Figure 3.4
Thermogravimetric analysis curves. Fe-BTC (red), Fe-BTC/PHQ (blue), Fe-BTC/PpPDA (green), Fe-BTC/PTA (pink) and Fe-BTC/PmAP (orange).

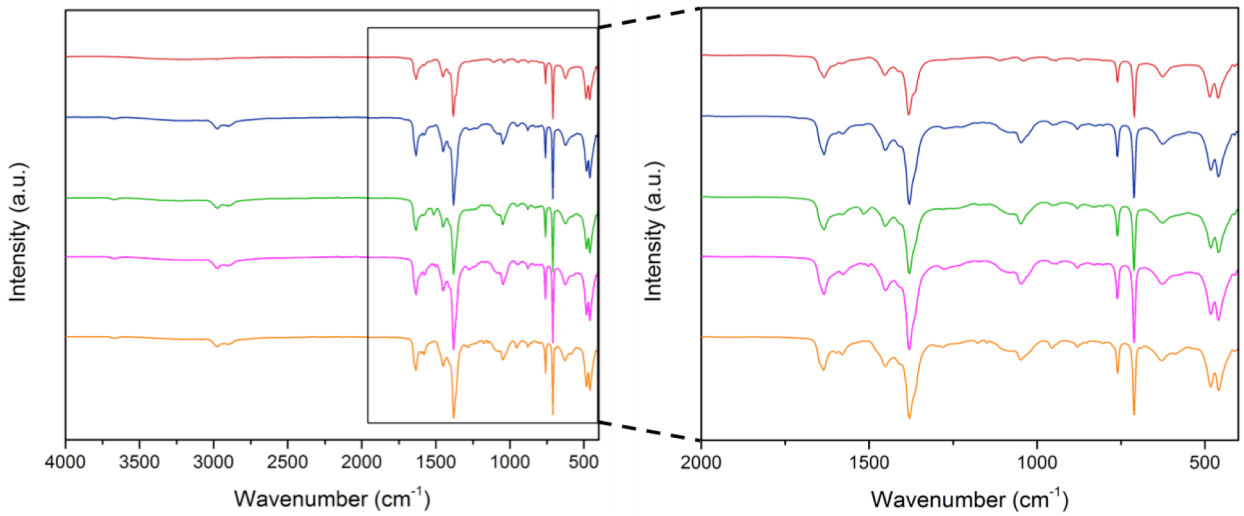

Figure 3.5
IATR Spectra. Fe-BTC (black), Fe-BTC (red), Fe-BTC/PHQ (blue), Fe-BTC/PpPDA (green), Fe-BTC/PTA (pink) and Fe-BTC/PmAP (orange).

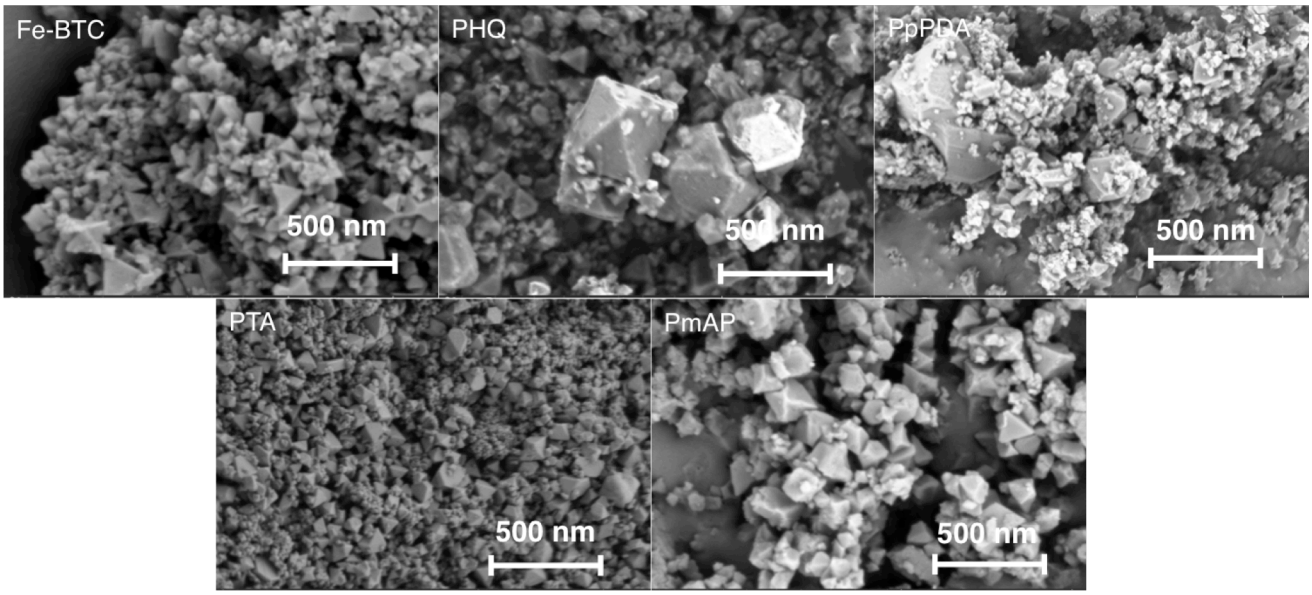

Figure 3.6
Scanning Electron Microscopy Images of the composites. Samples were sputtered with 7nm of iridium.

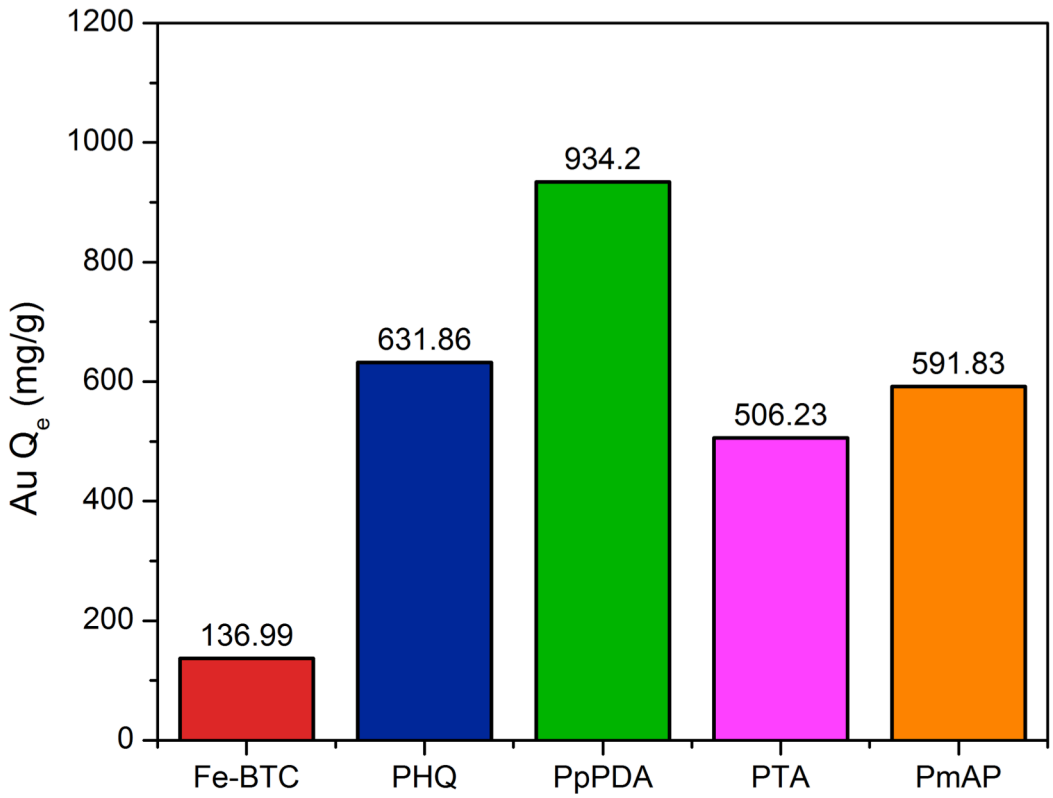

Figure 3.7
Removal Capacities (Q_e – mg/g) for Au from water. Samples were soaked in a 1000 ppm Au solution of distilled water for 24 hours.

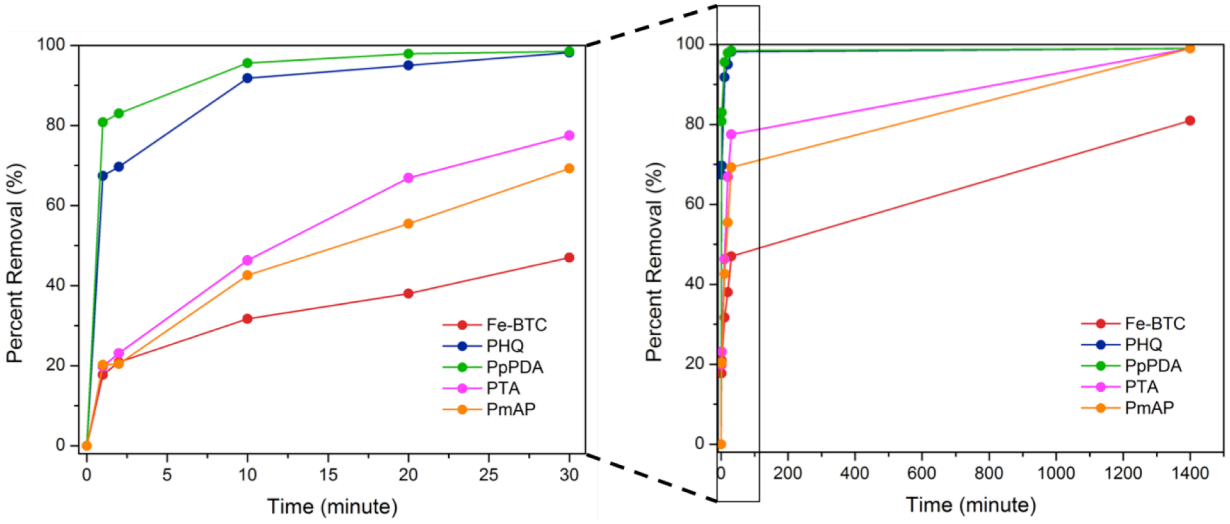

Figure 3.8
Removal rate for Au in river water. Percent removal of Au after treatment of a 1 ppm river water solution with the composite at different time points.

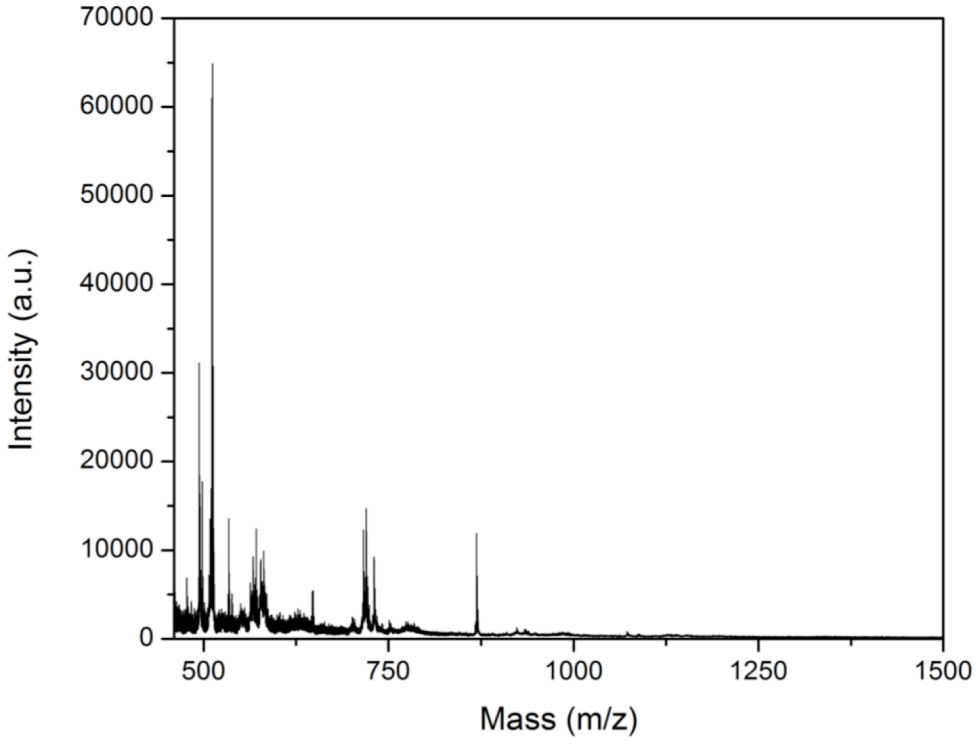

Figure 3.9
MALDI-TOF-MS. Spectrum of Fe-BTC/PpPDA after partially destroying the material in 4M HCl. The results indicate the polymerization of p-phenylenediamine

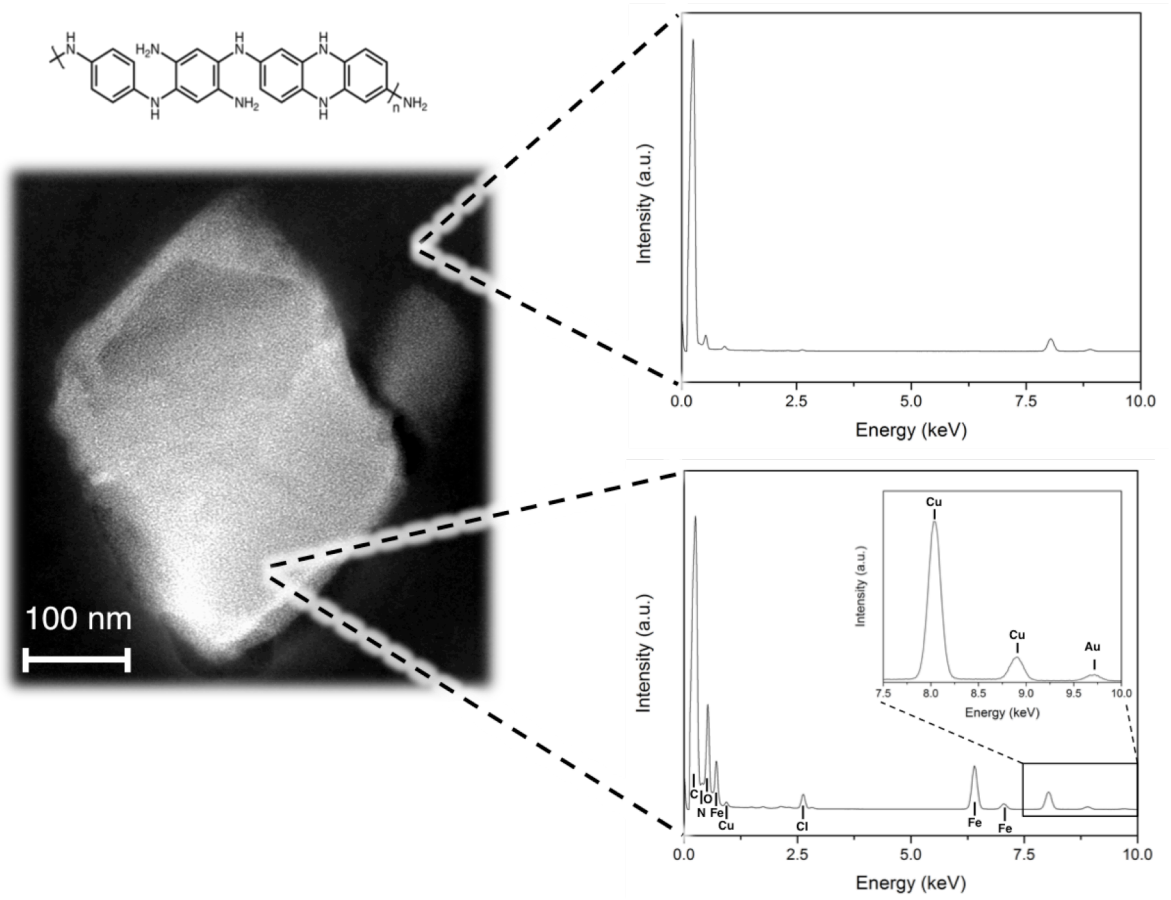

Figure 3.10
HAADF-STEM coupled with EDX. Fe-BTC/PpPDA was soaked in a gold solution and was cut into 100 nm slices using a microtome. EDX was performed on the substrate (top) and the sliced crystallie (bottom).

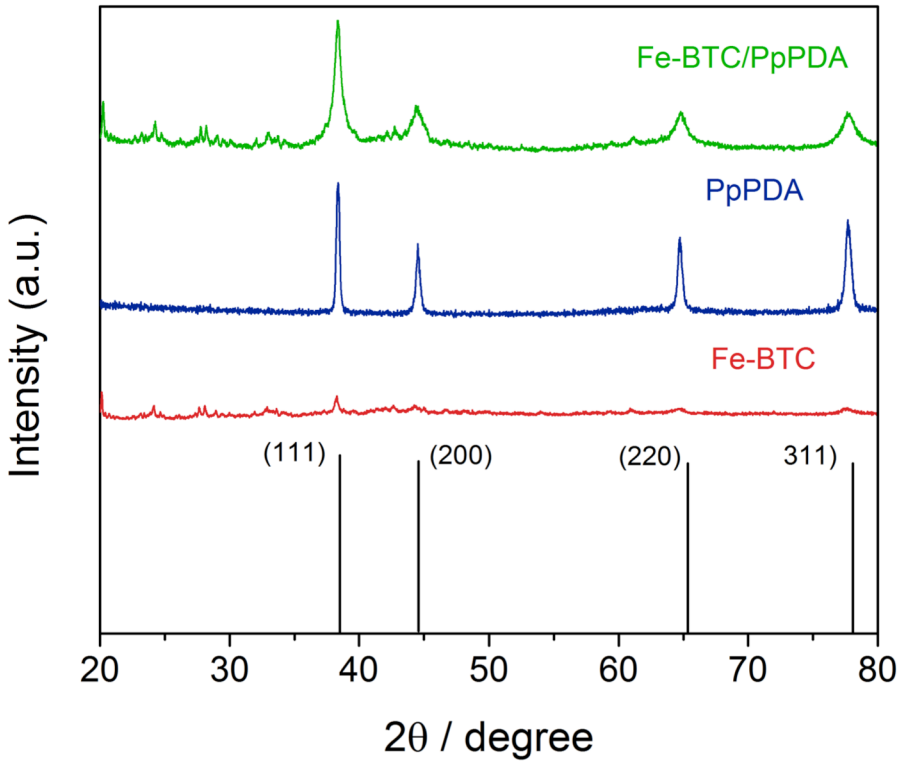

Figure 3.11
Powder x-ray diffraction pattern of Fe-BTC, PpPDA and Fe-BTC/PpPDA saturated with Au. All samples were soaked in a concentrated gold solution and PXRD was measured on the resulting powder. The peaks shown indicate the presence of neutral state Au in the powder.

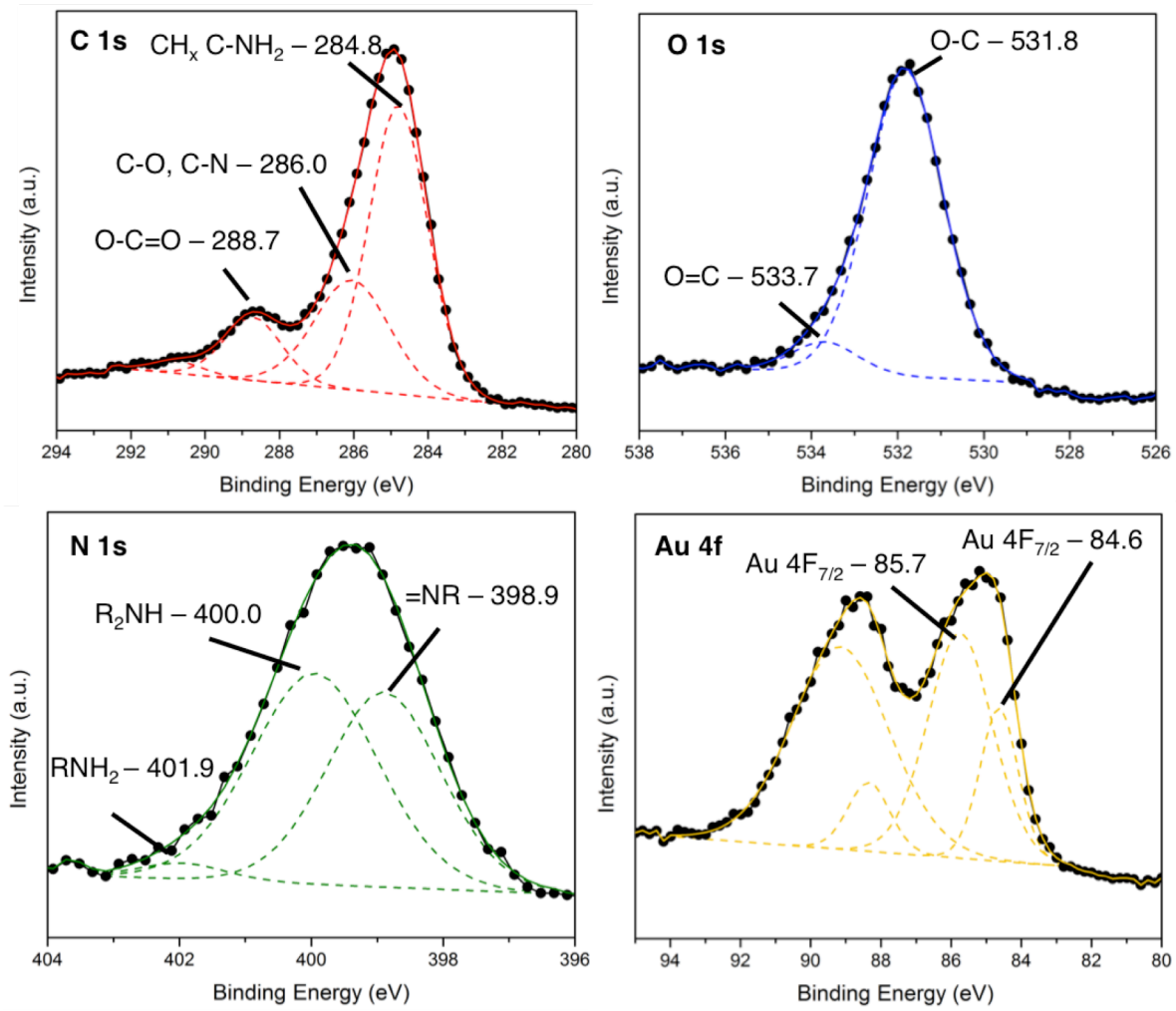

Figure 3.12
X-ray photoelectron spectra of Fe-BTC/PpPDA. XPS spectra of the C 1s region (top, left), the O 1s region (top, right), the N 1s region (bottom, right) and Au 4f region (bottom, right) of Fe-BTC/PpDA after being saturated with Au^{3+}.

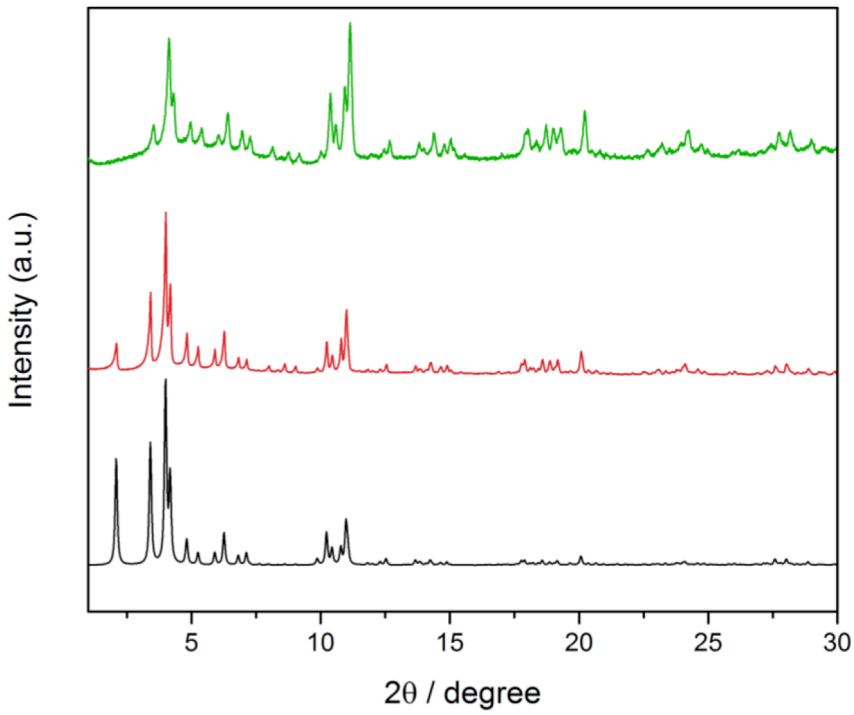

Figure 3.13
Stability experiments for Fe-BTC/PpPDA. Powder X-ray diffraction pattern of Fe-BTC/PpPDA after being soaked in river water spiked with 800 ppm of Cu and Ni for 2 months (green). Fe-BTC/PpPDA as synthesized (red). Simulated powder pattern of Fe-BTC (black)

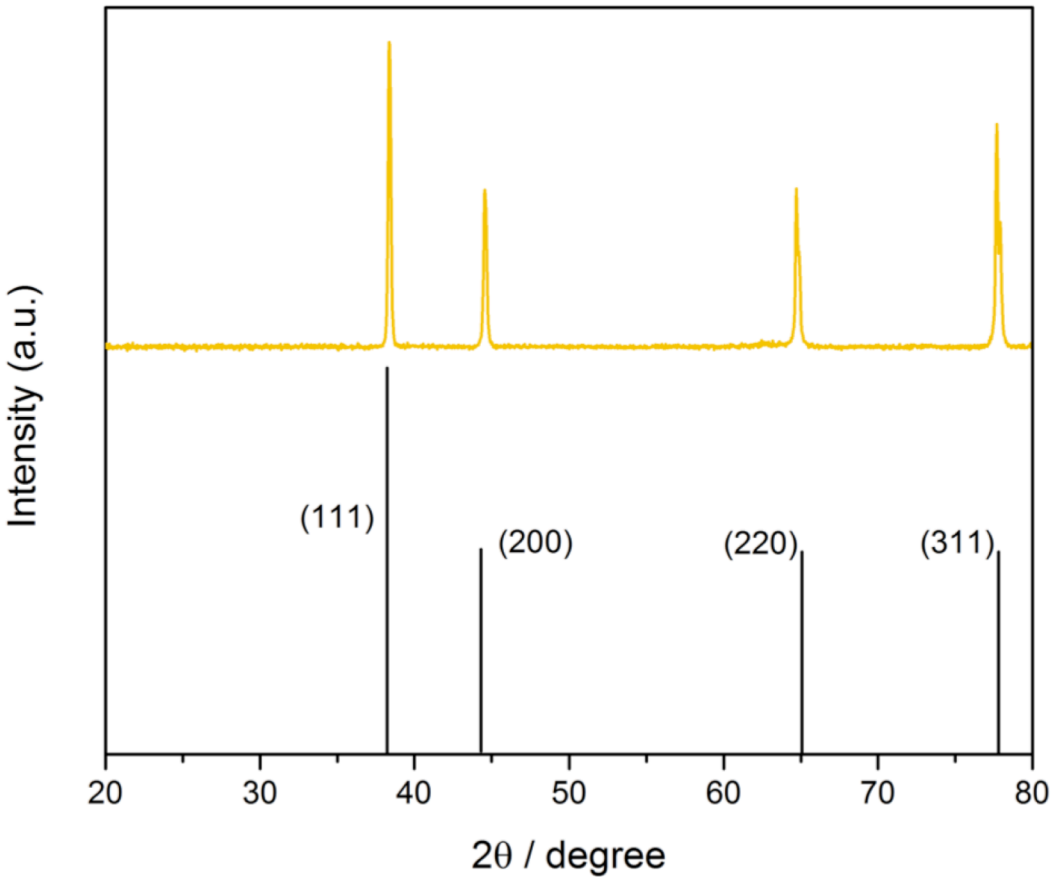

Figure 3.14
Purification of Au from Fe-BTC/PpPDA. Powder x-ray diffraction pattern of Au particles that was purified from Fe-BTC/PpPDA. The diffraction pattern indicate that Au^{3+} is reduced to Au^{0} after treatment with the composite.

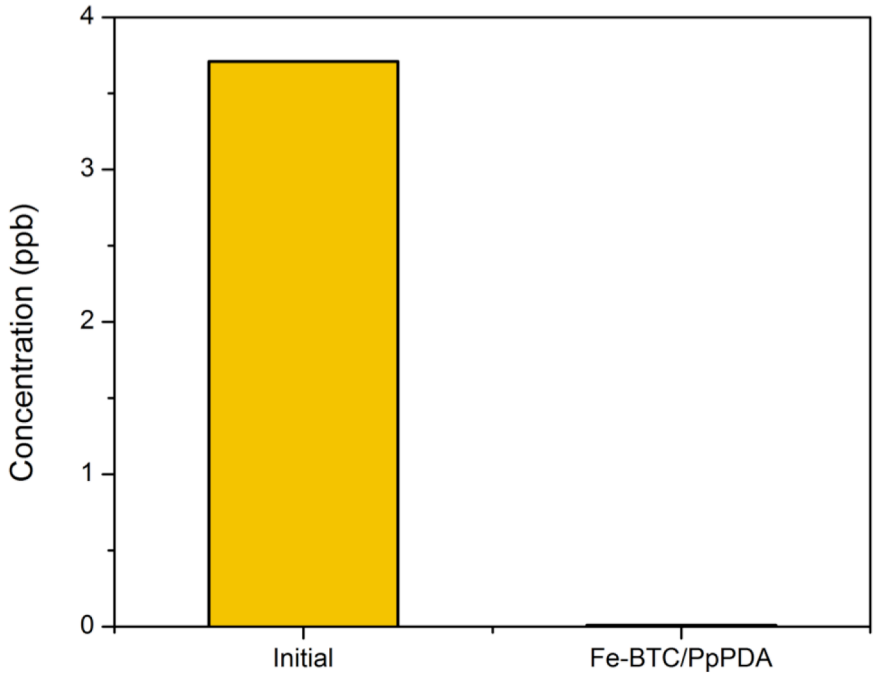

Figure 3.15
Concentration of Au from water provided by a waste water treatment plant. After treatment with Fe-BTC/PpPDA the concentration is reduced to under 0.010 ppb.

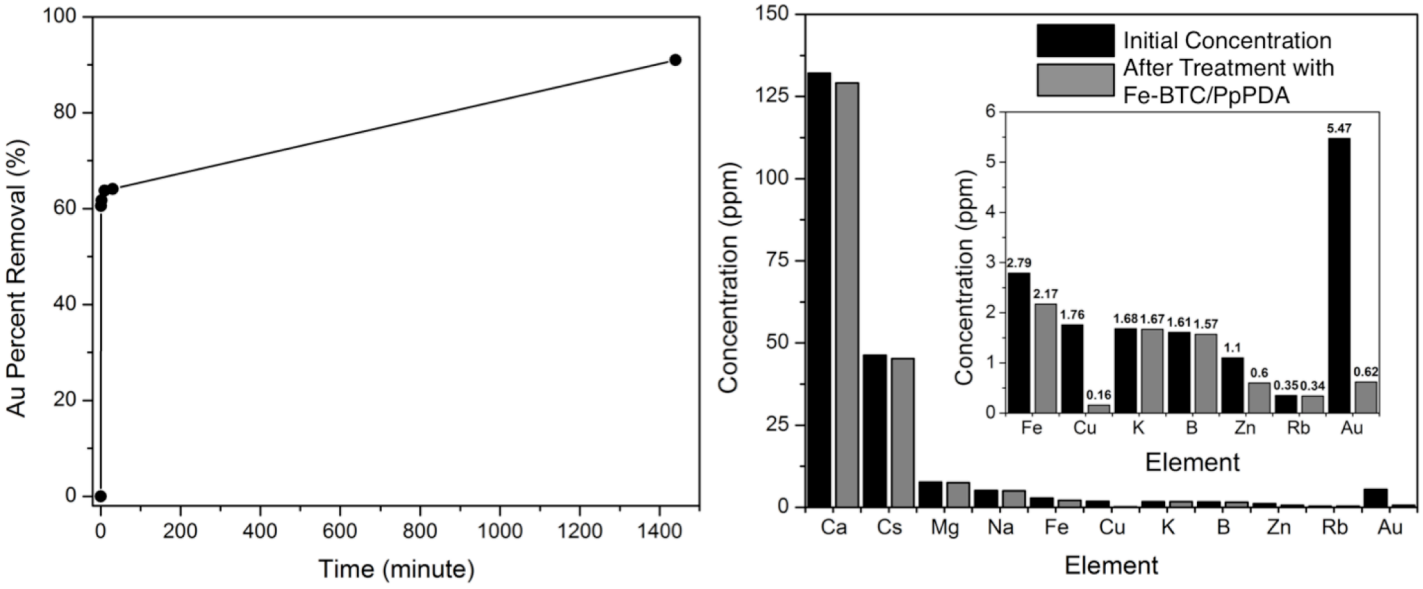

Figure 3.16
Extraction of Au from an incinerate sludge leaching solution. Incinerated sludge was soaked in a leaching solution and the solution was treated with Fe-BTC/PpPDA. The extraction rate (left) was determined by isolating the solution from the composite at different time points. The concentrations of all other metals present in the leaching solution (right) were determined after before and after equilibrium.

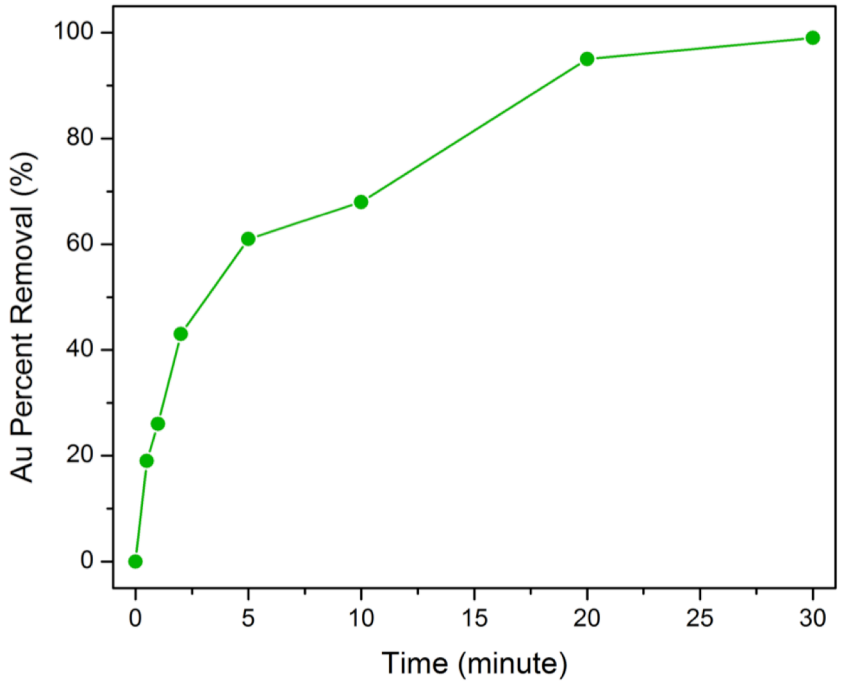

Figure 3.17
Extraction rate of Au from Mediterranean seawater. Seawater spiked with 1 ppm of Au was treated with Fe-BTC/PpPDA and the solution was isolated at different time points to calculate the percent removal.

Table 3.1
Elemental analysis and polymer loadings of the composites.

Polymer	C %	H %	N %	Polymer Wt. %
 Bare Framework	34.61	2.17	0	0
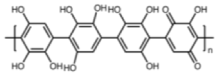 PHQ	40.06	2.57	1.54	19.69
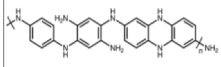 PpPDA	43.53	3.05	5.06	19.57
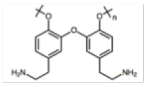 PTA	38.75	2.76	1.44	14.31
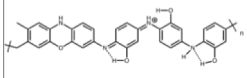 PmAP	40.35	2.78	2.12	16.54

Table 3.2
Comparison of top performing materials for gold extraction

Material	Surface Area (m^2/g)	Mechanism	% Removal	Speed to % Removal (min)	Au^{3+} Capacity (mg/g)	Regeneration	Selectivity	Purity of Au^0 (Out of 24K)	Ref.
Fe-BTC	2324	Adsorption	75.38	2	136.9	N.R.	N.R.	N.R.	This work
Fe-BTC/PpPDA	1034	Adsorption/Reduction	99	2	934	✔	✔	23.9	This work
3,5,5-trimethylhexanamide[a]	N.R.	Phase Extraction	86	60	N.R.	N.R.	✔	N.R.	181
$CaCu_6[(S,S)\text{-methox}]_3(OH)_2(H_2O)$[b]	N.R.	Adsorption	99	45	598	✔	✔	N.R.	180
Poly(vinylpyrrolidone) (PVP)[c]	N.R.	Reduction	99	6	N.R.	N.R.	✗	N.R.	200
DBC-$CONHNH_2$[d]	N.R.	Reduction	99	2880	2000	N.R.	✗	N.R.	185
PVBTAH~ZIF-8[e]	600	Ion-Exchange	90	5	N.R.	N.R.	N.R.	N.R.	182
NH_2-MCM-41[f*]	770	Adsorption	99	30	275	✔	N.R.	N.R.	201
UiO-66[g]	1551	Adsorption	N.R.	25	53	✔	✗	N.R.	184
UiO-66-NH_2[g]	1067	Adsorption	N.R.	180	76	✔	✗	N.R.	184
UiO-66-TU[h]	958	Adsorption	N.R.	90	326	✗	✔	N.R.	202
Fe_3O_4@DMSA[i]	N.R.	Adsorption	N.R.	480	340	N.R.	N.R.	N.R.	203
ZnO[j]	N.R.	Reduction	99	N.R.	N.R.	N.R.	N.R.	23.4	56
Bacteriophages[k]	N.R.	Adsorption/Reduction	96	1440	571	N.R.	N.R.	N.R.	183
L-lysine modified chitosan resin[l]	N.R.	Adsorption	N.R.	250	70.34	N.R.	N.R.	N.R.	204
Cross-linked Lignopyrogallol	N.R.	Adsorption/Reduction	80	1440	374.22	N.R.	✗	N.R.	205
Straw-SH[m]	N.R.	Adsorption	N.R.	120	450	N.R.	✗	N.R.	206
Starbon®[n]	631	Adsorption	99	N.R.	3800	N.R.	✗	N.R.	207
MPGC-900[o]	918.4	Adsorption	93	60	7.45	N.R.	✗	N.R.	208

N.R. – Not reported
✔ – Experiment performed with positive results
✗ – Experiment performed with negative results

a. Although the method has high selectivity for Au it is a solvent based homogenous extraction process using toluene, requiring 1-hour phase transferring times. There is no report of the material performance in applicable conditions with metal ions such as Na, Ca, Mg, etc and organics, which are present in river, sea and waste water matrixes. No trace experiments were done and gold purity is not reported.
b. 5 mg of MOF is soaked in 5 mL of a 0.02 M $AuCl_3$ solution. The concentration of the solution is high at 3939.2 ppm Au^{3+}. All experiments are performed in a 1 to 1 distilled water to methanol mixture. There is no report of the material performance in applicable conditions with metal ions such as Na, Ca, Mg, etc and organics, which are present in river, sea and waste water matrixes. No trace experiments or regeneration experiments were done and gold purity is not reported.
c. All experiments were done in distilled water. There is no report of the material performance in applicable conditions with metal ions such as Na, Ca, Mg, etc and organics, which are present in river, sea and waste water matrices. No trace experiments or regeneration experiments were done and gold purity is not reported.
d. The experiments are carried out in a 1969.6 ppm Au^{3+} solution. Further, the equilibrium times are 48 hours and all experiments were done in distilled water. No trace experiments or regeneration experiments were done and gold purity is not reported.

e. This method is an ion exchange thus a sacrificial anion must be present. These experiments are also done with KAuCN where $AuCN^-$ exchanges with another anion such as OH^- or Cl^-. There is no report of the material performance in applicable conditions with metal ions such as Na, Ca, Mg, etc and organics, which are present in river, sea and waste water matrixes. No trace experiments or regeneration experiments were done and gold purity is not reported.
f. Experiments were performed with distilled water containing Au concentrations at 787 ppm with 0.1 g of adsorbent to 0.1 L of solution. There is no report of the material performance in applicable conditions with metal ions such as Na, Ca, Mg, etc and organics, which are present in river, sea and waste water matrixes. No trace experiments or regeneration experiments were done and gold purity is not reported.
g. The equilibrium time was reported to be 25 min and 180 mins for UiO-66 and UiO-66-NH_2 respectively. Selectivity was tested only against Co, Ni, Cu and Zn. Also every experiment was performed in distilled water spiked with these metals and acidified with HCl. There is no report of the material performance in applicable conditions with metal ions such as Na, Ca, Mg, etc and organics, which are present in river, sea and waste water matrixes. No trace experiments were done and gold purity is not reported.
h. All experiments were done in distilled water. There is no report of the material performance in applicable conditions with metal ions such as Na, Ca, Mg, etc and organics, which are present in river, sea and waste water matrixes. No trace experiments or regeneration experiments were done and gold purity is not reported.
i. There is no report of the material performance in applicable conditions with metal ions such as Na, Ca, Mg, etc and organics, which are present in river, sea and waste water matrixes. No trace experiments or regeneration experiments were done and gold purity is not reported.
j. This paper illustrates a novel way of leeching gold from ores and electronic waste. They used a ZnO procedure taken from a patent and are able to purify 23.4K gold. Although their first step is great the separation of the oxidized gold ions is lacking detail. Our work focuses on this step and shows great improvements in the methodology as seen with the rapid extraction and reduction of gold resulting in 23.9K gold.
k. The authors only report capacity. There is no report of the material performance in applicable conditions with metal ions such as Na, Ca, Mg, etc and organics, which are present in river, sea and waste water matrixes. No trace experiments or regeneration experiments were done and gold purity is not reported.
l. There is no report of the material performance in applicable conditions with metal ions such as Na, Ca, Mg, etc and organics, which are present in river, sea and waste water matrixes. No trace experiments or regeneration experiments were done and gold purity is not reported.
m. Experimental procedures consist of using high concentrations of gold up to 500 ppm. There is no report of the material performance in applicable conditions with metal ions such as Na, Ca, Mg, etc and organics, which are present in river, sea and waste water matrixes. No trace experiments or regeneration experiments were done and gold purity is not reported.
n. Although they show high percent removal and claim capacities are over 3800 mg/g they do not show any data or isotherms related to these numbers. There is no report of the material performance in applicable conditions with metal ions such as Na, Ca, Mg, etc and organics, which are present in river, sea and waste water matrixes. No trace experiments or regeneration experiments were done and gold purity is not reported.
o. Magnetic porous graphitic carbons were used to treat solutions containing 10 ppm of Au. There is no report of the material performance in applicable conditions with metal ions such as Na, Ca, Mg, etc and organics, which are present in river, sea and waste water matrixes. No trace experiments or regeneration experiments were done and gold purity is not reported.

General Comments
Experiments are not being performed at trace concentrations (< 0.01 - 10 ppm)

APPENDIX to Chapter 4

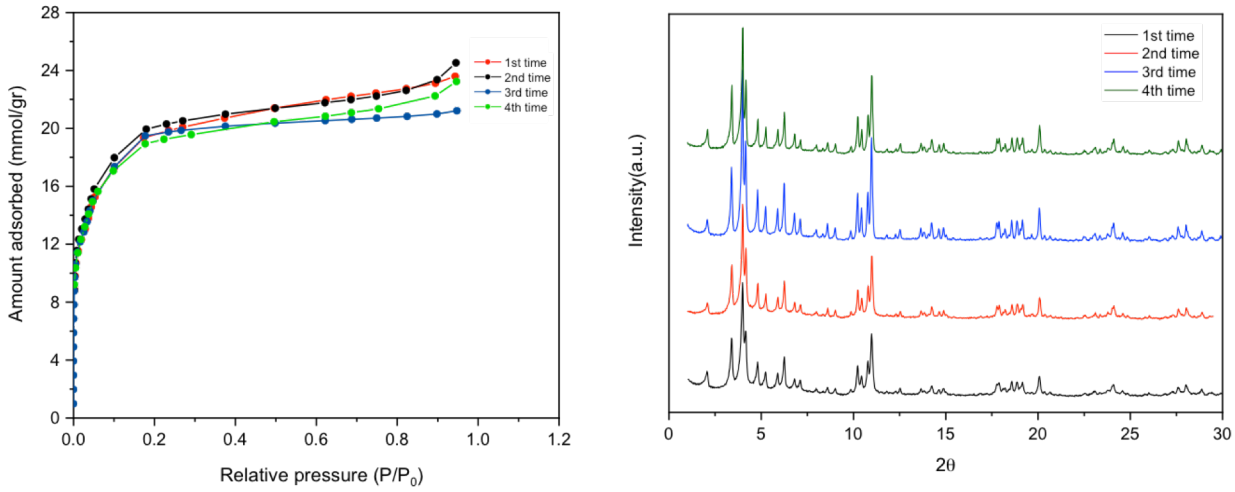

Figure 4.1. (Left) Nitrogen adsorption isotherms at 77K and (right) powder X-ray diffraction patterns for large scale Fe-BTC production and after reusing the mother liquor after the first reaction over many cycles.

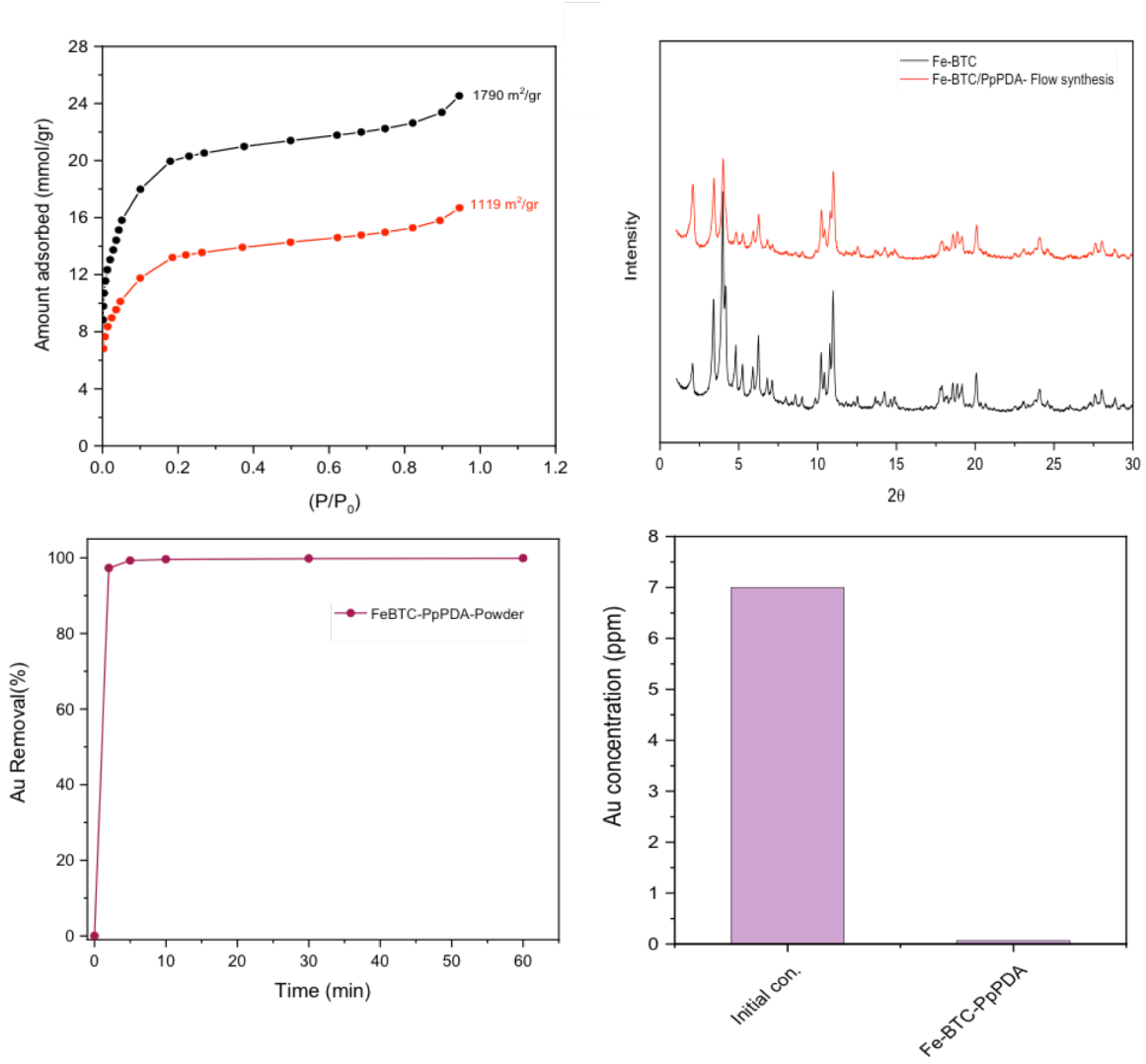

Figure 4.2. (Top, Left) Nitrogen adsorption isotherms at 77K for (black) Fe-BTC and (red) Fe-BTC/PpPDA made from the continuous flow through reactor. (Top, Right) Powder X-ray diffraction patterns for large scale (black) Fe-BTC and (red) Fe-BTC/PpPDA made from the continuous flow through reactor. (Bottom, Left) Gold extraction speed of scaled up Fe-BTC/PpPDA. (Bottom, Right) Concentration of the initial concentration of gold and after treatment with scaled up Fe-BTC/PpPDA.

Acknowledgements

First and foremost, I would like to thank my advisor, mentor and sensei Prof. Wendy L. Queen. Thank you for everything you have done for me these past years and taking a chance on me back in Berkeley. None of this work is possible without your input and guidance. Thank you for also developing me as a young professional, entrepreneur and scientist. I hope I have made you proud with my growth and scientific work. I will continue to better my self as a professional, scientist and entrepreneur.

Thank you to the current and previous members of Prof. Wendy L. Queen's Laboratory for Functional Inorganic Materials. This includes Prof. Li Peng, Dr. Safak Bulut, Dr. Shuliang Yang, Dr. Olga Trukhina, Dr. Jordi Espin, Dr. Pierre Dapsens, Dr. Mehrdad Asgari, Vikram V. Karve, Anita Justin, Ilia Kochetygov, Hassan Abedini, Till Schertenleib, Guanchu Lu, Martin W. Cull, Washington S. Reeder, Eunice Bae and Daniel Doeller. I consider you all my brothers and sisters and am grateful to you all for helping me all these years.

Thank you the EPFL Valais scientific staff. This includes Natalia Gasilova, Emad Oveisi, Pascal Schouwink and Mounir Mensi. Your expertise and help greatly enhanced the projects.

Thank you to EPFL Valais, its Magasin, Mechanical and Electronic workshop. This includes Marc-Andre Berclaz, Stephane Voeffray, Robin Cyril Deleze, Laurent Seydoux, Annabelle Coquoz, Cedric Passerini, Jean Perruchoud, Filipe Martins and Patrick Favre. The help over the years have been instrumental in the projects and I am grateful to you all.

Thank you to Laure Dayer for helping with many things over the years in LFIM. You are the best.

Thank you to Prof. Emily Jarvis and Prof. Jeremy McCallum for being great mentors during my Bachelor studies. You have been instrumental in the beginning of my career and I am forever grateful.

Thank you to all my friends and colleagues at EPFL. Especially Ski Squad.

Thank you to my family and friends for always supporting me on my endeavors.

Thank you to EPFL Vice Presidency of Innovation, Tech4Impact, the Swiss National Science Foundation and Innosuisse for supporting the project further.

References

1. Izatt, R. M.; Izatt, S. R.; Izatt, N. E.; Krakowiak, K. E.; Bruening, R. L.; Navarro, L., Industrial applications of molecular recognition technology to separations of platinum group metals and selective removal of metal impurities from process streams. *Green Chemistry* **2015,** *17* (4), 2236-2245.
2. Turner, A.; Crussell, M.; Millward, G. E.; Cobelo-Garcia, A.; Fisher, A. S., Adsorption Kinetics of Platinum Group Elements in River Water. *Environmental Science & Technology* **2006,** *40* (5), 1524-1531.
3. Sharma, S.; Rajesh, N., Augmenting the adsorption of palladium from spent catalyst using a thiazole ligand tethered on an amine functionalized polymeric resin. *Chem. Eng. J.* **2016,** *283*, 999-1008.
4. Cundy, C. S.; Cox, P. A., The hydrothermal synthesis of zeolites: Precursors, intermediates and reaction mechanism. *Microporous and Mesoporous Materials* **2005,** *82* (1), 1-78.
5. Ma, L.; Wang, Q.; Islam, S. M.; Liu, Y.; Ma, S.; Kanatzidis, M. G., Highly Selective and Efficient Removal of Heavy Metals by Layered Double Hydroxide Intercalated with the MoS42– Ion. *Journal of the American Chemical Society* **2016,** *138* (8), 2858-2866.
6. Asiabi, H.; Yamini, Y.; Shamsayei, M.; Tahmasebi, E., Highly selective and efficient removal and of heavy metals by layered double hydroxides intercalated with the diphenylamine-4-sulfonate: A comparative study. *Chemical Engineering Journal* **2017,** *323*, 212-223.
7. Hou, H.; Yu, C.-X.; Shao, C. Z., A functionalized metal-organic framework decorated with O- groups showing excellent performance for lead(II) removal from aqueous solution. *Chem. Sci.* **2017**.
8. He, R.; Li, W.; Deng, D.; Chen, W.; Li, H.; Wei, C.; Tang, Y., Efficient removal of lead from highly acidic wastewater by periodic ion imprinted mesoporous SBA-15 organosilica combining metal coordination and co-condensation. *Journal of Materials Chemistry A* **2015,** *3* (18), 9789-9798.
9. Zhang, Q.; Yang, Q.; Phanlavong, P.; Li, Y.; Wang, Z.; Jiao, T.; Peng, Q., Highly Efficient Lead(II) Sequestration Using Size-Controllable Polydopamine Microspheres with Superior Application Capability and Rapid Capture. *ACS Sustainable Chemistry & Engineering* **2017,** *5* (5), 4161-4170.
10. Rathore, E.; Pal, P.; Biswas, K., Layered Metal Chalcophosphate (K-MPS-1) for Efficient, Selective, and ppb Level Sequestration of Pb from Water. *The Journal of Physical Chemistry C* **2017,** *121* (14), 7959-7966.
11. Abney, C. W.; Gilhula, J. C.; Lu, K.; Lin, W., Metal-Organic Framework Templated Inorganic Sorbents for Rapid and Efficient Extraction of Heavy Metals. *Advanced Materials* **2014,** *26* (47), 7993-7997.
12. Gunathilake, C.; Kadanapitiye, M. S.; Dudarko, O.; Huang, S. D.; Jaroniec, M., Adsorption of Lead Ions from Aqueous Phase on Mesoporous Silica with P-Containing Pendant Groups. *ACS Appl. Mater. Interfaces* **2015,** *7* (41), 23144-23152.
13. Shin, Y.; Fryxell, G. E.; Um, W.; Parker, K.; Mattigod, S. V.; Skaggs, R., Sulfur-Functionalized Mesoporous Carbon. *Adv. Funct. Mater.* **2007,** *17* (15), 2897-2901.
14. Yantasee, W.; Warner, C. L.; Sangvanich, T.; Addleman, R. S.; Carter, T. G.; Wiacek, R. J.; Fryxell, G. E.; Timchalk, C.; Warner, M. G., Removal of Heavy Metals from Aqueous Systems with Thiol Functionalized Superparamagnetic Nanoparticles. *Environmental Science & Technology* **2007,** *41* (14), 5114-5119.
15. Manos, M. J.; Petkov, V. G.; Kanatzidis, M. G., H2xMnxSn3-xS6 (x = 0.11–0.25): A Novel Reusable Sorbent for Highly Specific Mercury Capture Under Extreme pH Conditions. *Advanced Functional Materials* **2009,** *19* (7), 1087-1092.

16. Yee, K.-K.; Reimer, N.; Liu, J.; Cheng, S.-Y.; Yiu, S.-M.; Weber, J.; Stock, N.; Xu, Z., Effective Mercury Sorption by Thiol-Laced Metal–Organic Frameworks: in Strong Acid and the Vapor Phase. *Journal of the American Chemical Society* **2013,** *135* (21), 7795-7798.

17. Li, B.; Zhang, Y.; Ma, D.; Shi, Z.; Ma, S., Mercury nano-trap for effective and efficient removal of mercury(II) from aqueous solution. **2014,** *5*, 5537.

18. Mon, M.; Lloret, F.; Ferrando-Soria, J.; Martí-Gastaldo, C.; Armentano, D.; Pardo, E., Selective and Efficient Removal of Mercury from Aqueous Media with the Highly Flexible Arms of a BioMOF. *Angew. Chem. Int. Ed.* **2016,** *55* (37), 11167-11172.

19. Rudd, N. D.; Wang, H.; Fuentes-Fernandez, E. M. A.; Teat, S. J.; Chen, F.; Hall, G.; Chabal, Y. J.; Li, J., Highly Efficient Luminescent Metal–Organic Framework for the Simultaneous Detection and Removal of Heavy Metals from Water. *ACS Appl. Mater. Interfaces* **2016,** *8* (44), 30294-30303.

20. Ahmed, S.; Brockgreitens, J.; Xu, K.; Abbas, A., A Nanoselenium Sponge for Instantaneous Mercury Removal to Undetectable Levels. *Advanced Functional Materials* **2017,** *27* (17), 1606572-n/a.

21. Meri-Bofi, L.; Royuela, S.; Zamora, F.; Ruiz-Gonzalez, M. L.; Segura, J. L.; Munoz-Olivas, R.; Mancheno, M. J., Thiol grafted imine-based covalent organic frameworks for water remediation through selective removal of Hg(ii). *Journal of Materials Chemistry A* **2017,** *5* (34), 17973-17981.

22. Sun, Q.; Aguila, B.; Perman, J.; Earl, L. D.; Abney, C. W.; Cheng, Y.; Wei, H.; Nguyen, N.; Wojtas, L.; Ma, S., Postsynthetically Modified Covalent Organic Frameworks for Efficient and Effective Mercury Removal. *J. Am. Chem. Soc.* **2017,** *139* (7), 2786-2793.

23. Zeng, X.; Mathews, J. A.; Li, J., Urban Mining of E-Waste is Becoming More Cost-Effective Than Virgin Mining. *Environmental Science & Technology* **2018,** *52* (8), 4835-4841.

24. Tan, M. X.; Sum, Y. N.; Ying, J. Y.; Zhang, Y., A mesoporous poly-melamine-formaldehyde polymer as a solid sorbent for toxic metal removal. *Energy & Environmental Science* **2013,** *6* (11), 3254-3259.

25. Li, B.; Zhou, F.; Huang, K.; Wang, Y.; Mei, S.; Zhou, Y.; Jing, T., Environmentally friendly chitosan/PEI-grafted magnetic gelatin for the highly effective removal of heavy metals from drinking water. **2017,** *7*, 43082.

26. Geoff Rayner-Canham, T. O., *Descriptive Inorganic Chemistry*. Fifth ed.; Clancy Marshall: New York, NY, USA, 2010; p 651.

27. Zheng, Y.; Li, X.; Dutta, P. K., Exploitation of unique properties of zeolites in the development of gas sensors. *Sensors* **2012,** *12* (4), 5170-5194.

28. Luo, X.; Ding, L.; Luo, J., Adsorptive Removal of Pb(II) Ions from Aqueous Samples with Amino-Functionalization of Metal–Organic Frameworks MIL-101(Cr). *Journal of Chemical & Engineering Data* **2015,** *60* (6), 1732-1743.

29. Marcus, Y., Thermodynamics of solvation of ions. Part 5.—Gibbs free energy of hydration at 298.15 K. *J. Chem. Soc., Faraday Trans.* **1991,** *87* (18), 2995-2999.

30. Ling, L.-L.; Liu, W.-J.; Zhang, S.; Jiang, H., Magnesium Oxide Embedded Nitrogen Self-Doped Biochar Composites: Fast and High-Efficiency Adsorption of Heavy Metals in an Aqueous Solution. *Environmental Science & Technology* **2017,** *51* (17), 10081-10089.

31. William F. Smith, J. H., *Foundations of Materials Science and Engineering*. 4th ed.; McGraw-Hill: 2006.

32. Cao, C.-Y.; Qu, J.; Wei, F.; Liu, H.; Song, W.-G., Superb Adsorption Capacity and Mechanism of Flowerlike Magnesium Oxide Nanostructures for Lead and Cadmium Ions. *ACS Applied Materials & Interfaces* **2012,** *4* (8), 4283-4287.

33. Paufler, P., R. F. Tylecote. A history of metallurgy. The Metals Society, London, 2nd impression 1979, 182 Seiten mit 149 Abbildungen, 76 Tabellen und 6 Karten, Preis £ 10,00, Übersee US $ 30.00. *Crystal Research and Technology* **1983,** *18* (7), 932-932.

34. Liu, L.; Corma, A., Metal Catalysts for Heterogeneous Catalysis: From Single Atoms to Nanoclusters and Nanoparticles. *Chem. Rev.* **2018,** *118* (10), 4981-5079.

35. Schmucker, S. C., THE ELECTROLYTIC SEPARATION OF THE METALS OF THE SECOND GROUP. *J. Am. Chem. Soc.* **1893,** *15* (4), 195-206.

36. Krishnamoorthy, L.; Cotruvo Jr, J. A.; Chan, J.; Kaluarachchi, H.; Muchenditsi, A.; Pendyala, V. S.; Jia, S.; Aron, A. T.; Ackerman, C. M.; Wal, M. N. V.; Guan, T.; Smaga, L. P.; Farhi, S. L.; New, E. J.; Lutsenko, S.; Chang, C. J., Copper regulates cyclic-AMP-dependent lipolysis. *Nat. Chem. Biol.* **2016,** *12*, 586.

37. Edelman, I. S.; Leibman, J., Anatomy of body water and electrolytes. *The American Journal of Medicine* **1959,** *27* (2), 256-277.

38. Tchounwou, P. B.; Yedjou, C. G.; Patlolla, A. K.; Sutton, D. J., Heavy Metal Toxicity and the Environment. In *Molecular, Clinical and Environmental Toxicology: Volume 3: Environmental Toxicology*, Luch, A., Ed. Springer Basel: Basel, 2012; pp 133-164.

39. Precious Metal Prices. https://www.perthmint.com/investment_invest_in_gold_precious_metal_prices.aspx.

40. Uranim Prices. https://www.indexmundi.com/commodities/?commodity=uranium&months=360.

41. Lithium Prices. https://www.metalary.com/lithium-price/.

42. Gleick, P. H., Global freshwater resources: soft-path solutions for the 21st century. *Science* **2003,** *302* (5650), 1524-1528.

43. World Health Organization: Drinking Water Fact Sheet. http://www.who.int/mediacentre/factsheets/fs391/en/ (accessed November 1, 2016).

44. Luu, T. T. G.; Sthiannopkao, S.; Kim, K.-W., Arsenic and other trace elements contamination in groundwater and a risk assessment study for the residents in the Kandal Province of Cambodia. *Environment International* **2009,** *35* (3), 455-460.

45. Beaumont, J. J.; Sedman, R. M.; Reynolds, S. D.; Sherman, C. D.; Li, L.-H.; Howd, R. A.; Sandy, M. S.; Zeise, L.; Alexeeff, G. V., Cancer Mortality in a Chinese Population Exposed to Hexavalent Chromium in Drinking Water. *Epidemiology* **2008,** *19* (1), 12-23.

46. Ingraham, C. This is how toxic Flint's water really is. https://www.washingtonpost.com/news/wonk/wp/2016/01/15/this-is-how-toxic-flints-water-really-is/ (accessed March 24, 2016).

47. M. B. Pell, J. S. Off the Charts: The thousands of U.S. locales where lead poisoning is worse than Flint. http://www.reuters.com/investigates/special-report/usa-lead-testing/.

48. Mohan, V. Across India, high levels of toxins in groundwater 2018. https://timesofindia.indiatimes.com/india/govt-body-finds-high-levels-of-groundwater-contamination-across-india/articleshow/65204273.cms.

49. Huang, D.; Liao, F.; Molesa, S.; Redinger, D.; Subramanian, V., Plastic-compatible low resistance printable gold nanoparticle conductors for flexible electronics. *J. Electrochem. Soc.* **2003,** *150* (7), G412-G417.

50. Ishiyama, T.; Matsuda, N.; Miyaura, N.; Suzuki, A., Platinum (0)-catalyzed diboration of alkynes. *J. Am. Chem. Soc.* **1993,** *115* (23), 11018-11019.

51. Meitner, L.; Frisch, O. R., Disintegration of uranium by neutrons: a new type of nuclear reaction. *A Century of Nature: Twenty-One Discoveries that Changed Science and the World* **1939**, 70.

52. Carbajo, J. J.; Yoder, G. L.; Popov, S. G.; Ivanov, V. K., A review of the thermophysical properties of MOX and UO2 fuels. *J. Nucl. Mater.* **2001,** *299* (3), 181-198.

53. Chan, C. K.; Peng, H.; Liu, G.; McIlwrath, K.; Zhang, X. F.; Huggins, R. A.; Cui, Y., High-performance lithium battery anodes using silicon nanowires. *Nat. Nanotechnol.* **2008,** *3* (1), 31.

54. C.P Balde, V. F., V. Gray, R. Kuehr, P. Stegmann *The Global E-waste Monitor 2017*; United Nations University, International Telecommunication Union & International Solid Waste Association: 2017.

55. Prichard, H. M.; Wedin, F.; Sampson, J.; Jackson, M. T.; Fisher, P. C., Precious metals in urban waste. *Water and Environment Journal* **2016,** *30* (1-2), 151-156.

56. Yue, C.; Sun, H.; Liu, W.-J.; Guan, B.; Deng, X.; Zhang, X.; Yang, P., Environmentally Benign, Rapid, and Selective Extraction of Gold from Ores and Waste Electronic Materials. *Angew. Chem. Int. Ed.* **2017,** *56* (32), 9331-9335.

57. Winter, T. C., *Ground water and surface water: a single resource*. DIANE Publishing Inc.: 1998; Vol. 1139.

58. Alsdorf, D. E.; Rodríguez, E.; Lettenmaier, D. P., Measuring surface water from space. *Reviews of Geophysics* **2007,** *45* (2).

59. Page, G. W., Comparison of groundwater and surface water for patterns and levels of contamination by toxic substances. *Environmental science & technology* **1981,** *15* (12), 1475-1481.

60. Kang, M.; Jackson, R. B., Salinity of deep groundwater in California: Water quantity, quality, and protection. *Proceedings of the National Academy of Sciences* **2016,** *113* (28), 7768-7773.

61. Meade, R. H.; Emery, K., Sea level as affected by river runoff, eastern United States. *Science* **1971,** *173* (3995), 425-428.

62. Lyman, J.; Fleming, R. H., Composition of sea water. *J. mar. Res* **1940,** *3* (2), 134-146.

63. McHugh, J., Concentration of gold in natural waters. *Journal of Geochemical Exploration* **1988,** *30* (1-3), 85-94.

64. Sholl, D. S.; Lively, R. P., Seven chemical separations to change the world. *Nature News* **2016,** *532* (7600), 435.

65. Kesler, S. E.; Gruber, P. W.; Medina, P. A.; Keoleian, G. A.; Everson, M. P.; Wallington, T. J., Global lithium resources: Relative importance of pegmatite, brine and other deposits. *Ore Geology Reviews* **2012,** *48*, 55-69.

66. Patterson, J. W., Industrial wastewater treatment technology. **1985**.

67. Dean, J. G.; Bosqui, F. L.; Lanouette, K. H., Removing heavy metals from waste water. *Environmental Science & Technology* **1972,** *6* (6), 518-522.

68. Harper, T. R.; Kingham, N. W., Removal of arsenic from wastewater using chemical precipitation methods. *Water Environment Research* **1992,** *64* (3), 200-203.

69. Bratby, J., *Coagulation and flocculation in water and wastewater treatment*. IWA publishing: 2016.

70. Molinari, R.; Gallo, S.; Argurio, P., Metal ions removal from wastewater or washing water from contaminated soil by ultrafiltration–complexation. *Water research* **2004,** *38* (3), 593-600.

71. Kadirvelu, K.; Thamaraiselvi, K.; Namasivayam, C., Removal of heavy metals from industrial wastewaters by adsorption onto activated carbon prepared from an agricultural solid waste. *Bioresource technology* **2001,** *76* (1), 63-65.

72. Rengaraj, S.; Yeon, K.-H.; Moon, S.-H., Removal of chromium from water and wastewater by ion exchange resins. *J. Hazard. Mater.* **2001,** *87* (1-3), 273-287.

73. Rubio, J.; Souza, M.; Smith, R., Overview of flotation as a wastewater treatment technique. *Minerals engineering* **2002,** *15* (3), 139-155.

74. Chen, G., Electrochemical technologies in wastewater treatment. *Sep. Purif. Technol.* **2004,** *38* (1), 11-41.

75. Nosier, S.; Sallam, S., Removal of lead ions from wastewater by cementation on a gas-sparged zinc cylinder. *Sep. Purif. Technol.* **2000,** *18* (2), 93-101.

76. Stephenson, T.; Brindle, K.; Judd, S.; Jefferson, B., *Membrane bioreactors for wastewater treatment*. IWA publishing: 2000.

77. Zhang, Y.; Liu, S.; Xie, H.; Zeng, X.; Li, J., Current status on leaching precious metals from waste printed circuit boards. *Procedia Environmental Sciences* **2012,** *16*, 560-568.

78. Aylmore, M. G.; Muir, D. M., Thiosulfate leaching of gold—a review. *Minerals engineering* **2001,** *14* (2), 135-174.

79. Cui, J.; Zhang, L., Metallurgical recovery of metals from electronic waste: a review. *J. Hazard. Mater.* **2008,** *158* (2-3), 228-256.

80. Rosenfeld, P. E.; Feng, L. G. H., 1 - Definition of Hazardous Waste. In *Risks of Hazardous Wastes*, Rosenfeld, P. E.; Feng, L. G. H., Eds. William Andrew Publishing: Boston, 2011; pp 1-10.

81. Hoffmann, J. E., Recovering precious metals from electronic scrap. *JOM* **1992,** *44* (7), 43-48.

82. Fleming, C., Hydrometallurgy of precious metals recovery. *Hydrometallurgy* **1992,** *30* (1-3), 127-162.

83. Ilyas, S.; Lee, J. c., Biometallurgical recovery of metals from waste electrical and electronic equipment: a review. *ChemBioEng Reviews* **2014,** *1* (4), 148-169.

84. Mecucci, A.; Scott, K., Leaching and electrochemical recovery of copper, lead and tin from scrap printed circuit boards. *Journal of Chemical Technology & Biotechnology: International Research in Process, Environmental & Clean Technology* **2002,** *77* (4), 449-457.

85. Brunner, G. H., *Supercritical fluids as solvents and reaction media*. Elsevier: 2004.

86. Baláž, P., Mechanochemistry in Minerals Engineering. In *Mechanochemistry in Nanoscience and Minerals Engineering*, Springer: 2008; pp 257-296.

87. Jenkin, G. R.; Al-Bassam, A. Z.; Harris, R. C.; Abbott, A. P.; Smith, D. J.; Holwell, D. A.; Chapman, R. J.; Stanley, C. J., The application of deep eutectic solvent ionic liquids for environmentally-friendly dissolution and recovery of precious metals. *Minerals Engineering* **2016,** *87*, 18-24.

88. Eissler, M., *The Cyanide Process for the Extraction of Gold and Its Practical Application on the Witwatersrand Goldfields and Elsewhere*. C. Lockwood: 1898.

89. Sun, D. T.; Peng, L.; Reeder, W. S.; Moosavi, S. M.; Tiana, D.; Britt, D. K.; Oveisi, E.; Queen, W. L., Rapid, Selective Heavy Metal Removal from Water by a Metal–Organic Framework/Polydopamine Composite. *ACS Cent. Sci.* **2018,** *4* (3), 349-356.

90. Sun, D. T.; Gasilova, N.; Yang, S.; Oveisi, E.; Queen, W. L., Rapid, Selective Extraction of Trace Amounts of Gold from Complex Water Mixtures with a Metal–Organic Framework (MOF)/Polymer Composite. *J. Am. Chem. Soc.* **2018,** *140* (48), 16697-16703.

91. Tang, W.-W.; Zeng, G.-M.; Gong, J.-L.; Liang, J.; Xu, P.; Zhang, C.; Huang, B.-B., Impact of humic/fulvic acid on the removal of heavy metals from aqueous solutions using nanomaterials: A review. *Sci. Total Environ.* **2014,** *468–469*, 1014-1027.

92. Shi, Q.; Terracciano, A.; Zhao, Y.; Wei, C.; Christodoulatos, C.; Meng, X., Evaluation of metal oxides and activated carbon for lead removal: Kinetics, isotherms, column tests, and the role of co-existing ions. *Sci. Total Environ.* **2019,** *648*, 176-183.

93. Rouquerol, J.; Rouquerol, F.; Llewellyn, P.; Maurin, G.; Sing, K. S., *Adsorption by powders and porous solids: principles, methodology and applications*. Academic press: 2013.

94. Shannon, M. A.; Bohn, P. W.; Elimelech, M.; Georgiadis, J. G.; Marinas, B. J.; Mayes, A. M., Science and technology for water purification in the coming decades. In *Nanoscience and technology: a collection of reviews from nature Journals*, World Scientific: 2010; pp 337-346.

95. Yaghi, O. M.; O'Keeffe, M.; Ockwig, N. W.; Chae, H. K.; Eddaoudi, M.; Kim, J., Reticular synthesis and the design of new materials. *Nature* **2003,** *423* (6941), 705-714.

96. Zhou, H.-C.; Long, J. R.; Yaghi, O. M., Introduction to Metal–Organic Frameworks. *Chem. Rev.* **2012,** *112* (2), 673-674.

97. Férey, G.; Mellot-Draznieks, C.; Serre, C.; Millange, F.; Dutour, J.; Surblé, S.; Margiolaki, I., A Chromium Terephthalate-Based Solid with Unusually Large Pore Volumes and Surface Area. *Science* **2005,** *309* (5743), 2040-2042.

98. Brown, G. P.; Aftergut, S., Bis(imidazolato)–metal polymers. *Journal of Polymer Science Part A: General Papers* **1964,** *2* (4), 1839-1845.

99. Lundberg, B., The crystal structure of di-imidazole-zinc(II) dichloride. *Acta Crystallogr.* **1966,** *21* (6), 901-909.

100. Hoskins, B. F.; Robson, R., Design and construction of a new class of scaffolding-like materials comprising infinite polymeric frameworks of 3D-linked molecular rods. A reappraisal of the zinc cyanide and cadmium cyanide structures and the synthesis and structure of the diamond-related frameworks [N(CH3)4][CuIZnII(CN)4] and CuI[4,4',4'',4'''-tetracyanotetraphenylmethane]BF4.xC6H5NO2. *J. Am. Chem. Soc.* **1990,** *112* (4), 1546-1554.

101. Yaghi, O. M.; Li, H., Hydrothermal Synthesis of a Metal-Organic Framework Containing Large Rectangular Channels. *J. Am. Chem. Soc.* **1995,** *117* (41), 10401-10402.

102. Kondo, M.; Yoshitomi, T.; Matsuzaka, H.; Kitagawa, S.; Seki, K., Three-Dimensional Framework with Channeling Cavities for Small Molecules: {[M2(4, 4′-bpy)3(NO3)4]·xH2O}n (M ⌋ Co, Ni, Zn). *Angewandte Chemie International Edition in English* **1997,** *36* (16), 1725-1727.

103. Li, H.; Eddaoudi, M.; Groy, T. L.; Yaghi, O. M., Establishing Microporosity in Open Metal–Organic Frameworks: Gas Sorption Isotherms for Zn(BDC) (BDC = 1,4-Benzenedicarboxylate). *J. Am. Chem. Soc.* **1998,** *120* (33), 8571-8572.

104. Yuan, S.; Feng, L.; Wang, K.; Pang, J.; Bosch, M.; Lollar, C.; Sun, Y.; Qin, J.; Yang, X.; Zhang, P.; Wang, Q.; Zou, L.; Zhang, Y.; Zhang, L.; Fang, Y.; Li, J.; Zhou, H.-C., Stable Metal–Organic Frameworks: Design, Synthesis, and Applications. *Adv. Mater.* **2018,** *30* (37), 1704303.

105. Queen, W. L.; Hudson, M. R.; Bloch, E. D.; Mason, J. A.; Gonzalez, M. I.; Lee, J. S.; Gygi, D.; Howe, J. D.; Lee, K.; Darwish, T. A.; James, M.; Peterson, V. K.; Teat, S. J.; Smit, B.; Neaton, J. B.; Long, J. R.; Brown, C. M., Comprehensive study of carbon dioxide adsorption in the metal–organic frameworks M2(dobdc) (M = Mg, Mn, Fe, Co, Ni, Cu, Zn). *Chem. Sci.* **2014,** *5* (12), 4569-4581.

106. Antonio, A. M.; Rosenthal, J.; Bloch, E. D., Electrochemically Mediated Syntheses of Titanium(III)-Based Metal–Organic Frameworks. *J. Am. Chem. Soc.* **2019,** *141* (29), 11383-11387.

107. Rieth, A. J.; Wright, A. M.; Skorupskii, G.; Mancuso, J. L.; Hendon, C. H.; Dinca, M., Record-Setting Sorbents for Reversible Water Uptake by Systematic Anion-Exchanges in Metal-Organic Frameworks. *J. Am. Chem. Soc.* **2019**.

108. Taylor, M. K.; Runčevski, T.; Oktawiec, J.; Bachman, J. E.; Siegelman, R. L.; Jiang, H.; Mason, J. A.; Tarver, J. D.; Long, J. R., Near-Perfect CO2/CH4 Selectivity Achieved through Reversible Guest Templating in the Flexible Metal–Organic Framework Co(bdp). *J. Am. Chem. Soc.* **2018,** *140* (32), 10324-10331.

109. Tu, M.; Reinsch, H.; Rodríguez-Hermida, S.; Verbeke, R.; Stassin, T.; Egger, W.; Dickmann, M.; Dieu, B.; Hofkens, J.; Vankelecom, I. F. J.; Stock, N.; Ameloot, R., Reversible Optical Writing and Data Storage in an Anthracene-Loaded Metal–Organic Framework. *Angew. Chem. Int. Ed.* **2019,** *58* (8), 2423-2427.

110. Kato, S.; Otake, K.-i.; Chen, H.; Akpinar, I.; Buru, C. T.; Islamoglu, T.; Snurr, R. Q.; Farha, O. K., Zirconium-Based Metal–Organic Frameworks for the Removal of Protein-Bound Uremic Toxin from Human Serum Albumin. *J. Am. Chem. Soc.* **2019,** *141* (6), 2568-2576.

111. Crawford, D.; Casaban, J.; Haydon, R.; Giri, N.; McNally, T.; James, S. L., Synthesis by extrusion: continuous, large-scale preparation of MOFs using little or no solvent. *Chem. Sci.* **2015,** *6* (3), 1645-1649.

112. Stavitski, E.; Goesten, M.; Juan-Alcañiz, J.; Martinez-Joaristi, A.; Serra-Crespo, P.; Petukhov, A. V.; Gascon, J.; Kapteijn, F., Kinetic Control of Metal–Organic Framework Crystallization Investigated by Time-Resolved In Situ X-Ray Scattering. *Angew. Chem. Int. Ed.* **2011,** *50* (41), 9624-9628.

113. Cohen, S. M., Postsynthetic Methods for the Functionalization of Metal–Organic Frameworks. *Chem. Rev.* **2012,** *112* (2), 970-1000.

114. Braun, E.; Chen, J. J.; Schnell, S. K.; Lin, L.-C.; Reimer, J. A.; Smit, B., Nanoporous Materials Can Tune the Critical Point of a Pure Substance. *Angew. Chem.* **2015,** *127* (48), 14557-14560.

115. Yoon, J. W.; Seo, Y.-K.; Hwang, Y. K.; Chang, J.-S.; Leclerc, H.; Wuttke, S.; Bazin, P.; Vimont, A.; Daturi, M.; Bloch, E.; Llewellyn, P. L.; Serre, C.; Horcajada, P.; Grenèche, J.-M.; Rodrigues, A. E.; Férey, G., Controlled Reducibility of a Metal–Organic Framework with Coordinatively Unsaturated Sites for Preferential Gas Sorption. *Angew. Chem. Int. Ed.* **2010,** *49* (34), 5949-5952.

116. Peng, Y.; Huang, H.; Zhang, Y.; Kang, C.; Chen, S.; Song, L.; Liu, D.; Zhong, C., A versatile MOF-based trap for heavy metal ion capture and dispersion. *Nat. Commun.* **2018,** *9* (1), 187.

117. Drout, R. J.; Otake, K.; Howarth, A. J.; Islamoglu, T.; Zhu, L.; Xiao, C.; Wang, S.; Farha, O. K., Efficient Capture of Perrhenate and Pertechnetate by a Mesoporous Zr Metal–Organic Framework and Examination of Anion Binding Motifs. *Chem. Mater.* **2018,** *30* (4), 1277-1284.

118. Percec, V., Introduction: Frontiers in Polymer Chemistry. *Chem. Rev.* **2001,** *101* (12), 3579-3580.

119. Duan, P.; Moreton, J. C.; Tavares, S. R.; Semino, R.; Maurin, G.; Cohen, S. M.; Schmidt-Rohr, K., Polymer Infiltration into Metal–Organic Frameworks in Mixed-Matrix Membranes Detected in Situ by NMR. *J. Am. Chem. Soc.* **2019,** *141* (18), 7589-7595.

120. Su, N. C.; Sun, D. T.; Beavers, C. M.; Britt, D. K.; Queen, W. L.; Urban, J. J., Enhanced permeation arising from dual transport pathways in hybrid polymer–MOF membranes. *Energy & Environmental Science* **2016,** *9* (3), 922-931.

121. Darunte, L. A.; Oetomo, A. D.; Walton, K. S.; Sholl, D. S.; Jones, C. W., Direct Air Capture of CO2 Using Amine Functionalized MIL-101(Cr). *ACS Sustainable Chem. Eng.* **2016,** *4* (10), 5761-5768.

122. Bloch, E. D.; Murray, L. J.; Queen, W. L.; Chavan, S.; Maximoff, S. N.; Bigi, J. P.; Krishna, R.; Peterson, V. K.; Grandjean, F.; Long, G. J.; Smit, B.; Bordiga, S.; Brown, C. M.; Long, J. R., Selective Binding of O2 over N2 in a Redox–Active Metal–Organic Framework with Open Iron(II) Coordination Sites. *J. Am. Chem. Soc.* **2011,** *133* (37), 14814-14822.

123. Calbo, J.; Golomb, M. J.; Walsh, A., Redox-active metal–organic frameworks for energy conversion and storage. *J. Mater. Chem. A.* **2019,** *7* (28), 16571-16597.

124. Kitagawa, S.; Kitaura, R.; Noro, S.-i., Functional Porous Coordination Polymers. *Angew. Chem. Int. Ed.* **2004,** *43* (18), 2334-2375.

125. Xiao, D. J.; Bloch, E. D.; Mason, J. A.; Queen, W. L.; Hudson, M. R.; Planas, N.; Borycz, J.; Dzubak, A. L.; Verma, P.; Lee, K.; Bonino, F.; Crocellà, V.; Yano, J.; Bordiga, S.; Truhlar, D. G.; Gagliardi, L.; Brown, C. M.; Long, J. R., Oxidation of ethane to ethanol by N2O in a metal–organic framework with coordinatively unsaturated iron(II) sites. *Nat Chem* **2014,** *6* (7), 590-595.

126. Tchounwou, P. B.; Yedjou, C. G.; Patlolla, A. K.; Sutton, D. J., Heavy Metals Toxicity and the Environment. *EXS* **2012,** *101*, 133-164.

127. Shannon, M. A.; Bohn, P. W.; Elimelech, M.; Georgiadis, J. G.; Marinas, B. J.; Mayes, A. M., Science and technology for water purification in the coming decades. *Nature* **2008,** *452* (7185), 301-310.

128. Lee, J.; Farha, O. K.; Roberts, J.; Scheidt, K. A.; Nguyen, S. T.; Hupp, J. T., Metal–organic framework materials as catalysts. *Chem. Soc. Rev.* **2009,** *38* (5), 1450-1459.

129. Peng, L.; Zhang, J.; Xue, Z.; Han, B.; Sang, X.; Liu, C.; Yang, G., Highly mesoporous metal–organic framework assembled in a switchable solvent. *Nat Commun* **2014,** *5*, 5465.

130. Zhu, Q.-L.; Li, J.; Xu, Q., Immobilizing Metal Nanoparticles to Metal–Organic Frameworks with Size and Location Control for Optimizing Catalytic Performance. *J. Am. Chem. Soc.* **2013,** *135* (28), 10210-10213.

131. Farha, O. K.; Eryazici, I.; Jeong, N. C.; Hauser, B. G.; Wilmer, C. E.; Sarjeant, A. A.; Snurr, R. Q.; Nguyen, S. T.; Yazaydın, A. Ö.; Hupp, J. T., Metal–Organic Framework Materials with Ultrahigh Surface Areas: Is the Sky the Limit? *J. Am. Chem. Soc.* **2012,** *134* (36), 15016-15021.

132. Furukawa, H.; Cordova, K. E.; O'Keeffe, M.; Yaghi, O. M., The Chemistry and Applications of Metal-Organic Frameworks. *Science* **2013,** *341* (6149).

133. Wang, C.; Liu, X.; Keser Demir, N.; Chen, J. P.; Li, K., Applications of water stable metal-organic frameworks. *Chem. Soc. Rev.* **2016,** *45* (18), 5107-5134.

134. Demessence, A.; D'Alessandro, D. M.; Foo, M. L.; Long, J. R., Strong CO2 Binding in a Water-Stable, Triazolate-Bridged Metal–Organic Framework Functionalized with Ethylenediamine. *J. Am. Chem. Soc.* **2009,** *131* (25), 8784-8786.

135. Singh, V.; Guo, T.; Xu, H.; Wu, L.; Gu, J.; Wu, C.; Gref, R.; Zhang, J., Moisture resistant and biofriendly CD-MOF nanoparticles obtained via cholesterol shielding. *Chem. Commun.* **2017,** *53*, 9246-9249.

136. Uemura, T.; Yanai, N.; Kitagawa, S., Polymerization reactions in porous coordination polymers. *Chem. Soc. Rev.* **2009,** *38* (5), 1228-1236.

137. Alsbaiee, A.; Smith, B. J.; Xiao, L.; Ling, Y.; Helbling, D. E.; Dichtel, W. R., Rapid removal of organic micropollutants from water by a porous β-cyclodextrin polymer. *Nature* **2016,** *529* (7585), 190-194.

138. Li, B.; Zhang, Y.; Ma, D.; Shi, Z.; Ma, S., Mercury nano-trap for effective and efficient removal of mercury(II) from aqueous solution. *Nat Commun* **2014,** *5*.

139. Knight, A. S.; Zhou, E. Y.; Pelton, J. G.; Francis, M. B., Selective Chromium(VI) Ligands Identified Using Combinatorial Peptoid Libraries. *J. Am. Chem. Soc.* **2013,** *135* (46), 17488-17493.

140. Horcajada, P.; Chalati, T.; Serre, C.; Gillet, B.; Sebrie, C.; Baati, T.; Eubank, J. F.; Heurtaux, D.; Clayette, P.; Kreuz, C.; Chang, J.-S.; Hwang, Y. K.; Marsaud, V.; Bories, P.-N.; Cynober, L.; Gil, S.; Ferey, G.; Couvreur, P.; Gref, R., Porous metal-organic-framework nanoscale carriers as a potential platform for drug delivery and imaging. *Nat Mater* **2010,** *9* (2), 172-178.

141. Férey, G.; Serre, C.; Mellot-Draznieks, C.; Millange, F.; Surblé, S.; Dutour, J.; Margiolaki, I., A Hybrid Solid with Giant Pores Prepared by a Combination of Targeted Chemistry, Simulation, and Powder Diffraction. *Angew. Chem. Int. Ed.* **2004,** *43* (46), 6296-6301.

142. Horcajada, P.; Surble, S.; Serre, C.; Hong, D.-Y.; Seo, Y.-K.; Chang, J.-S.; Greneche, J.-M.; Margiolaki, I.; Ferey, G., Synthesis and catalytic properties of MIL-100(Fe), an iron(iii) carboxylate with large pores. *Chem. Commun.* **2007,** (27), 2820-2822.

143. Lee, H.; Dellatore, S. M.; Miller, W. M.; Messersmith, P. B., Mussel-Inspired Surface Chemistry for Multifunctional Coatings. *Science* **2007,** *318* (5849), 426-430.

144. Seo, Y.-K.; Yoon, J. W.; Lee, J. S.; Lee, U. H.; Hwang, Y. K.; Jun, C.-H.; Horcajada, P.; Serre, C.; Chang, J.-S., Large scale fluorine-free synthesis of hierarchically porous iron(III) trimesate MIL-100(Fe) with a zeolite MTN topology. *Microporous and Mesoporous Materials* **2012,** *157*, 137-145.

145. Dhakshinamoorthy, A.; Alvaro, M.; Horcajada, P.; Gibson, E.; Vishnuvarthan, M.; Vimont, A.; Grenèche, J.-M.; Serre, C.; Daturi, M.; Garcia, H., Comparison of Porous Iron Trimesates Basolite F300 and MIL-100(Fe) As Heterogeneous Catalysts for Lewis Acid and Oxidation Reactions: Roles of Structural Defects and Stability. *ACS Catal.* **2012,** *2* (10), 2060-2065.

146. El-Ayaan, U.; Herlinger, E.; F. Jameson, R.; Linert, W., Anaerobic oxidation of dopamine by iron(III). *J. Chem. Soc., Dalton Trans.* **1997,** (16), 2813-2818.

147. Zangmeister, R. A.; Morris, T. A.; Tarlov, M. J., Characterization of Polydopamine Thin Films Deposited at Short Times by Autoxidation of Dopamine. *Langmuir* **2013,** *29* (27), 8619-8628.

148. Liu, Y.; Ai, K.; Lu, L., Polydopamine and Its Derivative Materials: Synthesis and Promising Applications in Energy, Environmental, and Biomedical Fields. *Chem. Rev.* **2014,** *114* (9), 5057-5115.

149. Ang, J. M.; Du, Y.; Tay, B. Y.; Zhao, C.; Kong, J.; Stubbs, L. P.; Lu, X., One-Pot Synthesis of Fe(III)–Polydopamine Complex Nanospheres: Morphological Evolution, Mechanism, and Application of the Carbonized Hybrid Nanospheres in Catalysis and Zn–Air Battery. *Langmuir* **2016,** *32* (36), 9265-9275.

150. Sever, M. J.; Weisser, J. T.; Monahan, J.; Srinivasan, S.; Wilker, J. J., Metal-Mediated Cross-Linking in the Generation of a Marine-Mussel Adhesive. *Angew. Chem. Int. Ed.* **2004,** *43* (4), 448-450.

151. Guo, Z.; Ni, K.; Wei, D.; Ren, Y., Fe3+-induced oxidation and coordination cross-linking in catechol-chitosan hydrogels under acidic pH conditions. *RSC Advances* **2015,** *5* (47), 37377-37384.

152. Rowsell, J. L. C.; Yaghi, O. M., Effects of Functionalization, Catenation, and Variation of the Metal Oxide and Organic Linking Units on the Low-Pressure Hydrogen Adsorption Properties of Metal–Organic Frameworks. *J. Am. Chem. Soc.* **2006,** *128* (4), 1304-1315.

153. Zhang, X.; Jia, X.; Zhang, G.; Hu, J.; Sheng, W.; Ma, Z.; Lu, J.; Liu, Z., Efficient removal and highly selective adsorption of Hg2+ by polydopamine nanospheres with total recycle capacity. *Appl. Surf. Sci.* **2014,** *314*, 166-173.

154. Lee, M.; Rho, J.; Lee, D.-E.; Hong, S.; Choi, S.-J.; Messersmith, P. B.; Lee, H., Water Detoxification by a Substrate-Bound Catecholamine Adsorbent. *ChemPlusChem* **2012,** *77* (11), 987-990.

155. Huang, G.; Yang, Q.; Xu, Q.; Yu, S.-H.; Jiang, H.-L., Polydimethylsiloxane Coating for a Palladium/MOF Composite: Highly Improved Catalytic Performance by Surface Hydrophobization. *Angew. Chem. Int. Ed.* **2016,** *55* (26), 7379-7383.

156. Kerrich, R., Nature's Gold Factory. *Science* **1999,** *284* (5423), 2101-2102.

157. Council, W. G. How much gold has been mined>. https://www.gold.org/about-gold/gold-supply/gold-mining/how-much-gold-has-been-mined.

158. Commission, E., Report on Critial Raw Materials for the EU.

159. Monitor, M. Who what why: How much gold can we get from mpbile phones? 2014. https://www.bbc.com/news/blogs-magazine-monitor-28802646.

160. Doyle, A. Electronic waste at new high, squandering gold, other metals -study. https://af.reuters.com/article/commoditiesNews/idAFL8N1OD2WB.

161. Shultz, D. Nearly $2 million in gold flows through Swiss sewers every year 2017. http://www.sciencemag.org/news/2017/10/nearly-2-million-gold-flows-through-swiss-sewers-every-year.

162. M., P. H.; Francis, W.; Jean, S.; T., J. M.; C., F. P., Precious metals in urban waste. *Water and Environment Journal* **2016,** *30* (1-2), 151-156.

163. Cornwall, W. Sewage sludge could contain millions of dollars worth of gold 2015. http://www.sciencemag.org/news/2015/01/sewage-sludge-could-contain-millions-dollars-worth-gold.

164. CNN, Scientists find gold worth $2 million in Swiss sewage. **2017**.

165. Devlin, H. Gold in faeces 'is worth millions and could save the environment' 2015. https://www.theguardian.com/science/2015/mar/23/gold-in-faeces-worth-millions-save-environment.

166. McHugh, J. B., Concentration of gold in natural waters. *Journal of Geochemical Exploration* **1988,** *30* (1), 85-94.

167. Caldwell, W. E., The gold content of sea water. *J. Chem. Educ.* **1938,** *15* (11), 507.

168. Koide, M.; Hodge, V.; Goldberg, E. D.; Bertine, K., Gold in seawater: a conservative view. *Applied Geochemistry* **1988,** *3* (3), 237-241.

169. Izatt, R. M.; Izatt, S. R.; Bruening, R. L.; Izatt, N. E.; Moyer, B. A., Challenges to achievement of metal sustainability in our high-tech society. *Chem. Soc. Rev.* **2014,** *43* (8), 2451-2475.

170. Sheberla, D.; Bachman, J. C.; Elias, J. S.; Sun, C.-J.; Shao-Horn, Y.; Dincă, M., Conductive MOF electrodes for stable supercapacitors with high areal capacitance. *Nat. Mater.* **2016,** *16*, 220.

171. Stassen, I.; Styles, M.; Grenci, G.; Gorp, Hans V.; Vanderlinden, W.; Feyter, Steven D.; Falcaro, P.; Vos, D. D.; Vereecken, P.; Ameloot, R., Chemical vapour deposition of zeolitic imidazolate framework thin films. *Nat. Mater.* **2015,** *15*, 304.

172. Furukawa, H.; Cordova, K. E.; O'Keeffe, M.; Yaghi, O. M., The Chemistry and Applications of Metal-Organic Frameworks. *Science* **2013,** *341* (6149), 1230444-1230444.

173. Queen, W. L.; Hudson, M. R.; Bloch, E. D.; Mason, J. A.; Gonzalez, M. I.; Lee, J. S.; Gygi, D.; Howe, J. D.; Lee, K.; Darwish, T. A.; James, M.; Peterson, V. K.; Teat, S. J.; Smit, B.; Neaton, J. B.; Long, J. R.; Brown, C. M., Comprehensive study of carbon dioxide adsorption in the metal-organic frameworks M2(dobdc) (M = Mg, Mn, Fe, Co, Ni, Cu, Zn). *Chem. Sci.* **2014,** *5* (12), 4569-4581.

174. Mondloch, J. E.; Katz, M. J.; Isley Iii, W. C.; Ghosh, P.; Liao, P.; Bury, W.; Wagner, G. W.; Hall, M. G.; DeCoste, J. B.; Peterson, G. W.; Snurr, R. Q.; Cramer, C. J.; Hupp, J. T.; Farha, O. K., Destruction of chemical warfare agents using metal–organic frameworks. *Nat. Mater.* **2015,** *14*, 512.

175. Liu, G.; Chernikova, V.; Liu, Y.; Zhang, K.; Belmabkhout, Y.; Shekhah, O.; Zhang, C.; Yi, S.; Eddaoudi, M.; Koros, W. J., Mixed matrix formulations with MOF molecular sieving for key energy-intensive separations. *Nat. Mater.* **2018,** *17* (3), 283-289.

176. McDonald, T. M.; Mason, J. A.; Kong, X.; Bloch, E. D.; Gygi, D.; Dani, A.; Crocellà, V.; Giordanino, F.; Odoh, S. O.; Drisdell, W. S.; Vlaisavljevich, B.; Dzubak, A. L.; Poloni, R.; Schnell, S. K.; Planas, N.; Lee, K.; Pascal, T.; Wan, L. F.; Prendergast, D.; Neaton, J. B.; Smit, B.; Kortright, J. B.; Gagliardi, L.; Bordiga, S.; Reimer, J. A.; Long, J. R., Cooperative insertion of CO2 in diamine-appended metal-organic frameworks. *Nature* **2015,** *519*, 303.

177. Wang, Z.; Cohen, S. M., Postsynthetic modification of metal–organic frameworks. *Chem. Soc. Rev.* **2009,** *38* (5), 1315-1329.

178. Sun, D. T.; Peng, L.; Reeder, W. S.; Moosavi, S. M.; Tiana, D.; Britt, D. K.; Oveisi, E.; Queen, W. L., Rapid, Selective Heavy Metal Removal from Water by a Metal–Organic Framework/Polydopamine Composite. *ACS Central Science* **2018**.

179. Woong, Y. J.; You-Kyong, S.; Kyu, H. Y.; Jong-San, C.; Hervé, L.; Stefan, W.; Philippe, B.; Alexandre, V.; Marco, D.; Emily, B.; L., L. P.; Christian, S.; Patricia, H.; Jean-Marc, G.; E., R. A.; Gérard, F., Controlled Reducibility of a Metal–Organic Framework with Coordinatively Unsaturated Sites for Preferential Gas Sorption. *Angew. Chem. Int. Ed.* **2010,** *49* (34), 5949-5952.

180. Mon, M.; Ferrando-Soria, J.; Grancha, T.; Fortea-Pérez, F. R.; Gascon, J.; Leyva-Pérez, A.; Armentano, D.; Pardo, E., Selective Gold Recovery and Catalysis in a Highly Flexible Methionine-Decorated Metal–Organic Framework. *J. Am. Chem. Soc.* **2016,** *138* (25), 7864-7867.

181. Doidge, E. D.; Carson, I.; Tasker, P. A.; Ellis, R. J.; Morrison, C. A.; Love, J. B., A Simple Primary Amide for the Selective Recovery of Gold from Secondary Resources. *Angew. Chem. Int. Ed.* **2016,** *55* (40), 12436-12439.

182. Gao, L.; Li, C.-Y. V.; Chan, K.-Y.; Chen, Z.-N., Metal–Organic Framework Threaded with Aminated Polymer Formed in Situ for Fast and Reversible Ion Exchange. *J. Am. Chem. Soc.* **2014,** *136* (20), 7209-7212.

183. Setyawati, M. I.; Xie, J.; Leong, D. T., Phage Based Green Chemistry for Gold Ion Reduction and Gold Retrieval. *ACS Applied Materials & Interfaces* **2014,** *6* (2), 910-917.

184. Lin, S.; Kumar Reddy, D. H.; Bediako, J. K.; Song, M.-H.; Wei, W.; Kim, J.-A.; Yun, Y.-S., Effective adsorption of Pd(ii), Pt(iv) and Au(iii) by Zr(iv)-based metal-organic frameworks from strongly acidic solutions. *Journal of Materials Chemistry A* **2017,** *5* (26), 13557-13564.

185. Okesola, B. O.; Suravaram, S. K.; Parkin, A.; Smith, D. K., Selective Extraction and In Situ Reduction of Precious Metal Salts from Model Waste To Generate Hybrid Gels with Embedded Electrocatalytic Nanoparticles. *Angew. Chem.* **2016,** *128* (1), 191-195.

186. Bonilla-Petriciolet, A.; Mendoza-Castillo, D. I.; Reynel-Ávila, H. E., *Adsorption processes for water treatment and purification*. Springer: 2017.

187. Cruz-Olivares, J.; Pérez-Alonso, C.; Barrera-Díaz, C.; Ureña-Nuñez, F.; Chaparro-Mercado, M.; Bilyeu, B., Modeling of lead (II) biosorption by residue of allspice in a fixed-bed column. *Chem. Eng. J.* **2013,** *228*, 21-27.

188. Lee, C.; Yang, W., Heavy metal removal from aqueous solution in sequential fluidized-bed reactors. *Environ. Technol.* **2005,** *26* (12), 1345-1354.

189. Kieu, H. T.; Müller, E.; Horn, H., Heavy metal removal in anaerobic semi-continuous stirred tank reactors by a consortium of sulfate-reducing bacteria. *Water research* **2011,** *45* (13), 3863-3870.

190. Thomas, H. C., Heterogeneous Ion Exchange in a Flowing System. *J. Am. Chem. Soc.* **1944,** *66* (10), 1664-1666.

191. *Mnova NMR*, Mestrelab Research 2016.

192. Liebscher, J.; Mrówczyński, R.; Scheidt, H. A.; Filip, C.; Hădade, N. D.; Turcu, R.; Bende, A.; Beck, S., Structure of Polydopamine: A Never-Ending Story? *Langmuir* **2013,** *29* (33), 10539-10548.

193. Dreyer, D. R.; Miller, D. J.; Freeman, B. D.; Paul, D. R.; Bielawski, C. W., Elucidating the Structure of Poly(dopamine). *Langmuir* **2012,** *28* (15), 6428-6435.

194. Perdew, J. P.; Burke, K.; Ernzerhof, M., Generalized Gradient Approximation Made Simple. *Phys. Rev. Lett.* **1996,** *77* (18), 3865-3868.

195. Grimme, S., Semiempirical GGA-type density functional constructed with a long-range dispersion correction. *J. Comput. Chem.* **2006,** *27* (15), 1787-1799.

196. Poloni, R.; Smit, B.; Neaton, J. B., CO2 Capture by Metal–Organic Frameworks with van der Waals Density Functionals. *J. Phys. Chem. A* **2012,** *116* (20), 4957-4964.

197. Hendon, C. H.; Tiana, D.; Fontecave, M.; Sanchez, C.; D'arras, L.; Sassoye, C.; Rozes, L.; Mellot-Draznieks, C.; Walsh, A., Engineering the Optical Response of the Titanium-MIL-125 Metal–Organic Framework through Ligand Functionalization. *J. Am. Chem. Soc.* **2013,** *135* (30), 10942-10945.

198. Planas, N.; Dzubak, A. L.; Poloni, R.; Lin, L.-C.; McManus, A.; McDonald, T. M.; Neaton, J. B.; Long, J. R.; Smit, B.; Gagliardi, L., The Mechanism of Carbon Dioxide Adsorption in an Alkylamine-Functionalized Metal–Organic Framework. *J. Am. Chem. Soc.* **2013,** *135* (20), 7402-7405.

199. *CasaXPS: Processing Software for XPS, AES, SIMS and More* Casa Software Ltd: 2016.

200. Li, M.; Sun, Q.; Liu, C.-j., Preparation of Floating Au/PVP Film on Water for a Green and Rapid Extraction of Gold Ion. *ACS Sustainable Chemistry & Engineering* **2016,** *4* (6), 3255-3260.

201. Lam, K. F.; Yeung, K. L.; McKay, G., An Investigation of Gold Adsorption from a Binary Mixture with Selective Mesoporous Silica Adsorbents. *The Journal of Physical Chemistry B* **2006,** *110* (5), 2187-2194.

202. Wu, C.; Zhu, X.; Wang, Z.; Yang, J.; Li, Y.; Gu, J., Specific Recovery and In Situ Reduction of Precious Metals from Waste To Create MOF Composites with Immobilized Nanoclusters. *Industrial & Engineering Chemistry Research* **2017,** *56* (47), 13975-13982.

203. Odio, O. F.; Lartundo-Rojas, L.; Santiago-Jacinto, P.; Martínez, R.; Reguera, E., Sorption of Gold by Naked and Thiol-Capped Magnetite Nanoparticles: An XPS Approach. *The Journal of Physical Chemistry C* **2014,** *118* (5), 2776-2791.

204. Fujiwara, K.; Ramesh, A.; Maki, T.; Hasegawa, H.; Ueda, K., Adsorption of platinum (IV), palladium (II) and gold (III) from aqueous solutions onto l-lysine modified crosslinked chitosan resin. *Journal of Hazardous Materials* **2007,** *146* (1), 39-50.

205. Parajuli, D.; Adhikari, C. R.; Kuriyama, M.; Kawakita, H.; Ohto, K.; Inoue, K.; Funaoka, M., Selective Recovery of Gold by Novel Lignin-Based Adsorption Gels. *Industrial & Engineering Chemistry Research* **2006,** *45* (1), 8-14.

206. Wang, J.; Li, J.; Wei, J., Adsorption characteristics of noble metal ions onto modified straw bearing amine and thiol groups. *Journal of Materials Chemistry A* **2015,** *3* (35), 18163-18170.

207. Munoz Garcia, A.; Hunt, A. J.; Budarin, V. L.; Parker, H. L.; Shuttleworth, P. S.; Ellis, G. J.; Clark, J. H., Starch-derived carbonaceous mesoporous materials (Starbon[registered sign]) for the selective adsorption and recovery of critical metals. *Green Chemistry* **2015,** *17* (4), 2146-2149.

208. Sun, L.; Tian, C.; Wang, L.; Zou, J.; Mu, G.; Fu, H., Magnetically separable porous graphitic carbon with large surface area as excellent adsorbents for metal ions and dye. *Journal of Materials Chemistry* **2011,** *21* (20), 7232-7239.

Daniel T. Sun

Rue de L'Industrie 17, 1950 Sion
Phone: +41 21 69 58298 E-Mail: daniel.sun@epfl.ch

EDUCATION

2015 – present	**Ph.D in Chemistry and Chemical Engineering** École polytechnique fédérale de Lausanne Valais Wallais, Sion, Switzerland Prof. Wendy L. Queen – Research Advisor
2009 – 2013	**B.S. in Chemistry, Minor in Biochemistry, ACS Certified** Loyola Marymount University, Los Angeles, CA Prof. Jeremy McCallum and Prof. Emily Jarvis – Research Advisor

EMPLOYMENT HISTORY

2013 – 2015	**Research Assistant** Lawrence Berkeley National Laboratory, Principal Investigator – Wendy L. Queen
Summer 2012	**Rains Research Assistant** Loyola Marymount University, Prof. Jeremy McCallum
2011 – 2013	**Organic Chemistry Tutor** Loyola Marymount University, Academic Resource Center
2011 – 2013	**Organic Chemistry Laboratory Teaching Assistant** Loyola Marymount University, Department of Chemistry and Biochemistry
2011 – 2013	**Shipping and Receiving** Loyola Marymount University, Distribution Center
2011	**Media and Reserve Student Worker** Loyola Marymount University, Hannon Library

AWARDS AND SCHOLARSHIPS

2019	SNSF/Innosuisse Bridge Proof of Concept Grant
2019	Tech4Impact Playgrant
2019	Swiss Nanotechnology Ph.D Award
2018	MERCK 350 Innovation Research Grant Winner
2018	Swiss Academy of Sciences and Swiss Chemical Society Travel Award
2017	Best Poster Prize – International Symposium on Composites of Metal-Organic Frameworks
2012	McNair Scholars Program - Ronald E. McNair Postbaccalaureate Achievement Program
2012	Loyola Marymount University O'Malley Scholarship

PEER-REVIEWED MANUSCRIPTS

1. "Efficient reductive amination of HMF with well dispersed Pd nanoparticles immobilized in a porous MOF/polymer composite", V. V. Karve, **D. T. Sun**, O. Trukhina, S. Yang, E. Oveisi, J. Luterbacher, W. L. Queen, Green Chem., 2019, just accepted.

2. "Mystical Material Might Help Solve Global Energy Problems", **D. T. Sun** and W. L. Queen, ACS Cent. Sci., 2019, 5, 8, 1307-1309.

3. "A new post-synthetic polymerization strategy makes metal-organic frameworks more stable", S. Yang, L. Peng, **D. T. Sun**, M. Agari, E. Oveisi, O. Trukhina, S. Bulut, A. Jamali, W. L. Queen, *Chem. Sci.,* 2019, 10, 4542 – 4549.

4. "Rapid, Selective Extraction of Trace Amounts of Gold from Complex Water Mixtures with a MOF/Polymer Composite", **D. T. Sun**, N. Gasilova, S. Yang, E. Oveisi, W. L. Queen, *J. Am. Chem. Soc.*, 2018, 140, 16697. **ACS Editors Choice. Featured in C&E and RTS News.** Patent Application Ser. No: 62/547,988 US

5. "MOF/polymer composite synthesized using a double solvent method offers enhanced water and CO2 adsorption properties" L. Peng, S. Yang, **D. T. Sun**, M. Asgari, W. L. Queen, *Chem. Commun*. 2018, 54, 10602.

6. "A metal-organic framework derived Co3S4 hollow nanobox for the selective reduction of nitroarenes" S. Yang, L. Peng, **D. T. Sun**, E. Oveisi, S. Bulut, and W. L. Queen, *ChemSusChem* 2018, 11, 3131.

7. "Rapid, Selective Heavy Metal Removal from Water by a Metal-organic Framework /Polydopamine Composite", **D. T. Sun,** L. Peng, W. S. Reeder, S. M. Moosavi, D. Tiana, D. K. Britt, E. Oveisi, W. L. Queen, *ACS Cent. Sci.,* 2018, 4 (3), 349-356. **Featured Front Cover Article. Featured in RTS News.** Patent Application Ser. No: PCT/US2017/028865

8. "MOF-Derived Cobalt Phosphide/Carbon Nanocubes for Selective Hydrogenation of Nitroarenes to Anilines" Shuliang Yang, Li Peng, Emad Oveisi, Safak Bulut, **Daniel T. Sun**, Mehrdad Asgari, Olga Trukhina, Wendy L. Queen, Chem. Eur. J., 2018, 24, 4234-4238

9. "Using predefined $M_3(\mu_3\text{-O})$ clusters as building blocks for an isostructural series of metal-organic frameworks" L. Peng, M. Asgari, P. Mieville, P. Schouwink, S. Bulut, **Daniel T. Sun**, Z. Zhou, P. Pattison, W. vanBeek, and W. L. Queen, 2017, *ACS Appl. Mater, Interfaces*. 2017, 9, 23957

10. "Understanding the formation mechanism of metal nanocrystal@MOF-74 hybrids", I. Luz, A. Loiudice, **D. T. Sun,** W. L. Queen, R. Buonsanti. *Chem. Mater.,* 2016 (11), 3839

11. "Transparent and Robust Metal-Organic Framework/Polymer Mixed Matrix Membranes as Water Vapor Barriers", Y. J. Bae, E. S. Cho, F. Qiu, **D. T. Sun**, T. E. Williams, J. J. Urban, W L. Queen, *ACS Appl Material Interfaces*, 2016, 8, 10098 U.S. Patent Application Ser. No: 62/485,241.

12. "Enhanced Permeation Arising from Dual Transport Pathways in Hybrid Polymer-MOF Membranes", N. C. Su, **D. T. Sun**, C. M. Beavers, D. K. Britt, W. L. Queen, J. J. Urban, Energy Environ. Sci, 2016, 9, 922 (featured cover article). U.S. Patent Application Ser. No: 62/417,954

13. "Multifunctional Purification and Sensing of Toxic Hydride Gases by CuBTC Metal-Organic Framework" Gregory W. Peterson, David K. Britt, **Daniel T. Sun**, John J. Mahle, Matthew Browe, Tyler Demasky, Shirmonda Smith, Amanda Jenkin and Joseph A. Rossin. *Ind. Eng. Chem. Res,* 2015, 54 (14).

RESEARCH PRESENTATIONS

October 2019	Invited 1 hour Seminar (Los Angeles, CA) Oral Presentation Loyola Marymount University, Department of Chemistry and Biochemistry The Clean Water Initiative
October 2019	Invited Lecture to McNair Scholars (Los Angeles, CA) Lecture Loyola Marymount University, Department of Chemistry and Biochemistry From Humble Beginning to the Clean Water Initiative
September 2019	Swiss Chemical Society Fall Meeting (Zurich, Switzerland) Poster Presentation Design of Porous Composites for Selective and Enhanced Chemical Separations in Aqueous Media
December 2018	MOF Conference 2018 (Auckland, New Zealand) Oral Presentation Design of Porous Composites for Selective and Enhanced Chemical Separations in Aqueous and Aerial Media
November 2017	2nd EuroMOF 2017 (Delft, Amsterdam) Poster Presentation Design of Porous Composites for Environmental Applications

September 2017	International Symposium on Composites of Metal and Covalent Organic Frameworks: Fundamental Design & Applications (Granada, Spain) Poster Presentation **(Best Poster Prize)** Design of Porous Composites for Environmental Applications
November 2014	Loyola Marymount University, Department of Chemistry and Biochemistry (Los Angeles, CA USA) Invited 1 hour Oral Presentation Tuning Metal-Organic Frameworks
April 2013	McNair Scholars Program (Los Angeles, CA USA) Oral Research Proposal Synthesis of Surface-Induced Aromatic Stabilized Charged and Metallic Molecules
March 2013	Loyola Marymount University Undergraduate Research Symposium (Los Angeles, CA USA) Poster Presentation Investigation into Photosensitized Oxidation of Indole Derivatives
February 2013	McNair Scholar Program (Los Angeles, CA USA) Oral Presentation Investigation into Photosensitized Oxidation of Indole Derivatives
November 2012	Southern California Conference for Undergraduate Research (Malibu, CA USA) Poster Presentation Investigation into Photosensitized Oxidation of Indole Derivatives Prof. Jeremy McCallum and Prof. Emily Jarvis – Research Advisor

“Be Coachable”